NASA CONTRACTOR REPORT

NASA CR-2140

NASA CR-2140

EXPERIMENTAL INVESTIGATION OF A 4½-STAGE TURBINE WITH VERY HIGH STAGE LOADING FACTOR

I - Turbine Design

by D. C. Evans and J. M. Hill

Prepared by
GENERAL ELECTRIC COMPANY
Cincinnati, Ohio 45215
for Lewis Research Center

NATIONAL AERONAUTICS AND SPACE ADMINISTRATION • WASHINGTON, D. C. • JANUARY 1973

1. Report No.	2. Government Accession No.	3. Recipient's Catalog No.
NASA CR-2140		

4. Title and Subtitle	5. Report Date
EXPERIMENTAL INVESTIGATION OF A $4\frac{1}{2}$-STAGE TURBINE WITH VERY HIGH STAGE LOADING FACTOR I - TURBINE DESIGN	January 1973
	6. Performing Organization Code
7. Author(s)	8. Performing Organization Report No.
D. C. Evans and J. M. Hill	None
	10. Work Unit No.
9. Performing Organization Name and Address	
General Electric Company Cincinnati, Ohio 45215	11. Contract or Grant No. NAS 3-15322
	13. Type of Report and Period Covered
12. Sponsoring Agency Name and Address	Contractor Report
National Aeronautics and Space Administration Washington, D.C. 20546	14. Sponsoring Agency Code

15. Supplementary Notes

Project Manager, Warren J. Whitney, Fluid System Components Division, NASA Lewis Research Center, Cleveland, Ohio

16. Abstract

The results of the Task I and II turbine design work are reported. Preliminary design is discussed. Blading detailed design is discussed, and design data are summarized. Predicted performance maps are presented. Steady-state stresses and vibratory behavior are discussed, and the results of the mechanical design analysis are presented.

17. Key Words (Suggested by Author(s))	18. Distribution Statement
Turbines High stage loading Fan engines	Unclassified - unlimited

19. Security Classif. (of this report)	20. Security Classif. (of this page)	21. No. of Pages	22. Price*
Unclassified	Unclassified	125	$3.00

* For sale by the National Technical Information Service, Springfield, Virginia 22151

TABLE OF CONTENTS

LIST OF TABLES

LIST OF ILLUSTRATIONS

LIST OF ILLUSTRATIONS (Continued)

LIST OF ILLUSTRATIONS (Continued)

LIST OF ILLUSTRATIONS (Concluded)

I. Summary

The results of the Task I velocity diagram and the Task II detailed design of the highly loaded four and one half stage fan turbine are presented. The effect of stage leaving swirl, stage energy split, and streamline slope and curvature were investigated and the results presented. The design procedure for the outlet turning vanes is presented. Final vector diagram calculations were made taking into account streamline slope and curvature effects. The number of vanes and rotors was selected using the Zweifel loading criteria. Vane and rotor section coordinates were generated and detailed design data was summarized. Velocity distributions for the flow through the blades was analyzed by two dimensional incompressible and compressible techniques and by a quasi-three dimensional technique. Velocity distributions at root, pitch, and tip for all the blade sections are presented. Predicted turbine performance maps were generated. Steady state stresses and vibratory behavior were predicted. No stress problems are expected during air turbine testing.

II. Introduction

Advanced research investigations of the propulsion requirements for direct lift fan engine systems indicate these systems will have high bypass ratio turbofan engines. The underlying reason for the expanding role of the turbofan engine stems from its inherent design flexibility to exploit the cycle advantage afforded through a small gas generator core in conjunction with a fan selected to provide improved fuel consumption and thrust characteristics.

Lift engine size is as important as weight. Twelve to fourteen of these engines must be installed on each airplane, and considerable pod area and weight are involved. If twelve of more lift engines are required per airplane, it is apparent that the cost of these engines will be a significant factor in the total airplane cost. Since number of parts and components has an effect on cost, there is an incentive to reduce the number of stages in the fan drive turbine.

The foregoing considerations of V/STOL engine requirements suggest the following fan drive turbine requirements:

1. Minimum number of stages (short, less cost).

2. Some SFC penalty acceptable (relative to cruise engine).

These requirements, combined with the low rotor speed (non-geared) imply a fan drive turbine with meanline average loading ($gJ\Delta h/2\Sigma U_p^2$) in the 2-2.5 range, with efficiencies in the 80% to 85% range for lift engine use. A fan drive turbine design of this type can result in a saving of 2-3 stages with minimum impact on lift engine fuel consumed, while having a beneficial effect on installation weight, drag, and cost. Since no test results are known to exist for this type of turbine, the need to design, build, and test a vehicle is apparent.

The specific objective of this program is to design, build, and test a very highly loaded four-stage fan drive turbine with outlet turning vanes.

This is an eighteen-month analytical and experimental investigation program to provide very high aerodynamic loading technology for fan drive turbines. The technology will be specifically applicable to multi-stage configurations for advanced high bypass ratio, direct lift turbofan propulsion system applications.

The program was divided into two phases encompassing nine task items of activity. The first phase covers Task Items I and II of this program which are the Velocity Diagram Study and Turbine Design, respectively. These tasks include the following sub-tasks:

- Investigate parametric turbine velocity diagram studies
- Select one design for building and testing
- Complete a detailed aerodynamic turbine design for an existing test rig

- Complete the detailed blading aerodynamic design for the rig
- Perform detailed blading mechanical design for the test rig
- Perform the turbine test rig mechanical design
- Prepare the turbine test rig modification drawings.

The second phase covers Task Items III through IX of this program to fabricate, procure vibration bench test, fatigue endurance test and inspect the turbine rig modifications, to instrument and calibrate the rig vehicle, to conduct a test program, and to report progress, analysis, and design, as well as test and performance results.

The purpose of this report is to present the Task I velocity diagram study results and the Task II detailed design of the turbine.

III. Preliminary Design

A. Requirements

The fan drive turbine investigated in this program has the following design requirements:

• Constant pitch diameter	19.00 in. (48.26 cm.)
• Number of stages	$4\frac{1}{2}$
• Equivalent weight flow	25.07 lbm/sec. (11.37 kg/sec.)
• Inlet swirl angle	0.0 degrees
• Exit swirl angle with turning vanes	0.0 degrees
• Velocity leaving outlet turning vanes related to inlet critical velocity	0.376
• D-Factor of outlet turning vanes at mean radius	0.4
• Average mean radius loading $(gJ\Delta h/2\Sigma U_p^2)$	2.5
• Equivalent specific work	25.88 BTU/lbm (60242.32 joules/leg)
• $w\sqrt{T_T}/P_T$ at inlet	38.84 lbm-°R/sec-Lbf/in^2 (25.55 kg-°R/sec-n/cm^2)
• $N/\sqrt{T_T}$	95.33

- Equivalent mean blade speed (constant for all stages) — 180 ft/sec (54.86 m/sec)

B. Design Studies

1. Flowpath and Velocity Diagram Studies

A velocity diagram study was made to show the relationships among the turbine design options such as stage energy split and stage leaving swirl for the turbine requirements.

The flowpath shape was specified to have a constant mean radius. The inlet and exit annulus areas were calculated to correspond to an inlet Mach number of 0.30 and an exit Mach number of 0.36. A free vortex velocity diagram parametric study was made in which stage energy extraction and stage leaving swirl was varied. With a pitchline D-factor for the outlet turning vane of 0.4 specified as one of the design requirements and the exit Mach number known, a value for the solidity of the outlet turning vane was determined for each turbine exit swirl calculated at the pitchline (Reference 1). With the pitchline turbine exit swirl known, a parametric study was made varying the distribution of the available energy among the stages. The results of this study showed that what appeared to be the best configuration was to let the stage pitch aerodynamic loading ($gJ\Delta h/2\Sigma U_p^2$) be approximately equal for stage one, two, and three with the stage four loading less than the previous stages but loaded high enough to prevent flow diffusion in the nozzle tip section.

A concern for such high aerodynamic loading is the high overall blade turning which results. To keep the turning reasonable and not penalize the turbine unnecessarily with high turning blading, the exit axial Mach numbers from stages one, two, and three were designed to be approximately 0.35.

To investigate the blade turning in more detail, the effect of streamline slope and curvature on the velocity diagram was calculated. This was accomplished by an analysis which satisfied the radial equilibrium equation which takes into effect the changes in annulus taper and blade thickness blockage gradients. This method of analysis is explained in detail in Section III-C. Figures 1, 2, 3, and 4 show the comparison between the angles with the effect of streamline slope and curvature and the free-vortex angles. The general trend shown for the velocity diagram angles is that the effect of streamline slope and curvature can change the angle from the free-vortex solution by an amount up to 3°. The effect is much less pronounced in stage 4, as might be expected, since stage 4 has cylindrical end walls through the rotor.

For the velocity diagram calculations, an efficiency was calculated on the basis of the following assumptions:

a) All stages had test factor equal to 0.96. The test factor is defined as the ratio of the turbine required energy extraction to the velocity diagram energy extraction.

b) Nozzle efficiencies were assumed to be 0.97 for stage one and 0.96 for stages two, three, and four.

c) Nozzle inlet pressure recovery factors were assumed equal to 0.97.

d) Rotor efficiencies were assumed equal to 0.95.

The calculated efficiency changes of the various velocity diagram configurations would then be due to changes in stator and rotor leaving kinetic energies.

2. Outlet Turning Vane Design

The outlet turning vanes are diffusing sections and require design techniques that are different from turbine vane design. The design requirements were that the pitchline diffusion factor (D-factor) was equal to 0.40, the flow leaving was axial, and the velocity leaving related to inlet critical velocity was 0.376.

The diffusion factor is defined in "Aerodynamic Design of Axial-Flow Compressors-Revised", (Reference 1) as $D = (1 - V_2/V_1) + \Delta V_\theta/2\sigma V_1$ which can also be represented compressibly as $D = 1 - [M_{Z2}/M_{Z1}]^{2/(\gamma+1)} \cos \beta_1 + 1/2\sigma \sin \beta_1$ if the exit angle from the turning vanes is axial. With the D-factor and leaving angle specified and the axial Mach number calculated leaving the outlet turning vanes, a parametric study was made of D-factor versus solidity and pressure loss versus D-factor at various values of entering angle and axial Mach number into the outlet turning vanes. These values were a function of the stage four energy extraction. The pressure loss estimates were obtained using correlations of annular cascade data contained in reference 1, and were used for the design case studies. For off-design outlet turning vane performance, pressure losses were estimated as a function of incidence angle. Figure 5 shows the predicted pressure loss across the outlet turning vane as a function of blade incidence angle.

On the basis of the pitchline requirement of the D-factor equal to 0.4 and the fourth stage exit swirl gradient determined from hub to tip for the most promising turbine velocity diagrams, the outlet guide vane was then designed. The basic design philosophy used was to design the blade shapes such that the diffusion on the suction surface was held to a minimum with the velocity distribution on the suction surface linear in deceleration from leading edge to trailing edge. Consistent with the pitchline calculation, parametric studies were made at hub and tip to determine the D-factor for the minimum loss across the outlet turning vanes. This corresponds quite closely to an outlet turning vane with constant axial width.

3. Turbine and Outlet Turning Vane Compatibility

Figures 6 and 7 combine the turbine velocity diagram and outlet turning vane studies. These results were a parametric study for an earlier similar design and not the final design as presented in the report. Although the values for the efficiency do not agree exactly with the final design, the figures do show the correct trends expected. Figure 6 shows the free vortex turbine total-to-total efficiency trends for a turbine design with and without the outlet turning vane loss. The curve represents a turbine design in which the

fourth stage exit swirl is varied by changing the stage energy extraction, maintaining a constant reaction. The remaining energy is distributed among the first three stages. With the D-factor at the pitch equal to 0.4 and the axial Mach number and inlet and exit angles to the outlet turning vane known, an outlet turning vane pressure loss estimate was made. The pressure loss was then put in terms of a total-to-total efficiency decrement which was subtracted from the four stage total-to-total turbine efficiency. The curve shows the interesting result that for a given D-factor there is a given fourth stage exit swirl angle corresponding with a stage energy extraction split that appears to give a maximum turbine efficiency.

Figure 7 shows another interesting trend concerning the value of D-factor. This curve is exactly the same as Figure 6 except a constant pitchline D-factor of 0.5 was considered. This curve shows that for increasing values of fourth stage exit swirl the maximum turbine total-to-total efficiency occurs at increasing values of D-factor, at least for the range studied here.

On the basis of these velocity diagram studies, it appeared that the most promising turbine would be one with a stage energy split (Δh stage/Δh turbine) of 28.5% on stage one, 26.5% on stage two, 26.0% on stage three, and 19.0% on stage four. The corresponding stage aerodynamic loading ($gJ\Delta h/2\Sigma U_p^2$) is 2.85, 2.65, 2.60, and 1.90 at the pitch on stages one, two, three, and four respectively. The design selected has a fourth stage pitchline exit swirl of 35.5° and a calculated total-to-total efficiency of 84.05% for the four and one half (4 stages plus the outlet turning vane) stage turbine. A summary of the velocity diagram calculation results for the 4½ stages is shown in Table I, and a description of the parameters for the blading design is presented in Tables II through X. The velocity diagram nomenclature and final design velocity diagrams are shown in Figure 9 and 10.

C. Quasi - Three Dimensional Flow Calculation

The quasi-three dimensional flow analysis through the turbine was performed with the aid of a digital computer program which describes the axisymmetric flow field in the region of turbomachinery blading. The overall calculation scheme of the computer program is summarized here. The flow is considered at a number of axial stations, and the radial-equilibrium equation, energy equation, and continuity condition are employed at each of them to determine the distribution of flow properties from hub to tip. It is necessary, however, that these distributions obtained separately at each station be consistent from station to station, and that the radial acceleration which a fluid particle undergoes as it passes from station to station be accounted for in the radial-equilibrium equation. This is done by assuming that the shape of a meridional streamline is adequately represented by a spline constrained at each axial station consistent with the continuity condition, and at upstream and downstream boundary stations by a selected orientation and shape. The radial acceleration is expressed in terms of the meridional streamline slope and curvature.

An iterative method of solution is implied. Meridional streamline shapes are assumed based on results from the previous iteration, and flow distributions at each axial station are found. These imply new meridional streamline shapes, and this iterative calculation is allowed to continue until the changes in streamline shapes between two successive calculations are small enough to satisfy a predetermined tolerance.

A significant feature of the computer program is the inclusion of terms in the radial-equilibrium equation which represent the blade action by a distributed body force field and the blade thickness by distributed blockage. The equation, which appears in Reference 3, wherein physical interpretation of the individual terms is presented, is restated here:

$$\frac{1\partial Ps}{\rho\partial r} = \left[\frac{1 - M_z^2}{1 - M_m^2}\right]\left[\frac{C_u^2}{r} - \frac{D^2 r}{Dz^2}\, C_z^2\right] + \frac{W_r C_z}{1 - M_m^2}\left[\frac{\partial(r \tan \phi)}{r\partial r} + \frac{1}{\lambda}\frac{D\lambda}{Dz}\right] - F_u \frac{M_r M_u}{1 - M_m^2} + F_r \qquad (1)$$

The heat addition term has been omitted since, in the absence of transients, the blade surface and the fluid adjacent to it are at the same temperature. As suggested in Reference 3, the computer program includes a term to represent the heating effect of internal fluid friction, which encompasses all loss sources including shock waves:

$$-\frac{W_r C_z}{1 - M_m^2}\left[1 - \frac{P_s}{P_{T_R}}\right]\frac{\bar{\omega}_z}{\ell} \qquad (2)$$

The loss-rate coefficient, $\bar{\omega}_z$, is defined in Reference 3.

The radial and tangential components of the blade force may be expressed in terms of the axial change in angular momentum by means of the following relationships:

$$F_u = \frac{C_z}{r}\frac{D(rC_u)}{Dz} \qquad (3)$$

and

$$F_r = F_u \tan \xi$$

By using the fact that the second derivative of the meridional streamline shape can be related to the meridional streamline curvature, $1/r_m$, and trigonometry to relate velocity components, equation (1) may be rewritten as follows:

$$\frac{1}{\rho}\frac{\partial P_s}{\partial r} = \frac{1 - M_z^2}{1 - M_m^2}\left\{\frac{C_u^2}{r} + \frac{C_z^2 \sec^3\phi}{r_m} + \frac{C_z^2 \tan\phi}{1 - M_z^2}\left[\frac{\partial (r \tan\phi)}{r\partial r} - \left(1 - \frac{P_s}{P_{T_R}}\right)\frac{\bar{\omega}_z}{\ell}\right]\right\} \tag{5}$$

$$+ \frac{1}{1 - M_m^2}\left\{C_z^2 \tan\phi \frac{1}{\lambda}\frac{D\lambda}{Dz} + \left[M_z^2 (U - C_u) \tan\phi + (1 - M_m^2) C_z \tan\xi\right]\frac{1}{r}\frac{D(rC_u)}{Dz}\right\}$$

The terms on the right-hand side of equation 5 have been grouped such that the first set of braces includes terms which are present anywhere in the flow field while the second set of braces includes terms which occur only when calculations inside the axial extent of a blade row are desired. By specification of the applicable input parameters, the intrabladerow calculation may be performed in order that the effects of stator lean and sweep may be determined.

At each axial station where the rotating bladerow is influential, the enthalpy of the fluid is related to the fluid swirl velocity by the energy equation which may be found in the following form in Chapter VIII of Reference 1:

$$(U C_u)_i - (UC_u)_{i-1} = g J c_p (T_{T_i} - T_{T_{i-1}}) \tag{6}$$

The static condition of the fluid is described by the use of the equation of state,

$$P_s = g\rho_s R T_s, \tag{7}$$

and the specific heats are assumed to be constant. Application of the continuity condition in the form found in Chapter VIII of Reference 4,

$$w = 2\pi g \int_{r_h}^{r_t} K_{bk} \rho C_z r dr, \tag{8}$$

in combination with the previous four equations yields a complete description of the flow at each axial station. With the flow field completely described, loading parameters and forces on the blading and walls are calculated from station data using geometric characteristics of the system where required.

The quasi-three dimensional flow along the blading surfaces can now be calculated. Considering Figure 8 the following equations can be written

$$\bar{C} = \bar{W} + \bar{U} \tag{9}$$

$$t = (1 - \lambda)\frac{2\pi r}{N} \tag{10}$$

or

$$dt = \frac{2\pi}{N} d\,[(1 - \lambda)\, r] = \frac{2\pi}{N}\,[(1 - \lambda)\, dr - r d\lambda].$$

Circulation is defined as $\Gamma = \oint \bar{V} \cdot d\bar{s}$.

Therefore circulation around AFDC can be written as

$$\Gamma_{AFDC} = \omega(r + dr)\,(t + dt) + (C_u + dC_u)\left[\frac{2\pi(r + dr)}{N} - (t + dt)\right]$$

$$- C_u\left(\frac{2\pi r}{N} - t\right) - \omega r t + Cds - Cds$$

or

$$\Gamma_{AFDC} = \omega d(rt) + \frac{2\pi}{N} d\,(\lambda r C_u). \tag{11}$$

Now consider the circulation around AFEB

$$\Gamma_{AFEB} = \bar{C}_p \cdot d\bar{s}_p - \bar{C}_s \cdot d\bar{s}_s + \bar{\omega} r t - \bar{\omega} \cdot (\bar{r} + d\bar{r})(t + dt)$$

$$\Gamma_{AFEB} = W_p ds_p - W_s ds_s + U_p ds_p - U_s ds_s + \omega d(rt).$$

But $U_p ds_p - U_s ds_s = -Udm(\tan \beta_p - \tan \beta_s)$.

Therefore the circulation around AFEB can be written

$$\Gamma_{AFEB} = W_p \frac{ds}{\cos \beta_p} - W_s \frac{dm}{\cos \beta_s} - Udm\,(\tan \beta_p - \tan \beta_s) + \omega d(rt) \tag{12}$$

The circulation around EDCB is equal to zero. Therefore $\Gamma_{AFDC} = \Gamma_{AFEB}$ and setting (11) equal to (12) and reducing

$$\omega d\,(rt) + \frac{2\pi}{N}\, d(\lambda r C_u) = W_p \frac{dm}{\cos \beta_p} - W_s \frac{dm}{\cos \beta_s} - Udm\,(\tan \beta_p - \tan \beta_s)$$

$$+ \omega d\,(rt)$$

or
$$\frac{W_p}{\cos \beta_p} - \frac{W_s}{\cos \beta_s} = \frac{2\pi}{N} \left(r W_u \frac{d\lambda}{dm} + \lambda \frac{d(rCu)}{dm} \right) . \quad (13)$$

By specification of the applicable input parameters of blade camber, thickness distribution, and meanline angle distribution, with the solution of equation 5, the difference in the velocity between the suction and pressure surfaces can be obtained. The actual velocities on the respective surfaces are solved for by adding one half of this difference to the circumferentially averaged solution (equation 5) for the suction surface and subtracting one half of the difference from the circumferentially averaged solution for the pressure surface.

IV. Blading Aerodynamic Design

A. Selection of Number of Vanes and Rotors

Vane and rotor solidities were determined through selection of Zweifel Numbers based on General Electric design experience using the Zweifel loading criteria. The vane and rotor axial widths and the number of vanes and rotors were set such that no performance loss would be expected due to trailing edge blockage.

After the vane and rotor axial widths had been determined, the aerodynamic flowpath was finalized and is presented in Figure 11.

B. Blading Profile Design

The vane and rotor throat openings were calculated using the following equations:

$$nd_{o_V} = \pi D \cos \alpha_1 \, (\sqrt{\eta_V}/C_f) \, \frac{h_{ex}}{h_{th}} \quad \text{and}$$

$$nd_{o_R} = \pi D \cos \beta_2 \, (\sqrt{\eta_R}/C_f) \, \frac{h_{ex}}{h_{th}}$$

These equations were the result of applying the law of conservation of mass between the throat and downstream of each blade row. The terms for these equations are shown in Figure 12.

The vane and rotor hub, pitch, and tip profiles were then generated with the aid of a computer program in which the section coordinates are developed from a small number of numerical inputs. An analysis of flow conditions through each blade section passage was conducted using an incompressible two dimensional potential flow cascade analysis computer program, and checked using a compressible two dimensional potential flow cascade analysis. Design iterations on the vane and rotor section profiles were made until satisfactory velocity distributions around each profile were obtained. The final blade shapes were analyzed by the quasi-three dimensional compressible analysis computer program.

C. Blade Stacking

The vane hub, pitch, and tip sections for stages two, three, and four were stacked on the minimum Y measurement on the suction surface and the axial width spaced such that the vane axial sweep angle was equal on the leading and trailing edges. The stage one vane was stacked on the trailing edge. The center of gravity was calculated for each rotor hub, pitch, and tip section, and the stacking axis was located to pass through each section's center of gravity. A summary of parameters describing the blading design is presented in Tables II through X. Figure 12 describes these parameters. The final vane and rotor hub, pitch, and tip airfoil flowpaths and velocity distributions are shown in Figures 13 through 48.

A computer program was employed to generate the coordinates of the sections intermediate to the hub, pitch, and tip. Sections were interpolated at 10%, 30%, 70%, and 90% of the trailing edge height for each vane and rotor. These coordinates were then used to generate the precision masters required for the fabrication of the vanes and rotors. Reduced copies of the vane and rotor precision masters are presented in Figures 48 through 57. Figures 58 through 66 show the stacked vane and rotor sections for each blade row.

D. Performance

The performance characteristics of the four-stage configuration was predicted with the aid of the "Analytical Procedure and Computer Program for Determining the Off-Design Performance of Axial Flow Turbines" (Reference 2). Pressure loss predictions were made for the outlet turning vane as discussed earlier in Section III-B-2.

Four and one half stage turbine predicted performance maps are presented in Figures 67 through 71 as follows:

Fig. 67 Equivalent torque vs. total-to-total pressure ratio

Fig. 68. Equivalent weight flow vs. total-to-total pressure ratio

Fig. 69. Equivalent specific work vs. total-to-total pressure ratio

Fig. 70. Total-to-total efficiency vs. blade-jet speed ratio

Fig. 71. Equivalent specific work vs. weight flow speed parameter with lines of constant total-to-total pressure ratio, constant speed, and efficiency contours.

V. Mechanical Design

A. Vibratory Behavior

In the analysis of a tip shrouded blade the fundamental question becomes one of chosing the appropriate shroud boundary conditions for both vibratory and steady-state operation. Conditions are generally chosen on the basis of such factors as blade length versus disc stiffness, shroud configuration, etc. Thus, several sets of conditions were chosen in an attempt to simulate various modes of behavior. From those conditions, the modes which seemed most likely to occur were extracted and are described below.

1. Cantilevered Mode - Cantilevered at the base of the shank, free at the tip shroud. This condition was used only to determine the amount of steady-state tip shroud twist or untwist and to obtain lower bounds on certain resonant frequencies.

2. Out of Phase Mode - Fixed at the base of the shank, pinned at the tip shroud. The flexure and torsion modes obtained for these conditions will probably exist under operating conditions.

3. Wheel Mode - Fixed at the base of the shank, restrained at the tip shroud in all directions except axially. Simulates blade behavior in a wheel mode. The flexure, axial, and torsion modes obtained for these conditions will exist under operating conditions.

4. Free Slip Mode - Fixed at the base of the shank, adjacent tip shrouds allowed to slip relative to each other. The axial and torsion modes obtained for these conditions may exist during turbine operation. Steady stresses obtained for this set of conditions are probably the most realistic.

Although the above four conditions appear to yield values covering a wide range of frequencies, the results are quite consistent and have been reduced to a set of "Most Probable Frequencies of Vibration" as shown on Campbell Diagrams in Figures 72 and 75 and tabulated below.

The following table summarizes the most probable modes of vibration of the various stages based upon 120% design speed (3153 rpm). Most of the modes will exhibit a change in frequency with speed due to the temperature effect and centrifugal stiffening. The results, however, will remain essentially the same.

Most Probable Frequencies of Vibration

Mode	Stage 1	Stage 2	Stage 3	Stage 4
First Flexure	--	3711 Hz	2342 Hz	1421 Hz
First Axial	2012 Hz	1347	749	664
First Torsional	--	3292	2504	2235
Second Flexure	--	--	2756	4078
Second Torsional	--	--	--	4487

Estimated vibratory capabilities are summarized in Table XI.

The vibratory behavior as summarized by stage is presented as follows:

- Stage One

There is no indication of resonance (1/rev, 2/rev, 3/rev, etc.) with any lower order vibratory mode within the operating range of 80% to 120% design speed of 3638 RPM. See Figure 72. The only probable mode is a first axial mode which is excited by nozzle passing frequency at about 80% of design speed. Due to the low excitation experienced in an air turbine at low RPM and the high vibratory allowable stresses predicted for this stage, this resonance should not present a problem. Furthermore, without a strong excitation, like a lower order resonance, an axial mode is hard to drive.

- Stage Two

As depicted on Figure 73, the stage two blade has two resonant frequencies excited by nozzle passing frequency between 100% and 120% design speed.

Usually this would be cause for concern. Past design experience shows that the level of vibratory stress would be low for this blade at nozzle passing frequency for the first flex and first torsion modes. Uncorrected gas bending stresses, an indicator of the level of separated flow vibratory response, is on the order of 6.5 KSI. Since there are no lower order resonances (1 to 10/rev), there is no indication of a serious vibratory stress problem for the stage two blade.

- Stage Three

As depicted on Figure 74, the stage three blade has three resonant frequencies that are excited by nozzle passing frequency between 80% and 100% design speed. The uncorrected gas bending stresses are on the order of 9.0 KSI which is low and the vibratory response should be low. No vibratory stress problem is anticipated with the stage three blade.

- Stage Four

The stage four blade has one resonant frequency near 120% design speed at nozzle passing frequency. As shown in Figure 75, second flex is a possible mode of vibration and due to blade to blade variations, second torsion might be activated by nozzle passing frequency. These are second order modes of vibrations and due to the low level of excitation in air turbine as compared to an actual engine, no strong response is anticipated. Furthermore, the uncorrected gas bending stresses are on the order of 9.8 KSI, which indicates a low level of separated flow vibratory response. The other three modes depicted on Figure 93 are activated by nozzle passing frequency low in the speed range and should experience no limiting vibratory stresses.

B. Steady State Behavior

Steady-state mechanical stresses were calculated for the Free Slip tip shroud boundary conditions. These conditions were felt to be the most realistic for steady-state operation. The stresses (centrifugal and gas bending) were found to be quite low for all four stages. The steady-state stress results are presented in Table XI. The mechanical analysis indicated that the shrouds on the first and second stages tended to unlock by a small amount (.005° and .03° respectively), and the third and fourth stages tends to lock up by a small amount (.06°). This analysis showed that the blades had very little twist or untwist in the centrifugal field. To insure that all the stages lock up, 0.5° of pretwist was designed into all the blading.

C. Key Detail Drawings

The mechanical design flowpath for the air turbine test rig is shown in Figure 76. Key detail drawings used for the assembly of the test rig are listed in Table XII.

REFERENCES

1. Lewis Research Center, NASA: "Aerodynamic Design of Axial Flow Compressors, Revised," NASA SP-36, 1965.

2. Flagg, E.E., "Analytical Procedure and Computer Program for Determining the Off-Design Performance of Axial Flow Turbines," NASA CR-710, March, 1966.

3. Smith, L.H., Sr.: "The Radial-Equilibrium Equation of Turbomachinery, "ASME Paper No. 65-WA/GTP-1, Journal of Engineering for Power, Trans. ASME, Series A, Vol 88, 1966.

4. Evans, D.C. and Wolfmeyer, G.W.: "Highly Loaded Multistage Fan Drive Turbine - Plain Blade Configuration Design," NASA CR-1964, February 1972.

LIST OF SYMBOLS

A	Area (in.^{2}, cm.^{2})
AW	Axial width (in., cm.)
C_f	Flow coefficient
D	Diameter (in., cm.)
d_o	Throat dimension (in., cm.)
d_i	Inlet throat dimension (in., cm.)
Δh	Turbine energy extraction (BTU/lbm, joules/kg.)
E	Turbine energy extraction (BTU/lbm, joules/kg.)
h_{ex}	Height at blade row exit (in., cm.)
h_{th}	Height at blade row throat (in., cm.)
M	Mach number
N	Rotational speed (rev/min.)
n	Number of vanes or rotors
P_s	Static pressure (psia, newtons/cm.^{2})
P_T	Total pressure (psia, newtons/cm.^{2})
T_{HLE}	Blade temperature at hub leading edge (°F)
T_s	Static temperature (°R)
T_T	Total temperature (°R)
t	Spacing (in., cm.)
t_e	Trailing edge thickness (in., cm.)
$t_{max.}$	Maximum thickness (in., cm.)
U	Wheel speed (ft/sec., m/sec.)
w	Mass flow rate (ft/sec, m/sec)
W	Relative Velocity (ft/sec, m/sec.)
$\bar{\omega}_z$	Loss rate coefficient
α_o	Vane inlet absolute flow angle (degrees)
α_1	Vane exit absolute flow angle (degrees)
β_1	Rotor inlet relative flow angle (degrees)
β_2	Rotor exit relative flow angle (degrees)
ϕ	Meridional angle; tan ϕ = Wr/Wz
Γ	Stage leaving swirl angle (degrees)

LIST OF SYMBOLS (Continued)

ξ	Rotor or vane lean angle (degrees)
μ	Angle of attack of outlet turning vane
i	Incidence angle of outlet turning vane (degrees)
γ_c	Chord angle of outlet turning vane (degrees)
δ	Deviation angle of outlet turning vane (degrees)
δ	Ratio of turbine pressure to pressure at standard sea level conditions
η_R	Rotor efficiency
η_{TT}	Total-to-total efficiency
η_v	Vane efficiency
ν	Blade-jet speed ratio
Γ	Circulation
σ	Stress (ksi, newtons/cm^2)
σ_c	Centrifugal stress (ksi, newtons/cm^2)
σ_{LE}	Stress at rotor leading edge (ksi, newtons/cm^2)
σ_{TE}	Stress at rotor trailing edge (ksi, newtons/cm^2)
σ_{Hi-c}	Stress at maximum distance from axis of least moment of inertia, convex surface (ksi, newtons/cm^2)
σ_{Midcv}	Stress at maximum distance from axis of least moment of inertia, concave surface (ksi, newtons/cm^2)
σ_{lmi}	Stress due to bending moment about axis of least moment of inertia (ksi, newtons/cm^2)
σ_{mmi}	Stress due to bending moment about axis of maximum moment of inertia (ksi, newtons/cm^2)
τ_{eq}	Equivalent torque (ft-lbf, m-newtons)
ψ_{zwei}	Zweifel number
$gJ\Delta h/2\Sigma u^2$	Loading factor
$E/\theta cr$	Equivalent specific work (BTU/lbm, joules/kg.)
$w\sqrt{\theta_{cr}}\ \varepsilon/\delta$	Equivalent weight flow (lbm/sec, kg/sec)
$N/\sqrt{\theta_{cr}}$	Equivalent rotative speed (rev/min)
$\frac{wN\varepsilon}{60\delta}$	Weight flow - speed parameter

LIST OF SYMBOLS (Concluded)

ε	Function of specific heat ratio
θ_{cr}	Squared ratio of critical velocity at turbine inlet temperature to critical velocity at standard sea level temperature
λ	Ratio of open circumference to total circumference

TABLE I. VELOCITY DIAGRAM CALCULATION RESULTS

OVERALL PERFORMANCE

Aerodynamic loading at mean radius	2.5
Inlet flow function; $w\sqrt{T_{T_0}}/P_{T_0}$	38.8
Total-to-total pressure ratio; P_{T_0}/P_{T_2} (psi)	2.70
Total-to-static pressure ratio; P_{T_0}/P_{S_3} (psi)	2.96
Total-to-total efficiency; η_{T_T}	84.05%
Weight flow-speed parameter; w Nε/608	908.6
Wheel speed; RPM	2628.1
Equivalent rotative speed; $N/\sqrt{\theta_{cr}}$	2173.5
Work extraction; Δh (Btu/Lbm)	37.85
Equivalent specific work; E/θ_{cr}	25.88

Table I (Continued)

STAGE 1

Blade	Station	Parameter	Hub	Pitch	Tip
Nozzle	Inlet	Dia (inches)	16.52	19.00	21.48
		T_T (° R)	760.0	760.0	760.0
		P_T (psi)	30.0	30.0	30.0
		T_S (° R)	746.7	746.7	746.7
		P_S (psi)	28.18	28.18	28.18
		M	0.300	0.300	0.300
		α (degrees)	0.0	0.0	0.0
	Exit	Dia (inches)	16.32	19.00	21.68
		T_S (° R)	672.2	690.3	702.0
		P_S (psi)	19.13	21.07	22.48
		M	0.815	0.716	0.647
		α (degrees)	63.80	60.4	57.5
Rotor	Inlet	Dia (inches)	16.27	19.00	21.73
		Relative T_T (°R)	734.3	735.3	736.5
		Relative P_T (psi)	26.16	26.35	26.54
		Relative M	0.684	0.571	0.492
		β (degrees)	57.7	51.3	44.1
	Exit	Dia (inches)	16.12	19.00	21.88
		Relative M	0.718	0.678	0.657
		β (degrees)	60.0	56.8	55.2
		Δh (Btu/Lbm)	10.91	10.90	10.88
		Reaction	0.091	0.209	0.303

Table I (Continued)

STAGE 2

Blade	Station	Parameter	Hub	Pitch	Tip
Nozzle	Inlet	Dia (inches)	16.04	19.00	21.96
		T_T (° R)	714.9	715.0	715.2
		P_T (psi)	23.15	23.25	23.33
		T_S (° R)	668.9	675.2	682.1
		P_S (psi)	18.47	19.16	19.91
		M	0.592	0.534	0.498
		α (degrees)	54.3	47.8	46.5
	Exit	Dia (inches)	15.75	19.00	22.25
		T_S (° R)	635.3	653.6	664.8
		P_S (psi)	14.91	16.61	17.73
		M	0.796	0.689	0.619
		α (degrees)	61.8	58.2	54.6
Rotor	Inlet	Dia (inches)	15.65	19.00	22.35
		Relative T_T (° R)	691.7	692.6	693.9
		Relative P_T (psi)	20.13	20.38	20.63
		Relative M	0.669	0.541	0.458
		β (degrees)	57.2	49.3	40.5
	Exit	Dia (inches)	15.45	19.00	22.55
		Relative M	0.706	0.663	0.645
		β (degrees)	60.0	56.1	54.6
		Δh (Btu/Lbm)	9.92	9.98	10.06
		Reaction	0.095	0.224	0.330

Table I (Continued)

STAGE 3

Blade	Station	Parameter	Hub	Pitch	Tip
Nozzle	Inlet	Dia (inches)	15.28	19.00	22.72
		T_T (° R)	674.0	673.7	673.4
		P_T (psi)	17.89	18.02	18.10
		T_S (° R)	631.9	638.8	645.1
		P_S (psi)	14.38	15.08	15.71
		M	0.582	0.512	0.474
		α (degrees)	54.2	46.1	41.8
	Exit	Dia (inches)	14.88	19.00	23.12
		T_S (° R)	594.3	617.0	628.4
		P_S (psi)	11.22	12.98	14.02
		M	0.821	0.680	0.597
		α	62.6	58.0	55.1
Rotor	Inlet	Dia (inches)	14.70	19.00	23.30
		Relative T_T (° R)	651.8	652.3	652.9
		Relative P_T (psi)	15.53	15.79	15.99
		Relative M	0.700	0.525	0.420
		β (degrees)	59.1	49.3	39.2
	Exit	Dia (inches)	14.40	19.00	23.60
		Relative M	0.760	0.689	0.664
		β (degrees)	62.8	57.4	58.2
		Δh (Btu/Lbm)	9.73	9.84	10.36
		Reaction	0.132	0.279	0.393

Table I (Continued)

STAGE 4

Blade	Station	Parameter	Hub	Pitch	Tip
Nozzle	Inlet	Dia (inches)	14.23	19.00	23.77
		T_T (° R)	633.7	632.9	631.0
		P_T (psi)	13.67	13.82	13.82
		T_S (° R)	586.4	597.3	604.3
		P_S (psi)	10.50	11.38	11.98
		M	0.639	0.534	0.474
		α (degrees)	57.4	47.4	41.8
	Exit	Dia (inches)	13.90	19.00	24.10
		T_S (° R)	577.1	594.6	601.7
		P_S (psi)	9.65	10.93	11.55
		M	0.702	0.569	0.494
		α (degrees)	61.6	53.1	48.2
Rotor	Inlet	Dia (inches)	13.90	19.00	24.10
		Relative T_T (° R)	616.6	617.2	617.0
		Relative P_T (psi)	12.18	12.46	12.62
		Relative M	0.587	0.437	0.357
		β (degrees)	55.2	39.3	22.1
	Exit	Dia (inches)	13.90	19.00	24.10
		Relative M	0.596	0.575	0.573
		β (degrees)	53.3	49.6	49.7
		Δh (Btu/Lbm)	6.91	7.03	7.24
		Reaction	0.051	0.300	0.435

Table I (Concluded)

OUTLET TURNING VANE

Station	Parameter	Hub	Pitch	Tip
Inlet	Dia (inches)	13.90	19.00	24.10
	T_T (° R)	605.1	603.0	601.1
	P_T (psi)	11.176	11.256	11.309
	T_S (° R)	575.9	577.6	579.4
	P_S (psi)	9.46	9.75	10.0
	M	0.494	0.458	0.423
	α (degrees)	44.3	35.5	29.3
Exit	Dia (inches)	13.90	19.00	24.10
	T_T (° R)	605.1	603.0	601.1
	P_T (psi)	10.913	11.110	11.112
	T_S (° R)	590.8	588.8	587.0
	P_S (psi)	10.041	10.222	10.224
	M	0.347	0.347	0.347
	α (degrees)	0.0	0.0	0.0

TABLE II. STAGE ONE VANE DESIGN DATA

PARAMETER	UNITS	HUB		PITCH		TIP	
	in. (cm)						
Dia. (T.E.)		16.32	(41.45)	19.00	(48.26)	21.68	(55.07)
α_1 (Degrees)		63.80		60.4		57.5	
ψ_{zwei}, Incompressible		.724		.812		.776	
AW		1.013	(2.57)	1.142	(2.90)	1.445	(3.67)
t		.916	(2.33)	1.066	(2.71)	1.216	(3.09)
n		56		56		56	
nd_o (C_f=.975, η_v=.97)		23.01	(58.24)	27.89	(70.56)	36.74	(93.52)
d_o = ndo/n		.411	(1.04)	.498	(1.26)	.656	(1.67)
t_e		.02	(.05)	.02	(.05)	.02	(.05)
$t_e/(t_e+d_o)$		.046		.039		.030	
chord		1.431	(3.63)	1.627	(4.13)	1.828	(4.64)
t_{max}, max thickness		.153	(.387)	.177	(.450)	.200	(.508)
Unguided Turning (Degrees)		7.5		8.5		9.2	
Overturning (Degrees)		1.6		1.8		2.2	
Wedge Angle (Degrees)		6.0		6.9		7.2	

Precision Master No. 4013164-009, 010

TABLE III. STAGE TWO VANE DESIGN DATA

PARAMETER	UNITS	HUB		PITCH		TIP	
	in. (cm)						
Dia. (T.E.)		15.80	(40.13)	19.00	(48.26)	22.26	(56.54)
α_1 (Degrees)		61.80		58.20		54.60	
ψ_{zwei}, Incompressible		.904		.872		.853	
AW		1.052	(2.67)	1.455	(3.70)	1.858	(4.72)
t		.689	(1.75)	.829	(2.11)	.971	(2.47)
n		72		72		72	
nd_o (C_f = .975, η_v = .96)		23.83	(60.55)	32.04	(81.36)	41.33	(105.12)
d_o = ndo/n		.331	(.841)	.445	(1.13)	.574	(1.46)
t_e		.02	(.05)	.02	(.05)	.02	(.05)
$t_e/(t_e+d_o)$		.057		.043		.033	
chord		1.100	(2.79)	1.516	(3.85)	1.930	(4.90)
t_{max}, max thickness		.120	(.305)	.139	(.353)	.158	(.401)
Unguided Turning (Degrees)		12.1		11.5		8.6	
Overturning (Degrees)		2.2		2.7		1.8	
Wedge Angle (Degrees)		4.6		4.8		4.8	

Precision Master No. 4013164-011, 012

TABLE IV. STAGE THREE VANE DESIGN DATA

PARAMETER	UNITS	HUB		PITCH		TIP	
	in. (cm)						
Dia. (T.E.)		14.90	(37.85)	19.00	(48.26)	23.24	(59.03)
α_1 (Degrees)		62.60		58.00		55.10	
ψ_{zwei}, Incompressible		.874		.863		.861	
AW		1.052	(2.67)	1.566	(3.98)	2.080	(5.28)
t		.709	(1.80)	.904	(2.30)	1.106	(2.81)
n		66		66		66	
nd_o (C_f = .975, η_v = .96)		21.91	(55.64)	32.21	(81.84)	42.64	(108.24)
d_o = ndo/n		.332	(.843)	.488	(1.24)	.646	(1.64)
t_e		.02	(.05)	.02	(.05)	.02	(.05)
$t_e/(t_e + d_o)$		.057		.039		.0300	
chord,		1.125	(2.86)	1.634	(4.15)	2.151	(5.46)
t_{max}, max thickness		.120	(.305)	.143	(.363)	.165	(.419)
Unguided Turning (Degrees)		10.6		9.2		8.5	
Overturning (Degrees)		1.6		2.2		1.8	
Wedge Angle (Degrees)		5.0		5.2		4.1	

Precision Master No. 4013164-013, 014

TABLE V. STAGE FOUR VANE DESIGN DATA

PARAMETER	UNITS	HUB		PITCH		TIP	
	in. (cm)						
Dia. (T.E.)		13.90	(35.31)	19.00	(48.26)	24.10	(61.21)
α_1 (Degrees)		61.60		53.10		48.20	
ψ_{zwei}, Incompressible		.750		.836		.862	
AW		1.102	(2.80)	1.563	(3.97)	2.022	(5.13)
t		.546	(1.39)	.746	(1.89)	.946	(2.40)
n		80		80		80	
nd_o (C_f = .975, η_v = .96)		6.96	(53.20)	36.16	(92)	50.72	(128.80)
d_o = ndo/n		.262	(.665)	.452	(1.15)	.634	(1.61)
t_e		.02	(.05)	.02	(.05)	.02	(.05)
$t_e/(t_e + d_o)$		.071		.042		.031	
chord		1.110	(2.82)	1.570	(3.99)	2.025	(5.14)
t_{max}, max thickness		.140	(.356)	.150	(.381)	.161	(.409)
Unguided Turning (Degrees)		8.5		8.6		8.6	
Overturning (Degrees)		1.0		1.0		2.3	
Wedge Angle (Degrees)		7.4		5.5		5.1	

Precision Master No. 4013164-015, 016

TABLE VI. OUTLET TURNING VANE DESIGN DATA

PARAMETER	UNITS	HUB		PITCH		TIP	
	in. (cm)						
Dia. (T.E.)		13.90	(35.31)	19.00	(48.26)	24.10	(61.21)
AW		1.507	(3.83)	1.508	(3.83)	1.509	(3.83)
t		.662	(1.68)	.904	(2.30)	1.147	(2.91)
n		66		66		66	
d_i		.412	(1.05)	.712	(1.81)	.974	(2.47)
t_e		.02	(.05)	.02	(.05)	.02	(.05)
chord		1.596	(4.05)	1.554	(3.95)	1.530	(3.88)
t_{max}, max thickness		.100	(.254)	.100	(.254)	.100	(.254)
β_1 (Degrees)		-44.3		-35.5		-29.3	
ξ (Degrees)		25.0		21.6		19.0	
i (Degrees)		0.0		1.0		2.0	
γ_c (Degrees)		-19.6		-14.2		-9.8	
β_2 (Degrees)		1.9		2.6		3.7	
δ (Degrees)		-3.1		-3.9		-4.3	

TABLE VII. STAGE ONE ROTOR DESIGN DATA

PARAMETER	UNITS	HUB		PITCH		TIP	
	in. (cm)						
Dia. (T.E.)		16.16	(41.05)	19.00	(48.26)	21.90	(55.63)
β_1 (Degrees)		57.7		51.3		44.1	
β_2 (Degrees)		60.0		56.8		55.2	
$\Delta\beta$ (Degrees)		117.7		108.1		99.3	
ψ_{zwei}, Incompressible		.979		.984		.959	
AW		.952	(2.42)	1.061	(2.69)	1.170	(2.97)
t		.540	(1.37)	.635	(1.61)	.732	(1.86)
n		94		94		94	
nd_o (C_f = .97, η_R = .95)		25.66	(65.14)	33.09	(84.04)	39.57	(100.58)
d_o = ndo/n		.273	(.693)	.352	(.894)	.421	(1.07)
t_e		.020	(.05)	.020	(.05)	.020	(.05)
$t_e/(t_e + d_o)$		.068		.054		.045	
Chord		.946	(2.40)	1.067	(2.71)	1.202	(3.05)
t_{max}, max thickness		.122	(.310)	.113	(.287)	.105	(.267)
Unguided Turning (Degrees)		13.2		13.6		14.5	
Overturning (Degrees)		2.0		2.4		4.1	
Wedge Angle (Degrees)		5.5°		4.5		4.3	
Precision Master No.		4013164-001, 002					

TABLE VIII. STAGE TWO ROTOR DESIGN DATA

PARAMETER	UNITS	HUB		PITCH		TIP	
	in.(cm)						
Dia. (T.E.)		15.47	(39.29)	19.00	(48.26)	22.55	(57.28)
β_1 (Degrees)		57.2		49.3		40.5	
β_2 (Degrees)		60.0		56.1		54.6	
$\Delta\beta$ (Degrees)		117.2		105.4		95.1	
ψ_{zwei}, Incompressible		.963		.986		.955	
AW		.952	(2.42)	1.071	(2.72)	1.190	(3.02)
t		.528	(1.34)	.649	(1.65)	.770	(1.95)
n		92		92		92	
nd_o (C_f = .97, η_R = .95)		24.56	(62.38)	33.76	(85.74)	41.67	(105.80)
$d_o = nd_o/n$		.267	(.678)	.367	(.932)	.453	(1.15)
t_e		.020	(.05)	.020	(.05)	.020	(.05)
$t_e/(t_e + d_o)$		.069		.052		.042	
Chord		.950	(2.41)	1.084	(2.75)	1.231	(3.12)
t_{max}, max thickness		.130	(.330)	.115	(.292)	.100	(.254)
Unguided Turning (Degrees)		12.5		12.5		12.5	
Overturning (Degrees)		1.3		3.6		5.0	
Wedge Angle (Degrees)		7.5		6.0		5.0	
Precision Master No.		4013164-003, 004					

TABLE IX. STAGE THREE ROTOR DESIGN DATA

PARAMETER	UNITS	HUB		PITCH		TIP	
	in. (cm)						
Dia. (T.E.)		14.35	(36.45)	19.00	(48.26)	23.73	(60.27)
β_1 (Degrees)		59.1		49.3		39.2	
β_2 (Degrees)		62.8		57.4		58.2	
$\Delta\beta$ (Degrees)		121.9		106.7		97.4	
ψ_{zwei}, Incompressible		1.013		1.034		.969	
AW		.952	(2.42)	1.155	(2.93)	1.358	(3.45)
t		.578	(1.47)	.765	(1.94)	.956	(2.43)
n		78		78		78	
nd_o (C_f = .97, η_R = .95)		20.83	(52.88)	32.53	(82.68)	39.94	(101.40)
$d_o = nd_o/n$		.267	(.678)	.417	(1.06)	.512	(1.30)
t_e		.020	(.05)	.020	(.05)	.020	(.05)
$t_e/(t_e + d_o)$		.070		.046		.038	
Chord		.958	(2.43)	1.199	(3.04)	1.469	(3.73)
t_{max}, max thickness		.130	(.330)	.122	(.310)	.114	(.290)
Unguided Turning (Degrees)		10.8		10.1		10.9	
Overturning (Degrees)		1.9		2.6		3.7	
Wedge Angle (Degrees)		5.5		5.9		4.0	
Precision Master No.		4013164-005, 006					

TABLE X. STAGE FOUR ROTOR DESIGN DATA

PARAMETER	UNITS	HUB		PITCH		TIP	
	in. (cm)						
Dia. (T.E.)		13.90	(35.31)	19.00	(48.26)	24.10	(61.21)
β_1 (Degrees)		55.2		39.3		22.10	
β_2 (Degrees)		53.3		49.6		49.70	
$\Delta\beta$ (Degrees)		108.50		88.9		71.70	
ψ_{zwei}, Incompressible		.979		.992		.906	
AW		.954	(2.42)	1.057	(2.68)	1.161	(2.95)
t		.464	(1.18)	.635	(1.61)	.805	(2.04)
n		94		94		94	
nd_o (C_f = .97, η_R = .95)		26.32	(66.83)	39.01	(98.70)	49.26	(125.02)
$d_o = nd_o/n$		.280	(.711)	.415	(1.05)	.524	(1.33)
t_e		.020	(.05)	.020	(.05)	.020	(.05)
$t_e/(t_e + d_o)$		.067		.046		.037	
Chord		.946	(2.40)	1.080	(2.74)	1.242	(3.15)
t_{max}, max thickness		.110	(.279)	.105	(.267)	.100	(.254)
Unguided Turning (Degrees)		11.1		9.6		10.3	
Overturning (Degrees)		1.7		1.9		3.6	
Wedge Angle (Degrees)		6.5		6.0		5.3	
Precision Master No.		4013164-007, 008					

TABLE XI. STEADY-STATE MECHANICAL STRESSES AND ESTIMATED VIBRATORY CAPABILITIES

Mechanical Stresses ksi (N/cm^2)		Stage 1	Stage 2	Stage 3	Stage 4
Airfoil Hub					
σ centrifugal		3.3 (2.28)	4.06 (2.80)	6.58 (4.54)	5.8 (4.0)
σ resultant span wise stress (free slip mode)	LE	9.54 (6.58)	11.06 (7.63)	19.91 (13.73)	14.16 (9.76)
	TE	9.91 (6.83)	10.77 (7.43)	16.17 (11.15)	15.93 (10.98)
	Hi-c	-.52 (-.36)	-.12 (-.08)	-.47 (-.32)	.37 (.26)
	Midcv	2.11 (1.45)	3.02 (2.08)	4.49 (3.10)	4.4 (3.03)
σ uncorrected gas bending (1 m i and m m i, free slip mode)	LE	5.2 (3.59)	6.4 (4.41)	9.0 (6.20)	9.8 (6.76)
	TE	5.4 (3.72)	6.2 (4.27)	8.2 (5.65)	10.2 (7.03)
	Hi-c	-3.1 (-2.14)	-3.8 (-2.62)	-5.2 (-3.59)	-5.9 (-4.07)
	Midcv	-.9 (-.62)	-.9 (-.62)	-1.50 (-1.03)	-1.5 (-1.03)
Under Tip Shroud					
σ centrifugal		1.21 (.83)	1.71 (1.18)	2.35 (1.62)	1.7 (1.17)
σ resultant span wise stress (free slip mode)	LE	2.69 (1.85)	3.16 (2.18)	12.38 (8.54)	-.04 (-.03)
	TE	2.75 (1.90)	3.2 (2.21)	10.92 (7.53)	1.1 (.76)
	Hi-c	.36 (.25)	.89 (.61)	-2.73 (-1.88)	2.47 (1.70)
	Midcv	.89 (.61)	1.39 (.46)	.47 (.32)	1.79 (1.23)
Estimated Vibratory Capabilities					
$\sigma_{mean} = \sigma_c + \sigma_{lmi} + \sigma_{mmi}$ ksi (n/cm^2) at Hub LE ($\sigma_{thermal\ neglected}$)		9.51 (6.56)	11.04 (7.61)	19.87 (13.70)	14.11 (9.73)
Estimated T_{HLE} (°F)		276 (190)	233 (161)	192 (132)	156 (108)
Estimated Minimum Margin Vibratory Allowable Stress (Based on APSI 410 Stainless Steel average strength less three standard deviations)		34.0 (23)	35.0 (24)	34.0 (23)	36.0 (25)

TABLE XII. KEY DETAIL DRAWING SUMMARY

Drawing No.	Title
4013098-552	Ring, Back-up - Stage 1 and OGV.
-553	Ring, Back-up - Stages 2, 3, and 4
-608	Shroud, Inner - Stages 2, 3, and 4
-609	Retainer, Blades - 1, 2, and 4
-610	Shroud, Outer - Stages 2 and 4
-611	Shroud, Outer - Stage 1
-612	Shroud, Outer - Stage 3
-615	Housing - Stage 2
-616	Housing - Stages 3 and 4
-617	Blade - Stage 1
-618	Blade - Stage 2
-619	Blade - Stage 3
-620	Blade - Stage 4
-621	Vane - Stage 1
-622	Vane - Stage 2
-623	Vane - Stage 3
-624	Vane - Stage 4
-625	Outlet Guide Vane
-626	Disc, Rotor - Stage 1
-627	Disc, Rotor - Stage 3 and 4
-628	Rotor Assembly
-629	Instrumentation Drawing
-630	Final Assembly
-945	Dowel Pin
-946	Ring, Torque - Stage 1
-947	Ring, Torque - Stage 3
-948	Ring, Torque - Stage 4
-949	Shaft, Main
-950	Spacer, Shaft
-951	Casing, Inner Inlet
-952	Housing, Assembly - Stage 1
-953	Housing - Stage 1

TABLE XII. KEY DETAIL DRAWING SUMMARY (Continued)

Drawing No.	Title
4013098-954	Ring, Seal - Stage 1 and OGV
-955	Housing, Assembly - Stage 2
-957	Housing, Assembly - Stages 3 and 4
-958	Bolt, Modified
-961	Ring, Half Vane
-962	Housing, Assembly O.G.V.
-963	Housing, O.G.V.
-965	Housing, Rear Instrumentation
-966	Housing, Inner Instrumentation
-967	Adapter, Bearing Housing
-975	Ring, Stage 2 Disc
-976	Housing, Rear Instrumentation
-977	Housing, Rear Instrumentation

Precision Master No.	Title
4013164-001	Blade 1
-002	Blade 1
-003	Blade 2
-004	Blade 2
-005	Blade 3
-006	Blade 3
-007	Blade 4
-008	Blade 4
-009	Vane 1
-010	Vane 1
-011	Vane 2
-012	Vane 2
-013	Vane 3
-014	Vane 3
-015	Vane 4

TABLE XII. KEY DETAIL DRAWING SUMMARY (Concluded)

Precision Master No.	Title
4013164-016	Vane 4
-017	Outlet Guide Vane
-018	Outlet Guide Vane

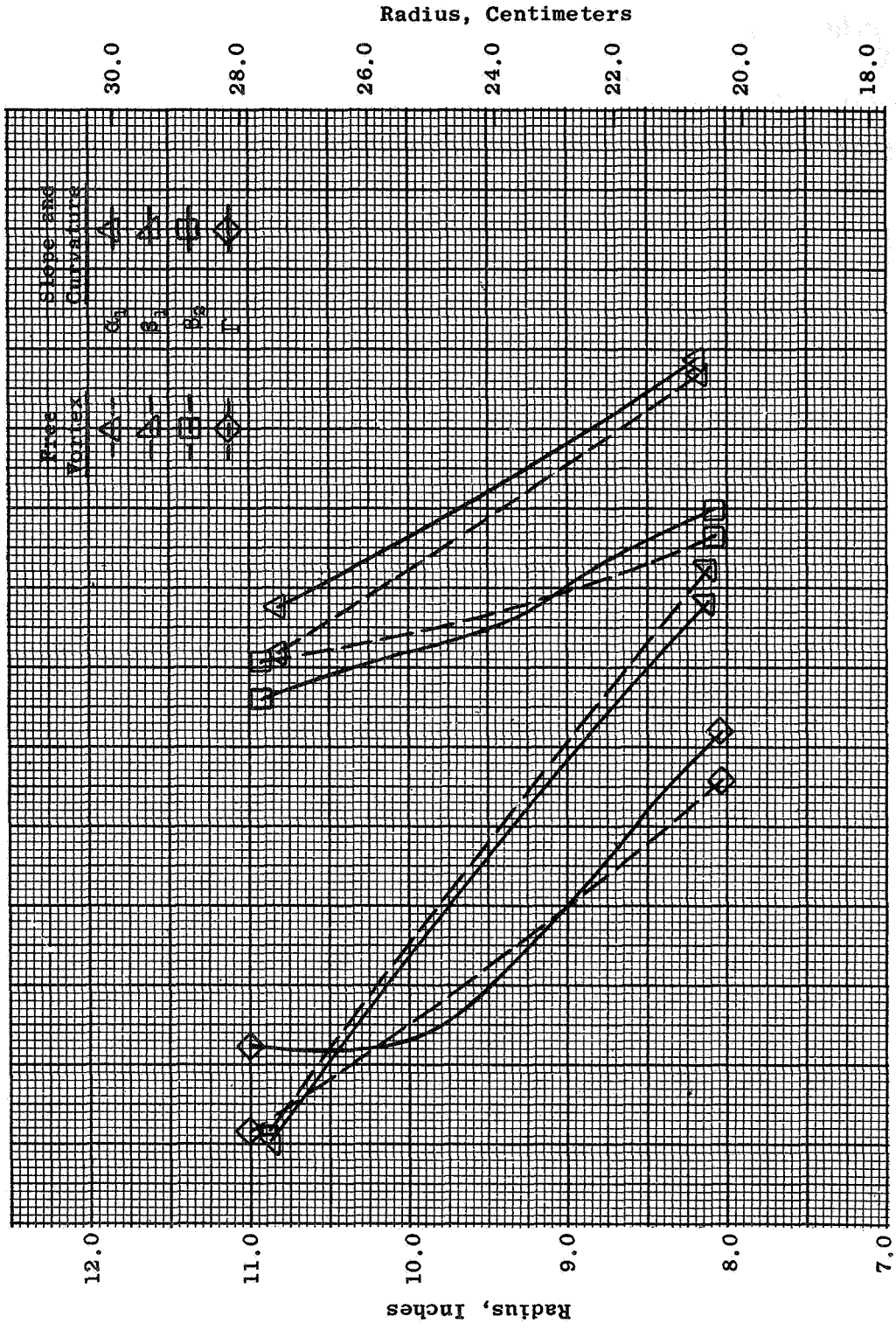

Figure 1. Effect of Flowpath Slope and Curvature on Angles, Stage One.

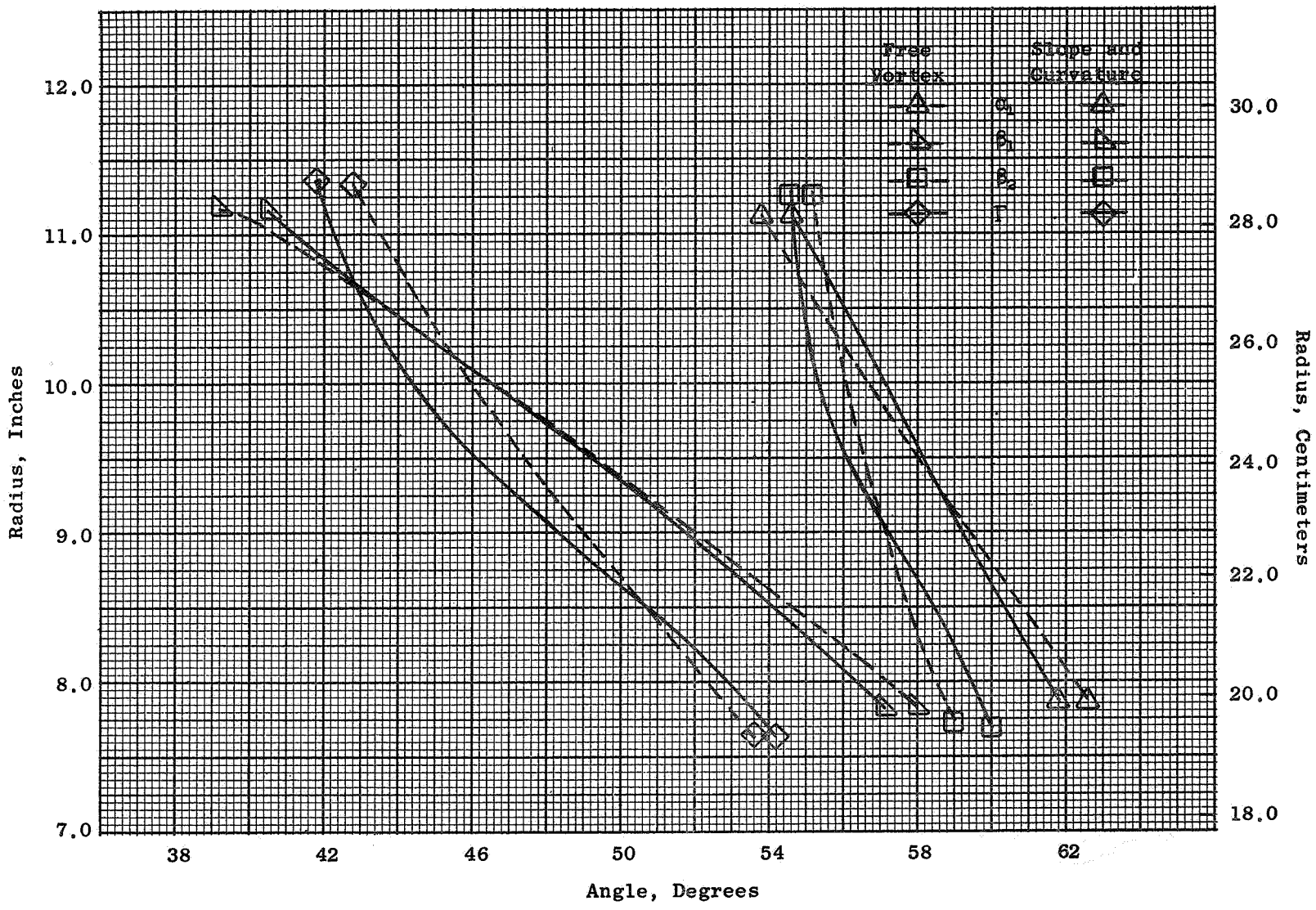

Figure 2. Effect of Flowpath Slope and Curvature on Angles, Stage Two.

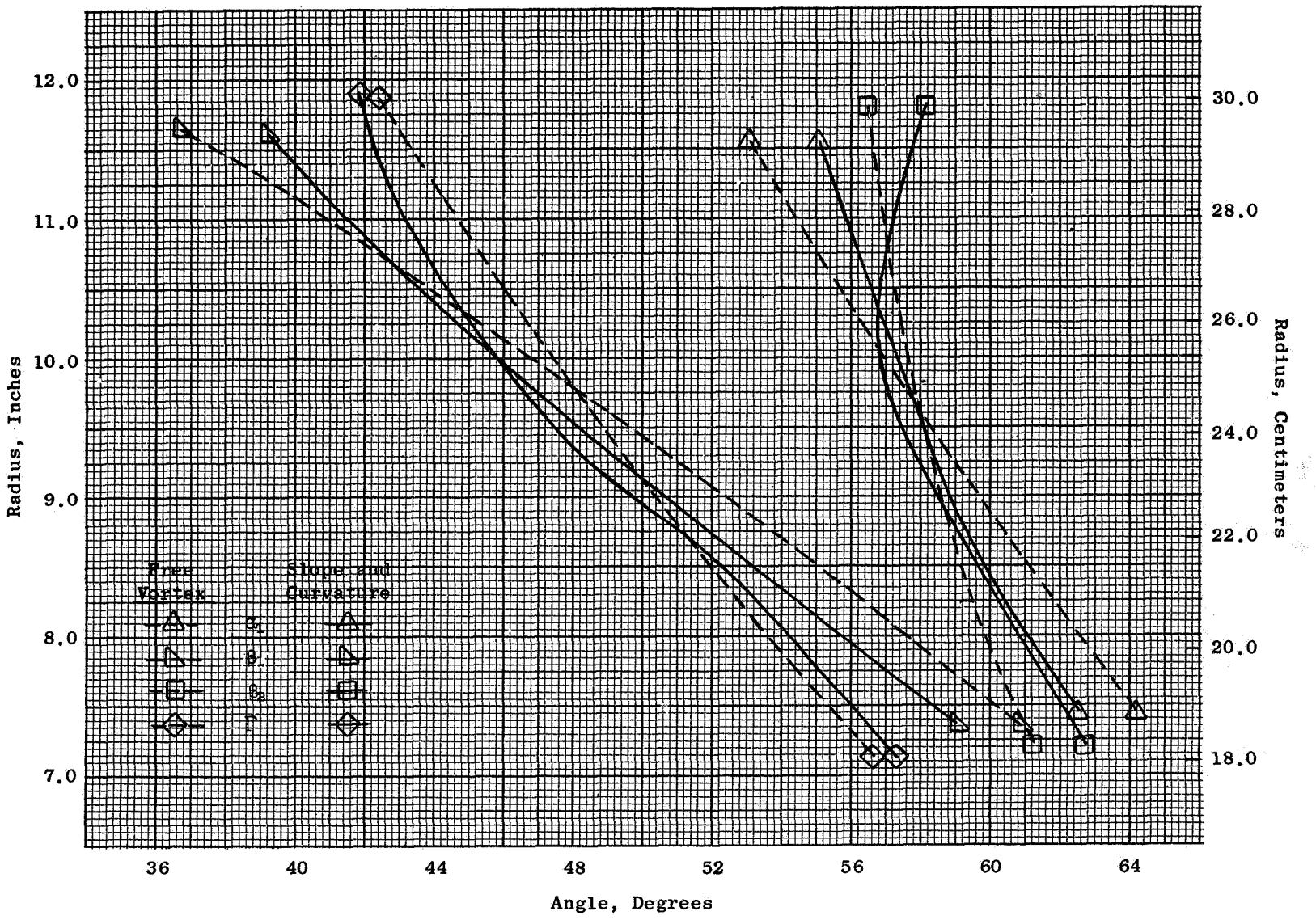

Figure 3. Effect of Flowpath Slope and Curvature on Angles, Stage Three.

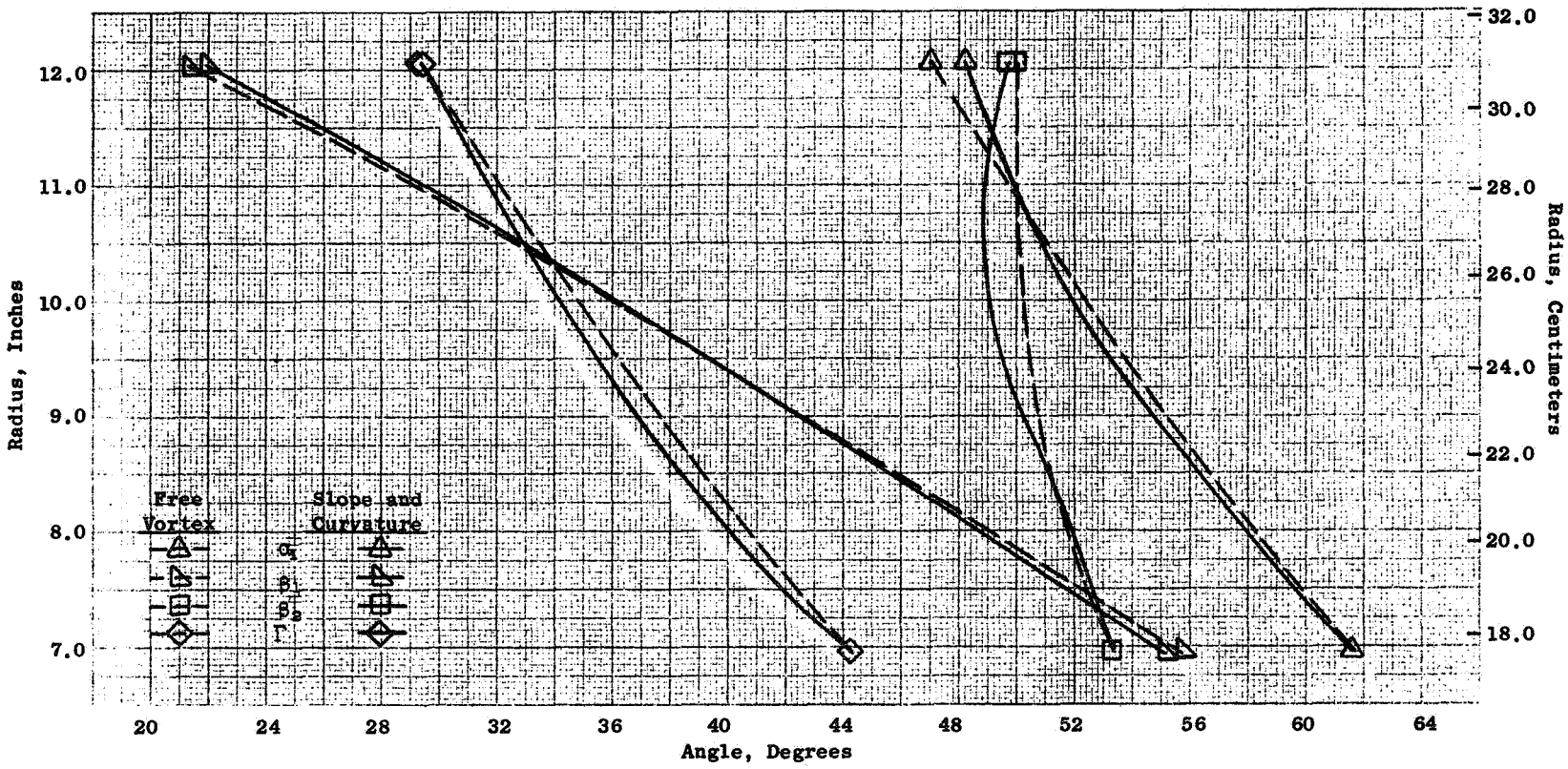

Figure 4. Effect of Flowpath Slope and Curvature on Angles, Stage Four.

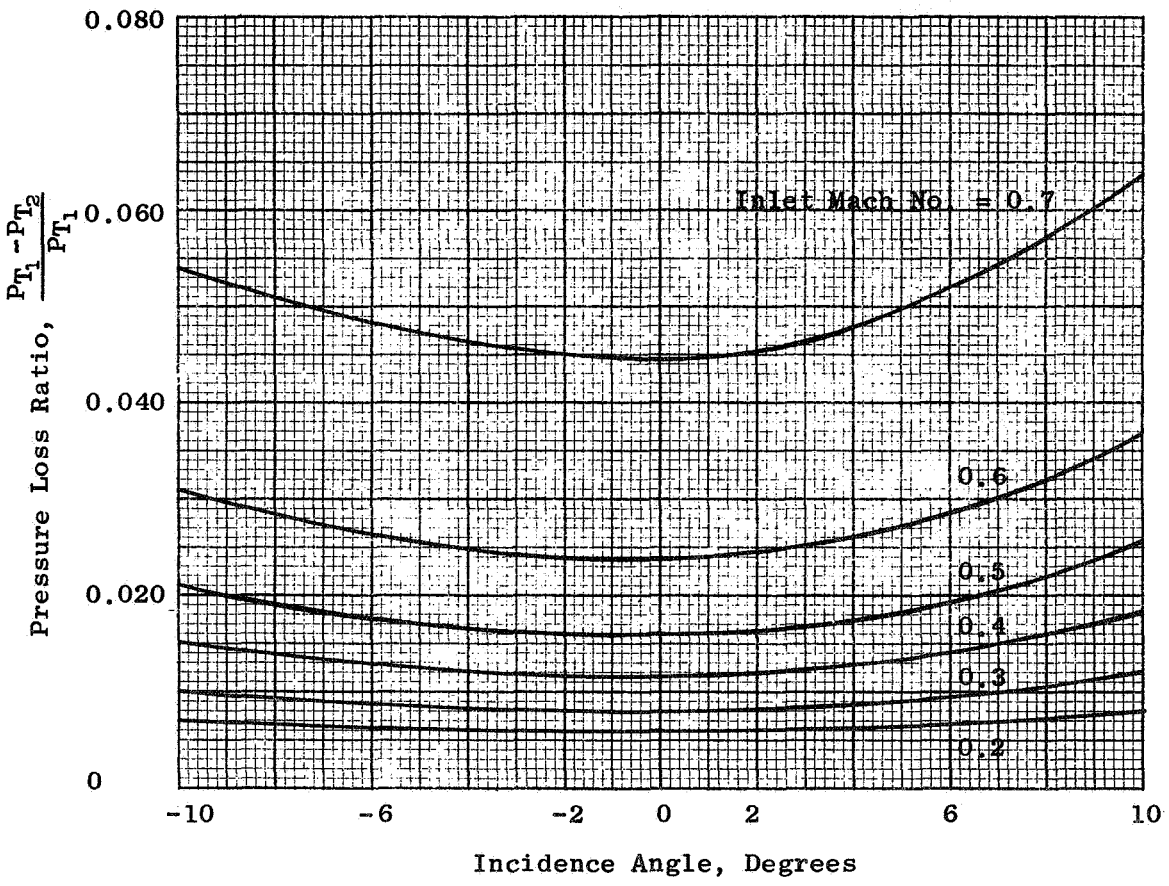

Figure 5. Pressure Loss Across Outlet Turning Vane Vs. Incidence Angle.

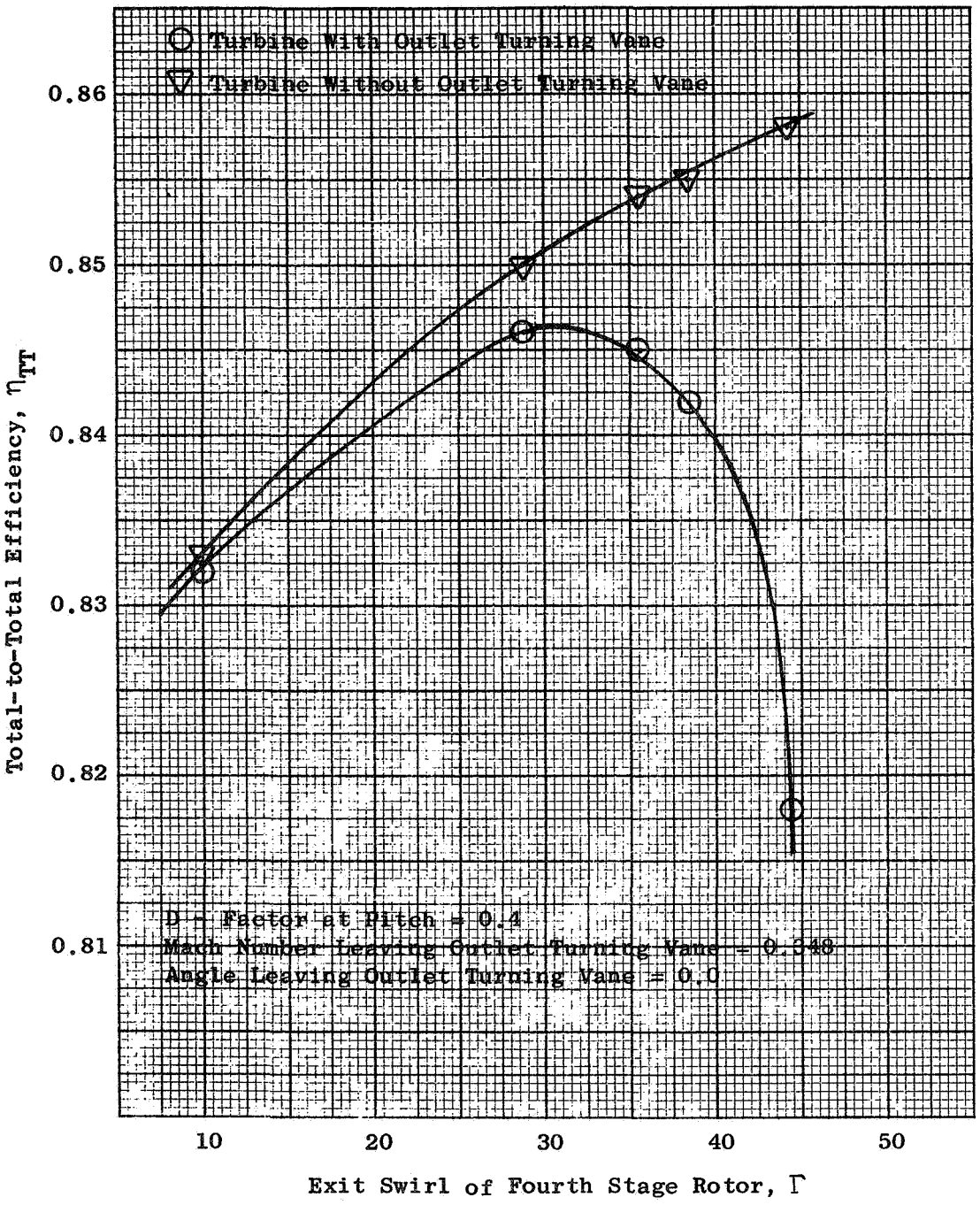

Figure 6. Total-to-Total Efficiency Vs. Fourth Stage Rotor Exit Swirl.

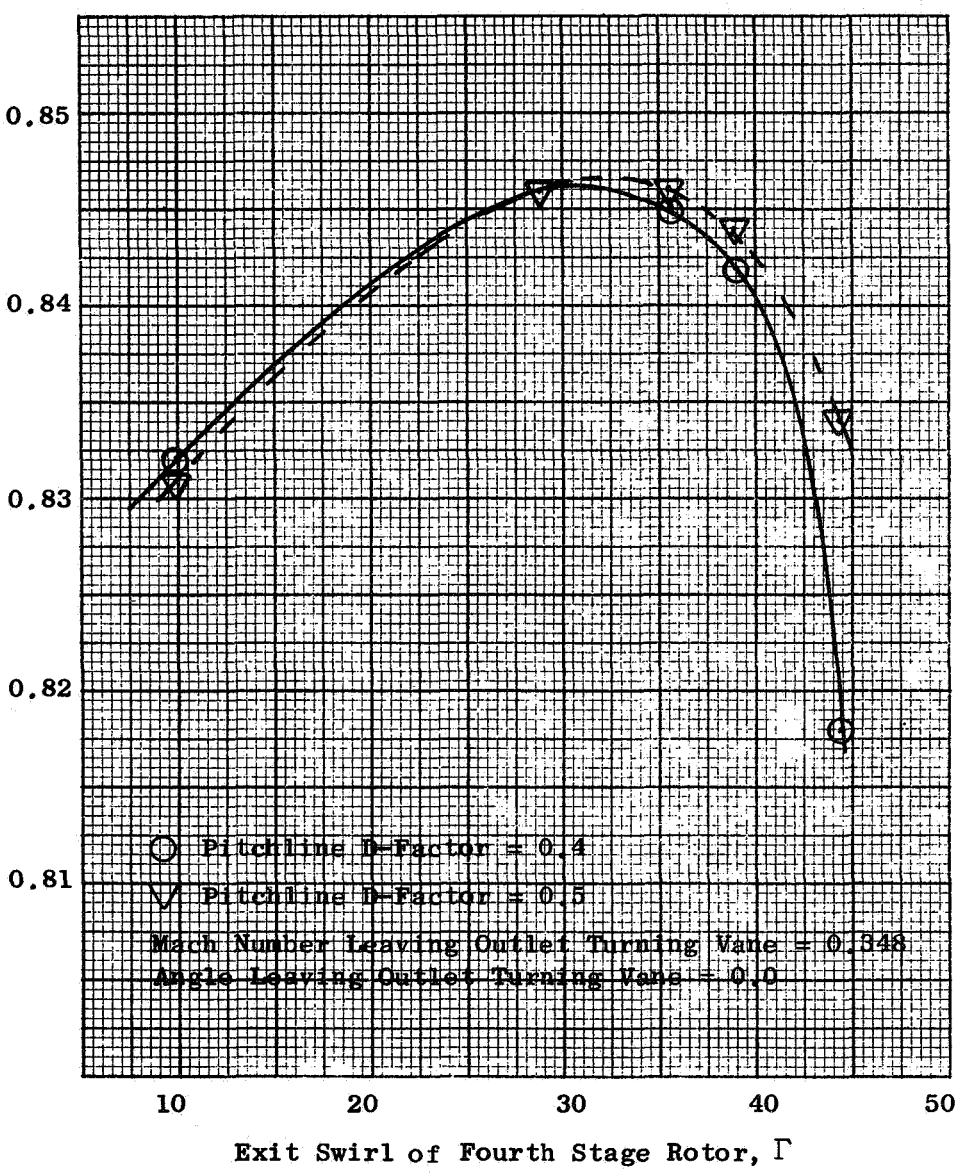

Figure 7. Total-to-Total Efficiency of Turbine and Outlet Turning Vane Vs. Fourth Stage Rotor Exit Swirl.

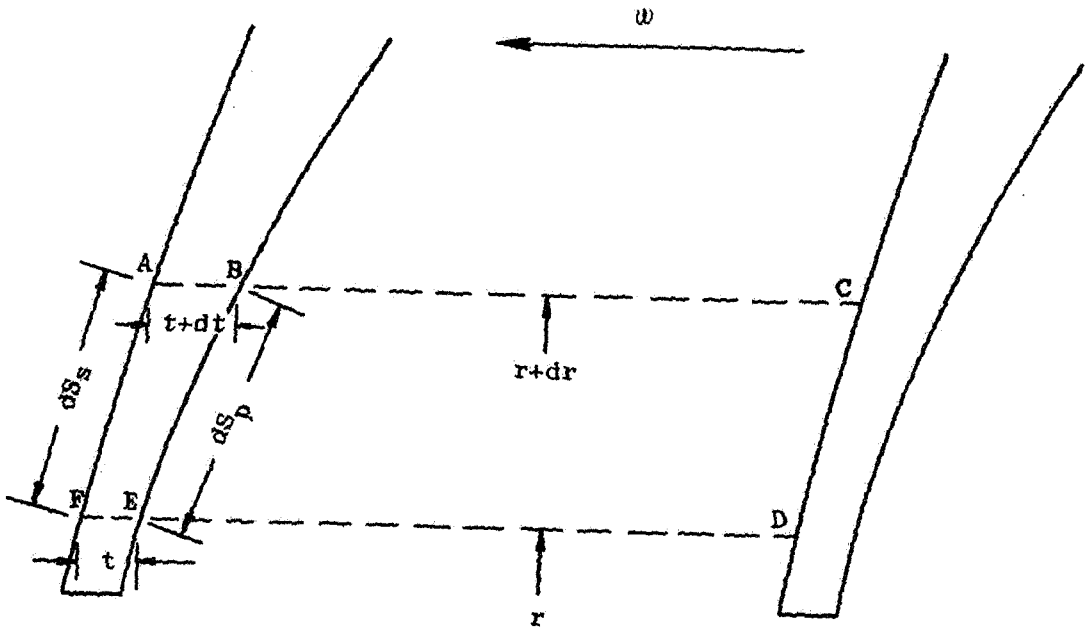

ω = Blade rotational speed, rpm
r = Radial distance from engine center line

Figure 8. Blade Circulation Schematic.

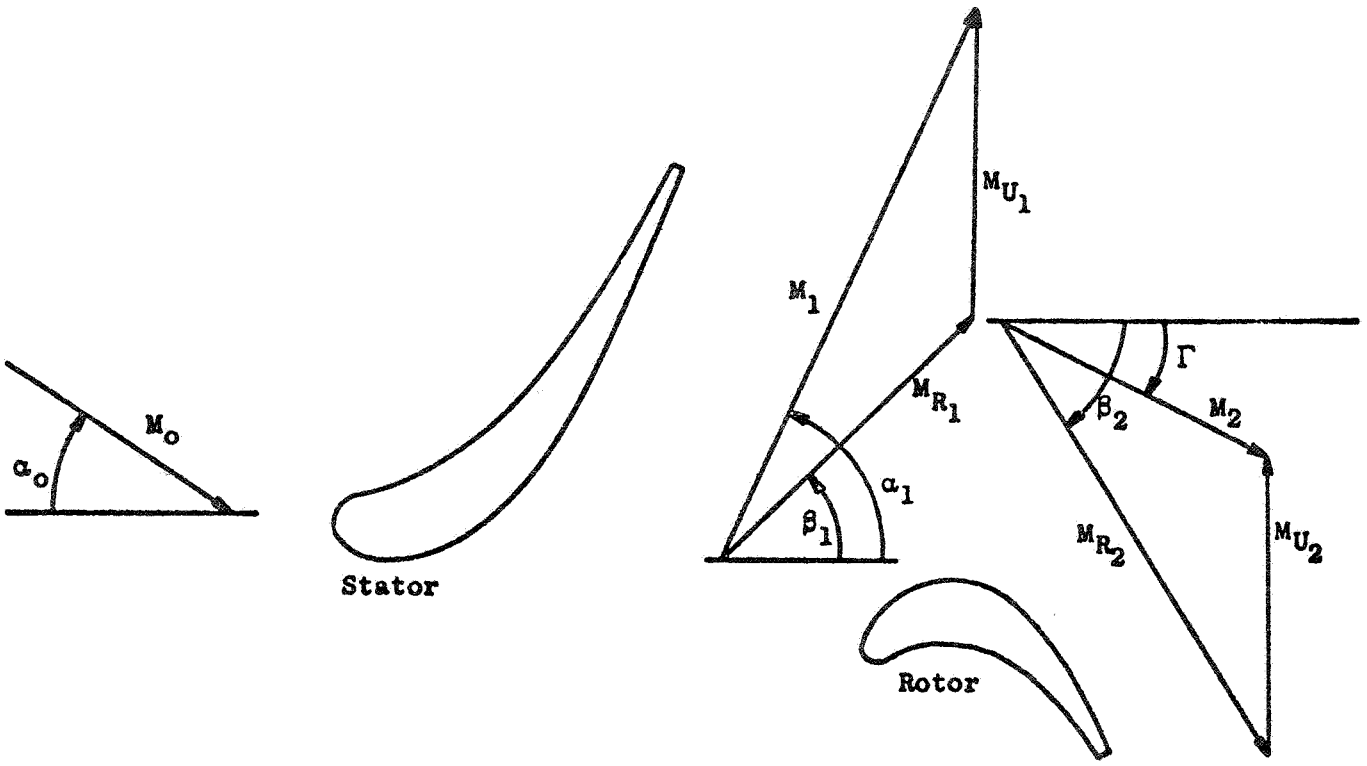

Figure 9. Velocity Diagram Nomenclature.

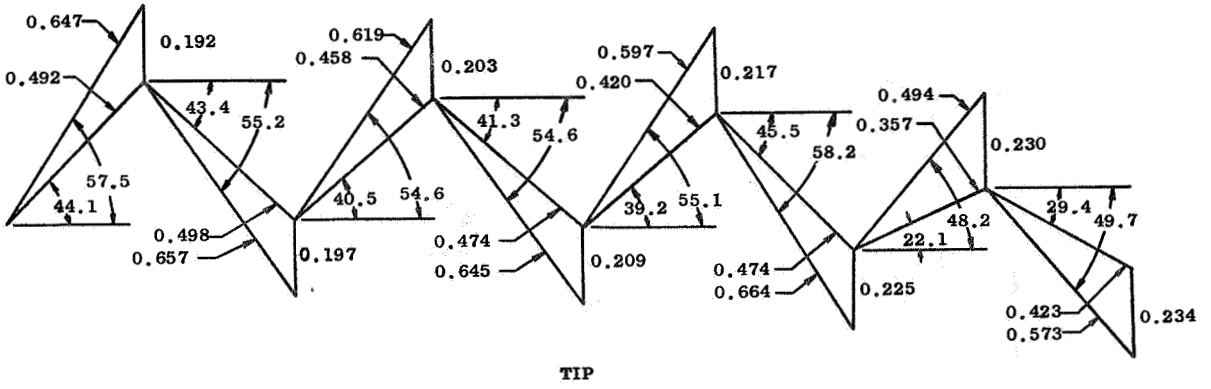

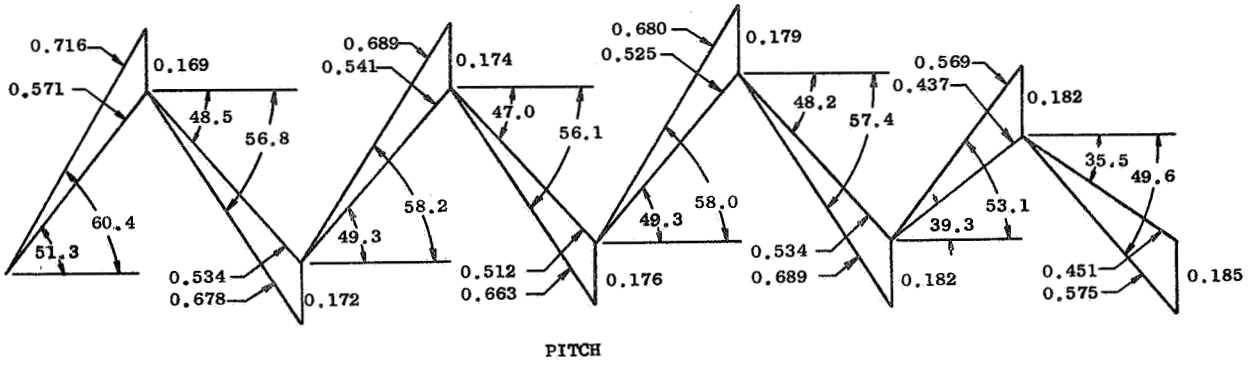

Numbers Shown on Velocity Diagrams are Angles in Degrees and Mach Numbers

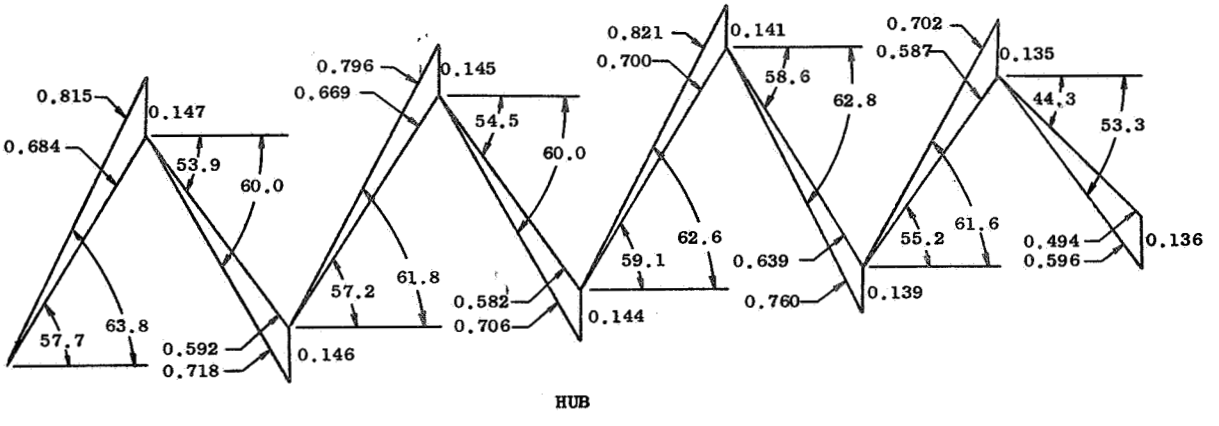

Figure 10. Velocity Diagrams.

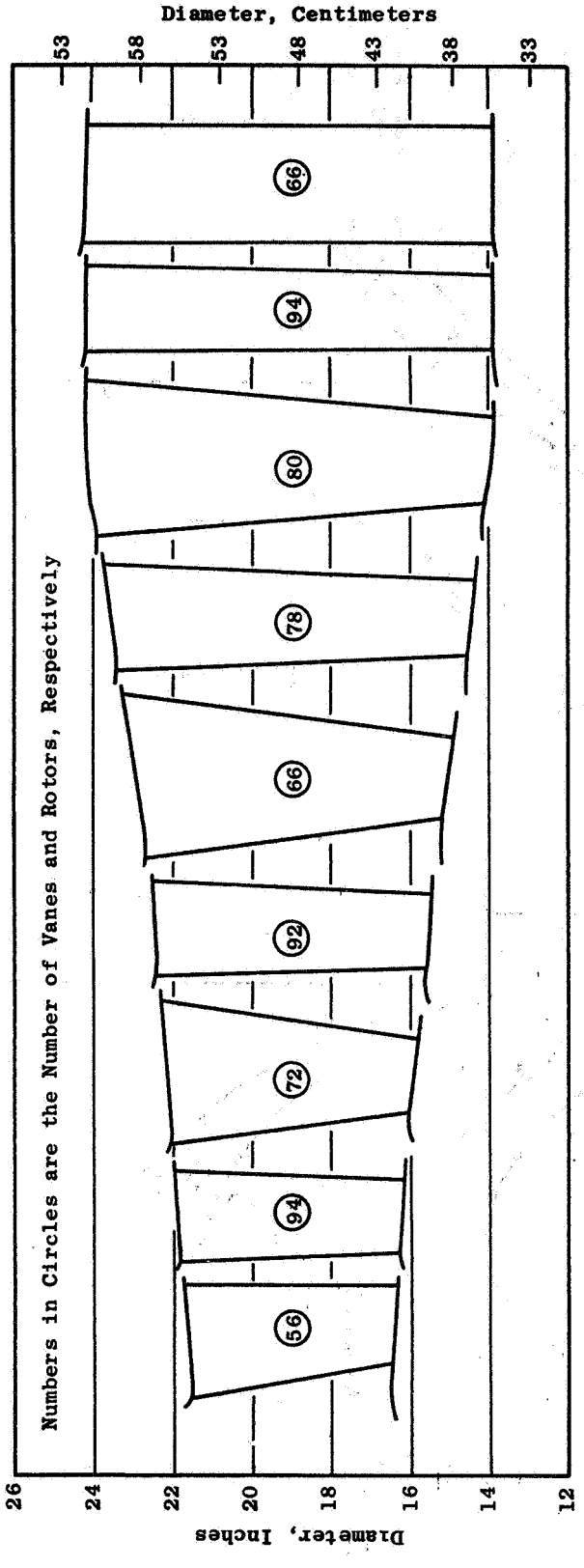

Figure 11. Aerodynamic Flowpath.

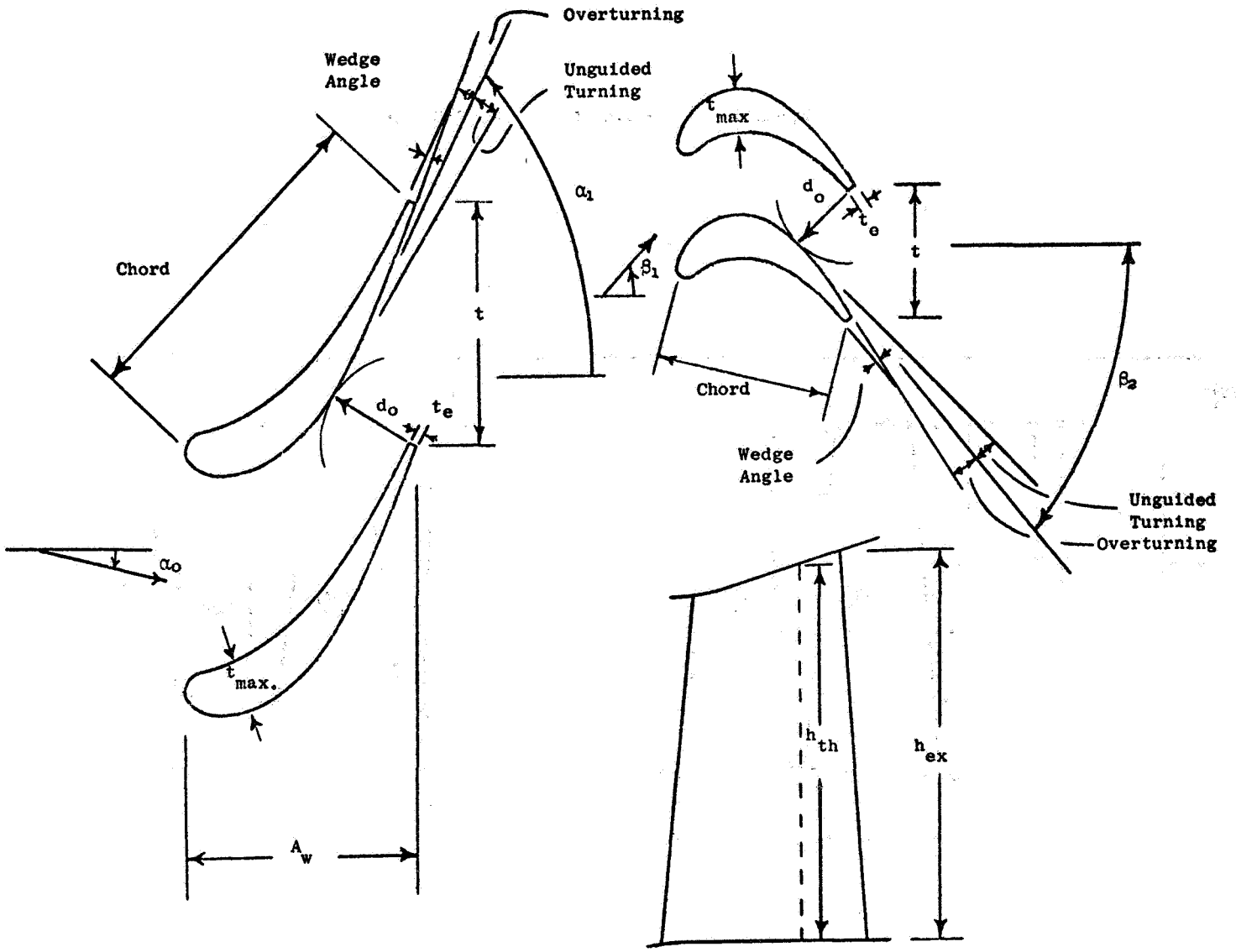

Figure 12. Design Data Nomenclature.

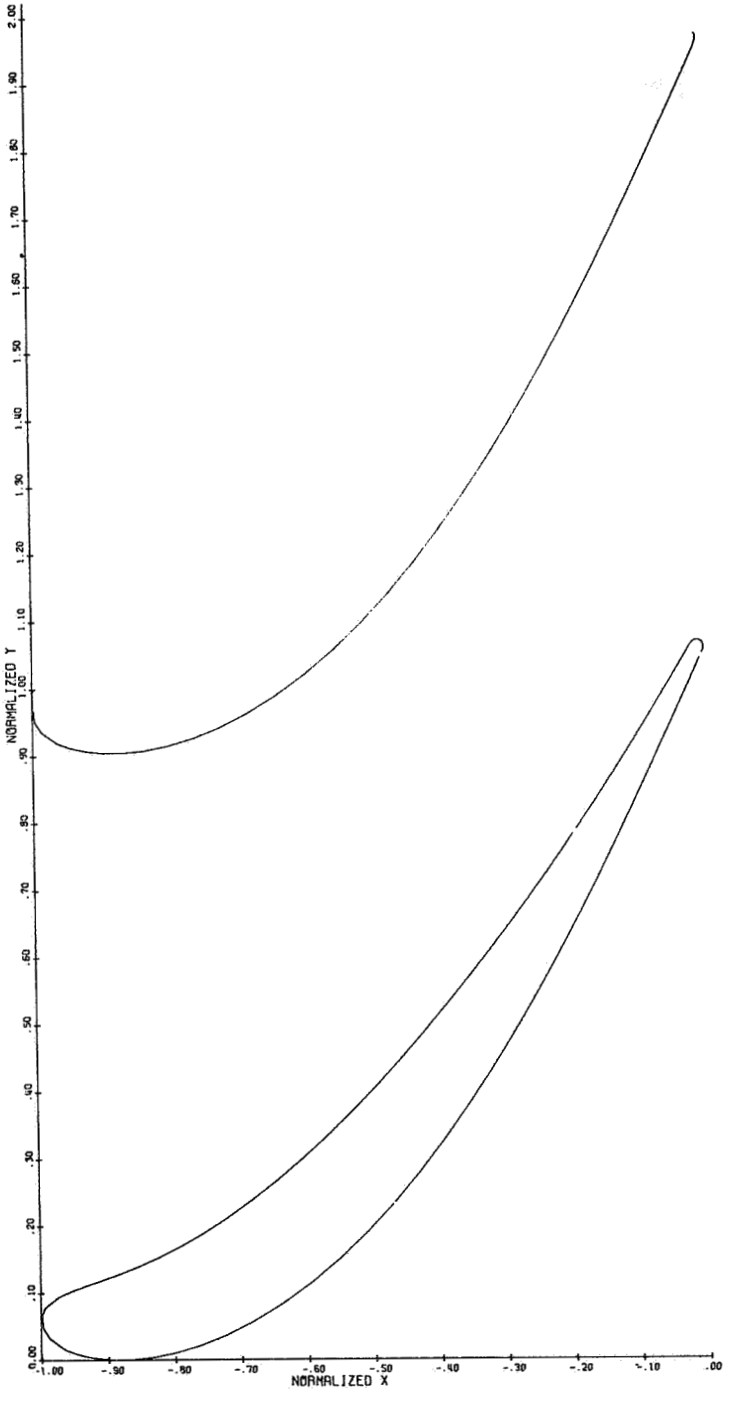

Figure 13. Stage One Vane Hub Airfoil Flowpath.

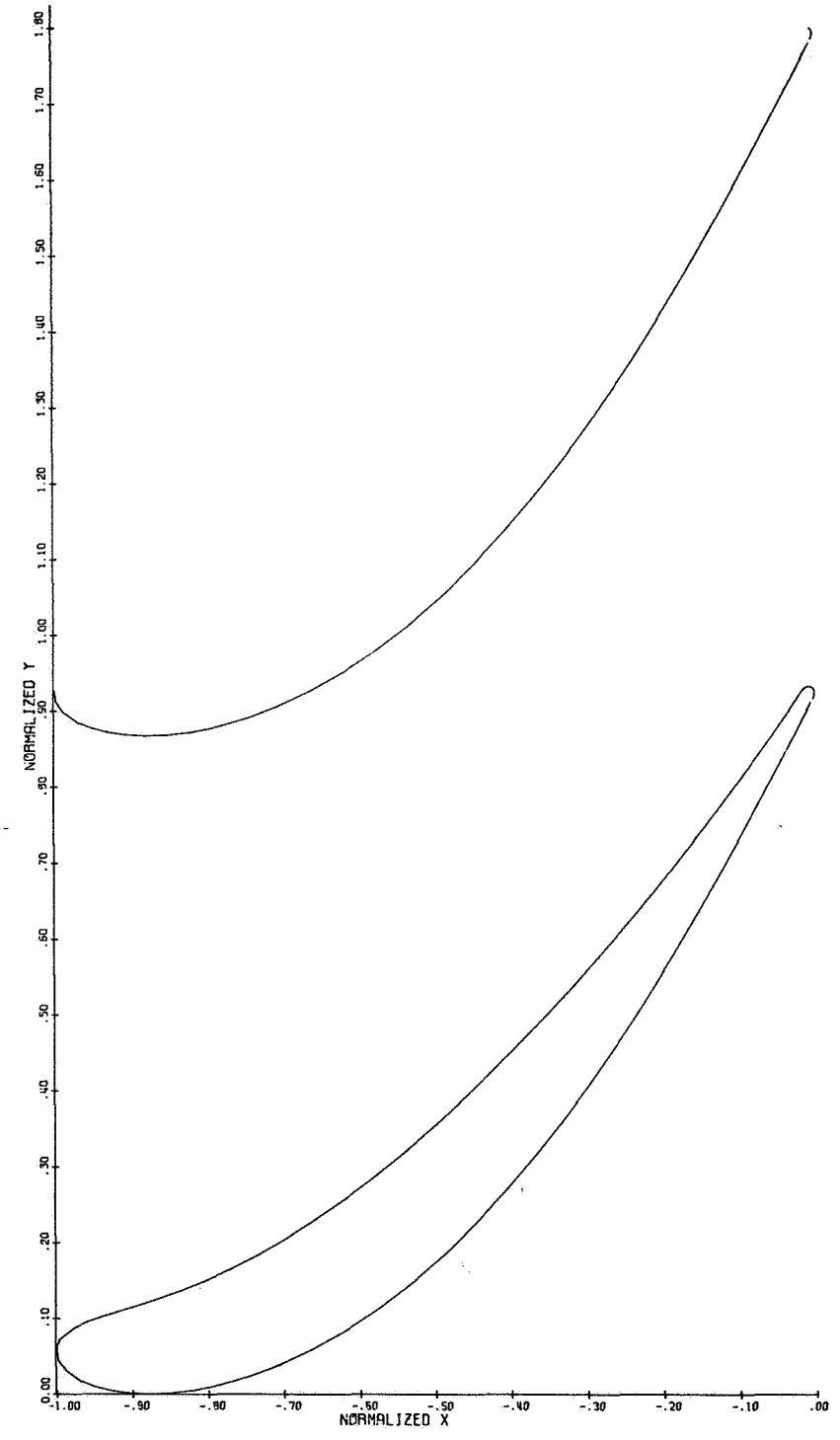

Figure 14. Stage One Vane Pitch Airfoil Flowpath.

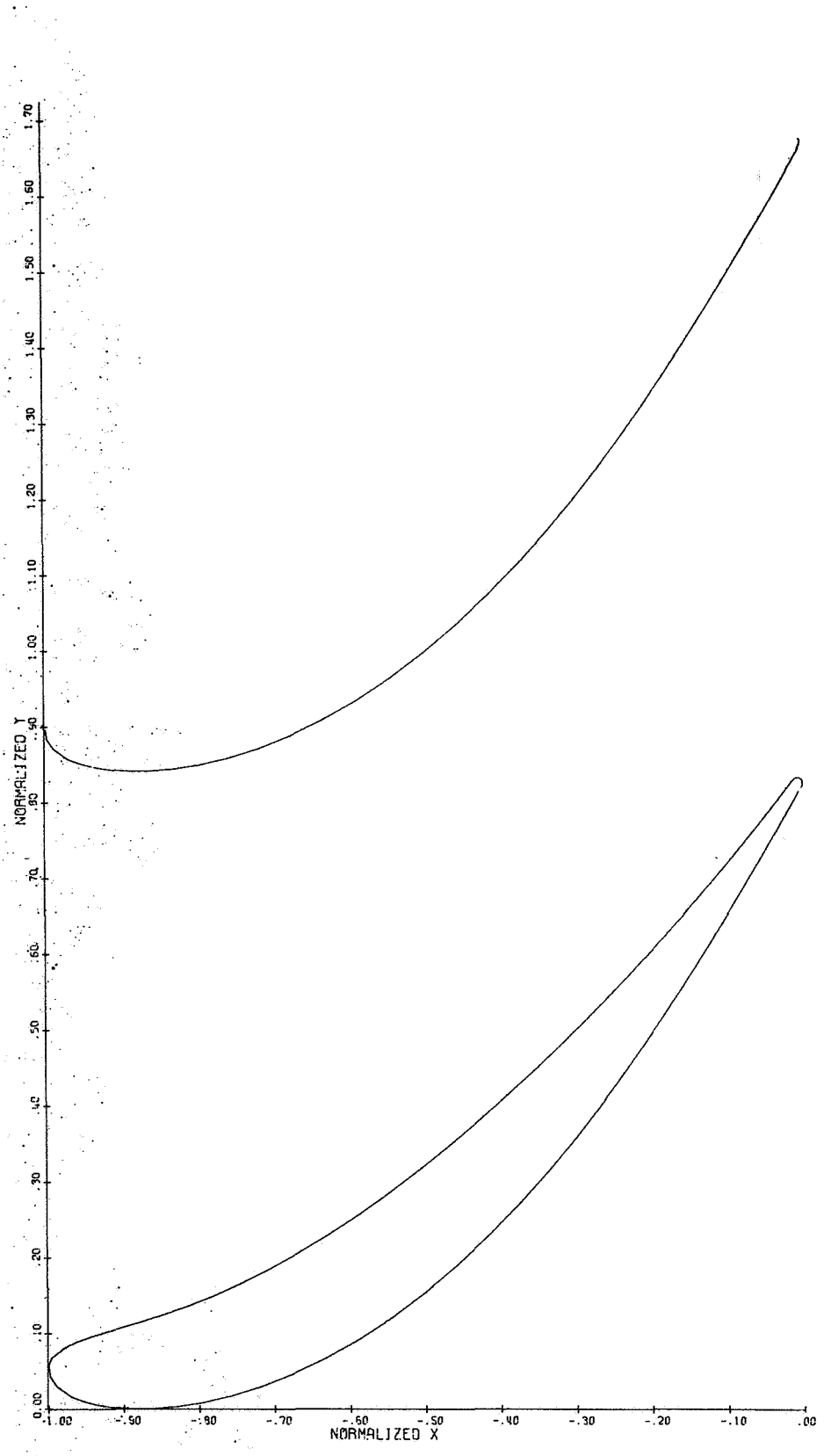

Figure 15. Stage One Vane Tip Airfoil Flowpath.

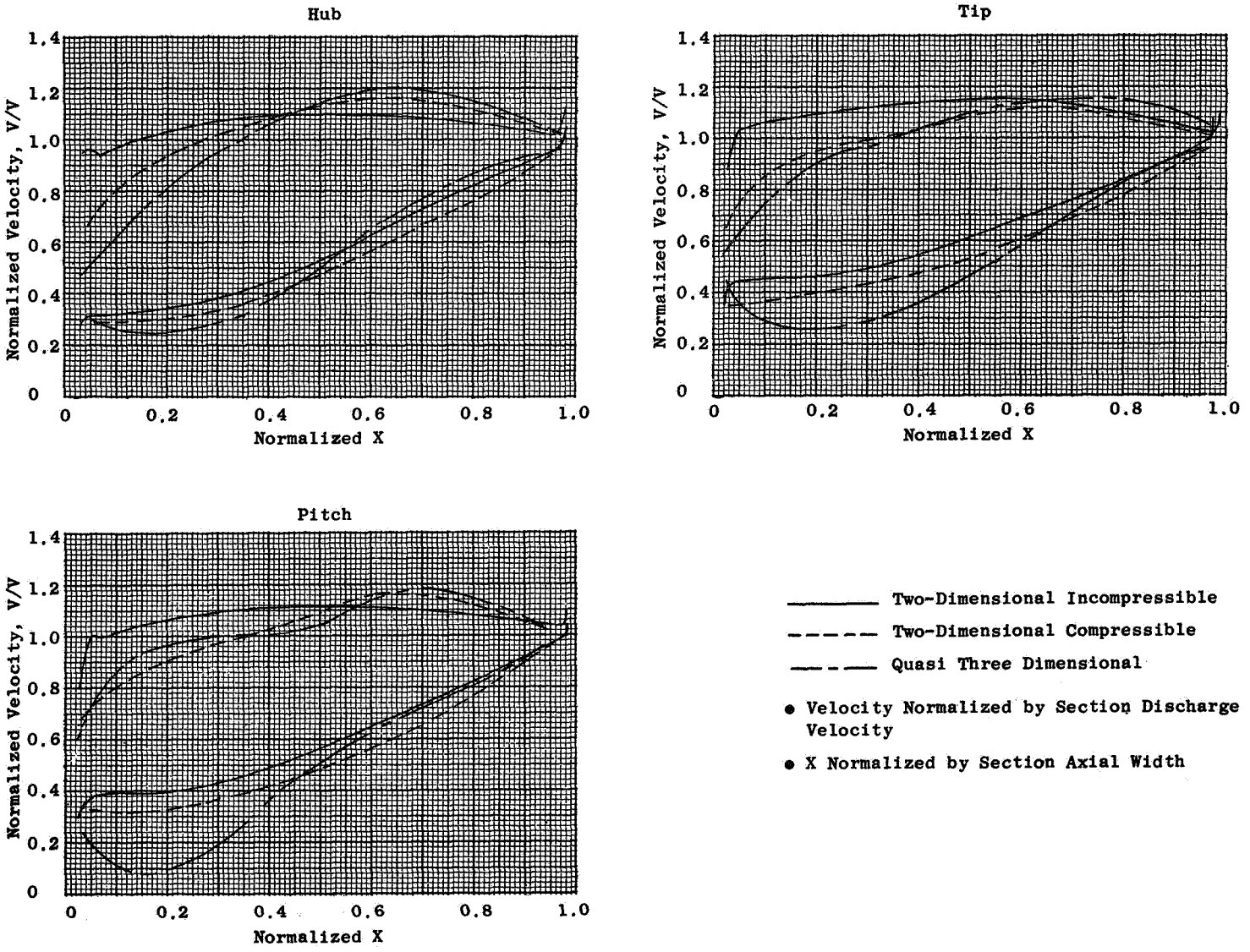

Figure 16. Stage One Vane Velocity Distribution.

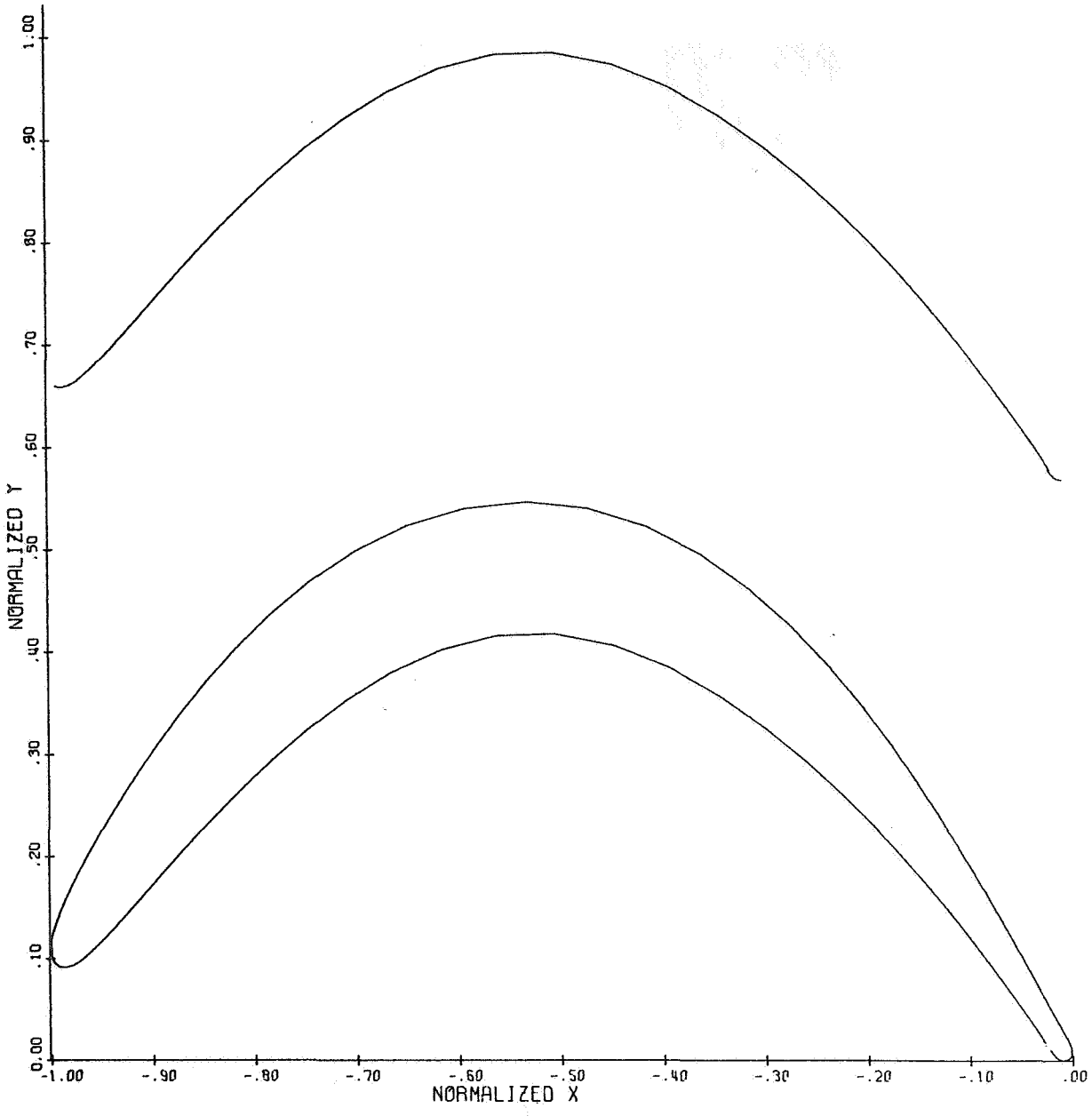

Figure 17. Stage One Rotor Hub Airfoil Flowpath.

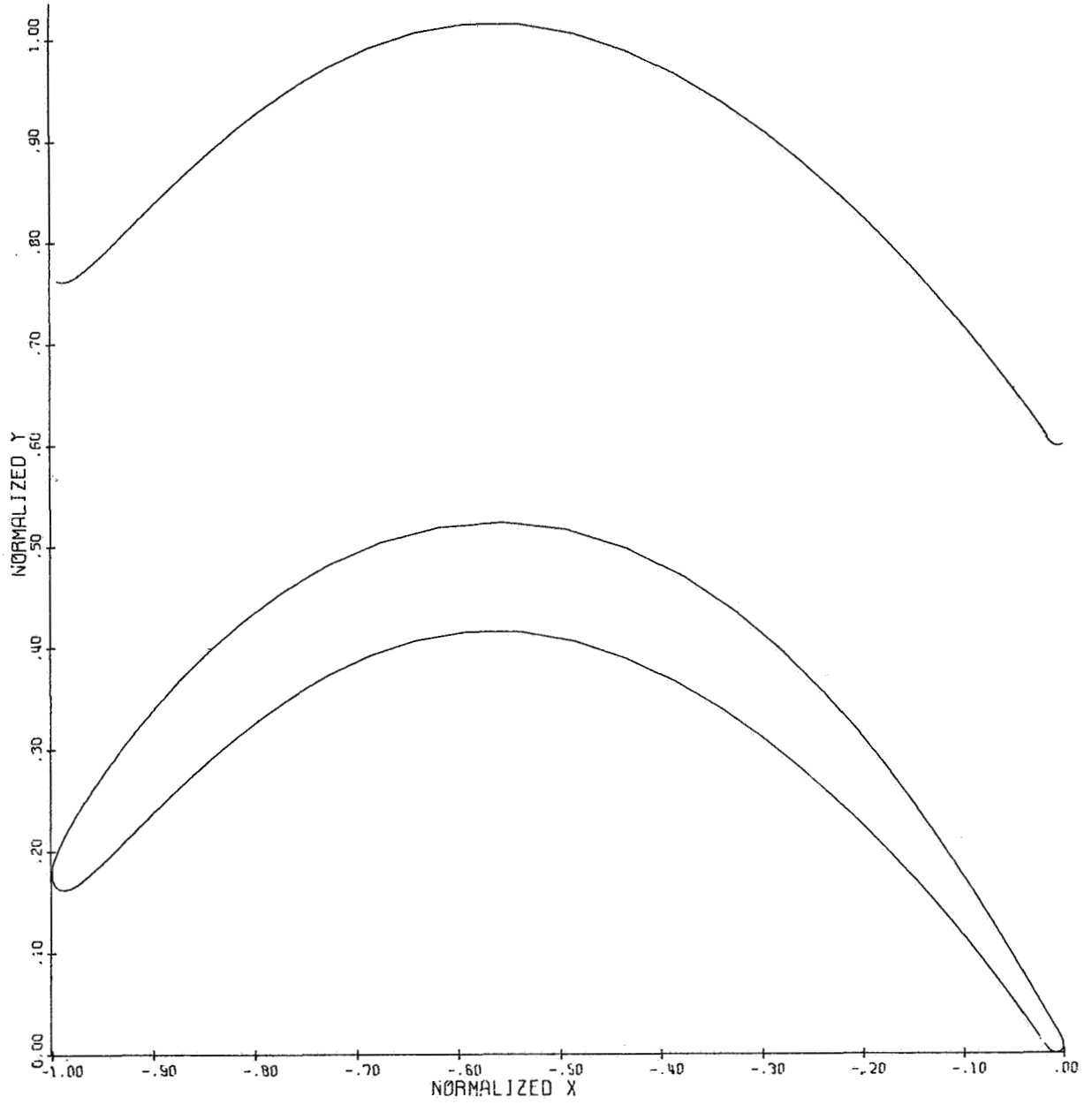

Figure 18. Stage One Rotor Pitch Airfoil Flowpath.

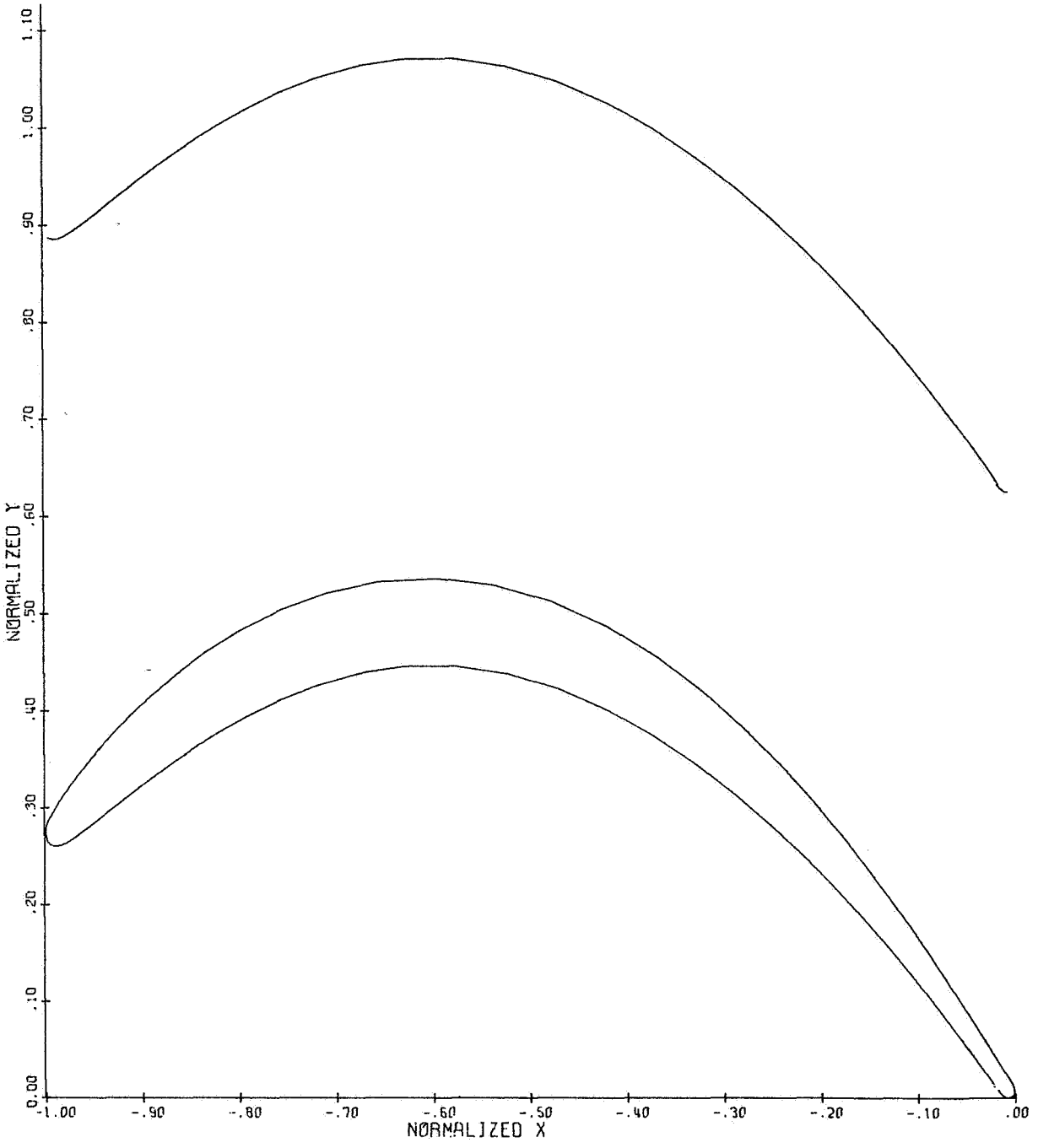

Figure 19. Stage One Rotor Tip Airfoil Flowpath.

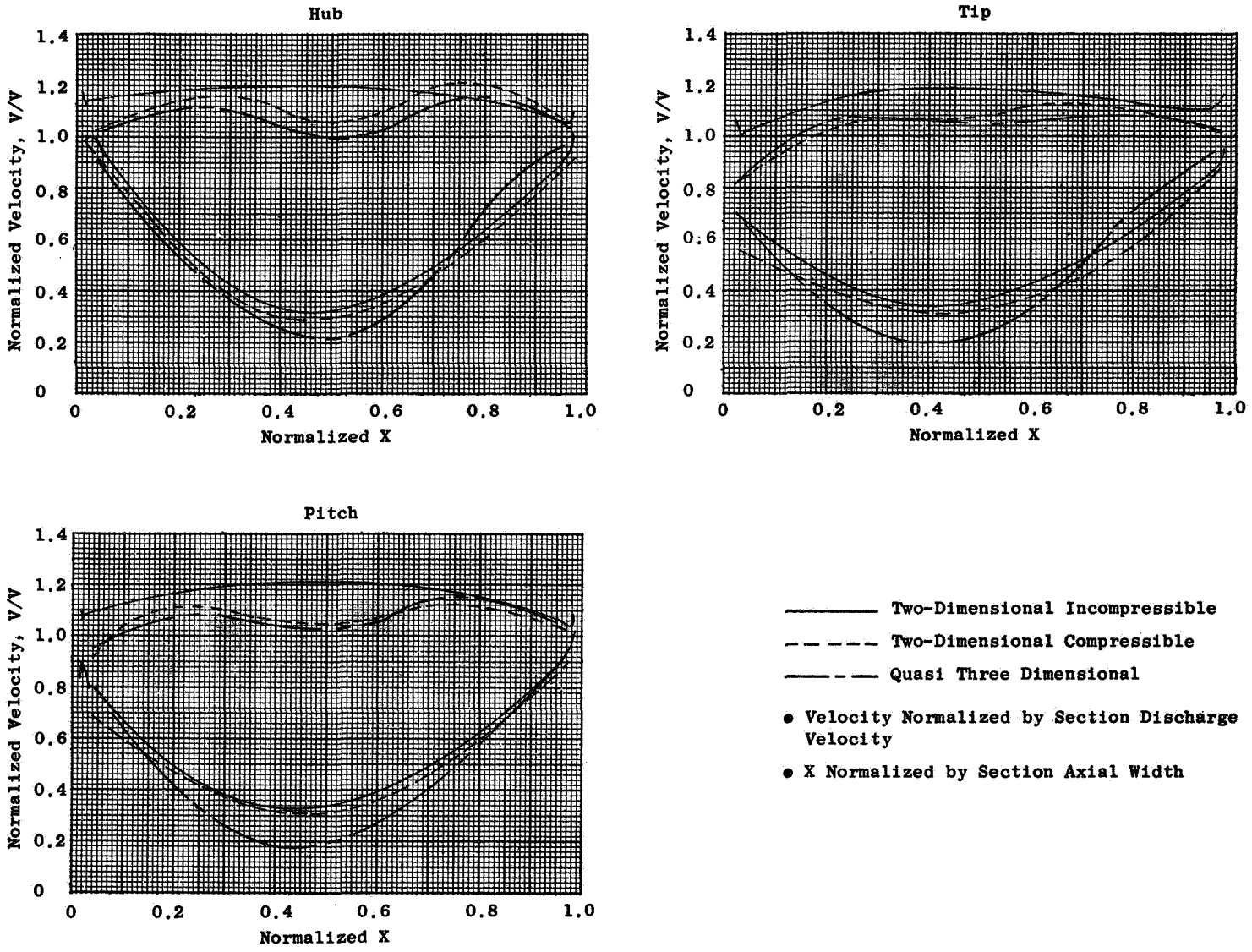

Figure 20. Stage One Rotor Velocity Distribution.

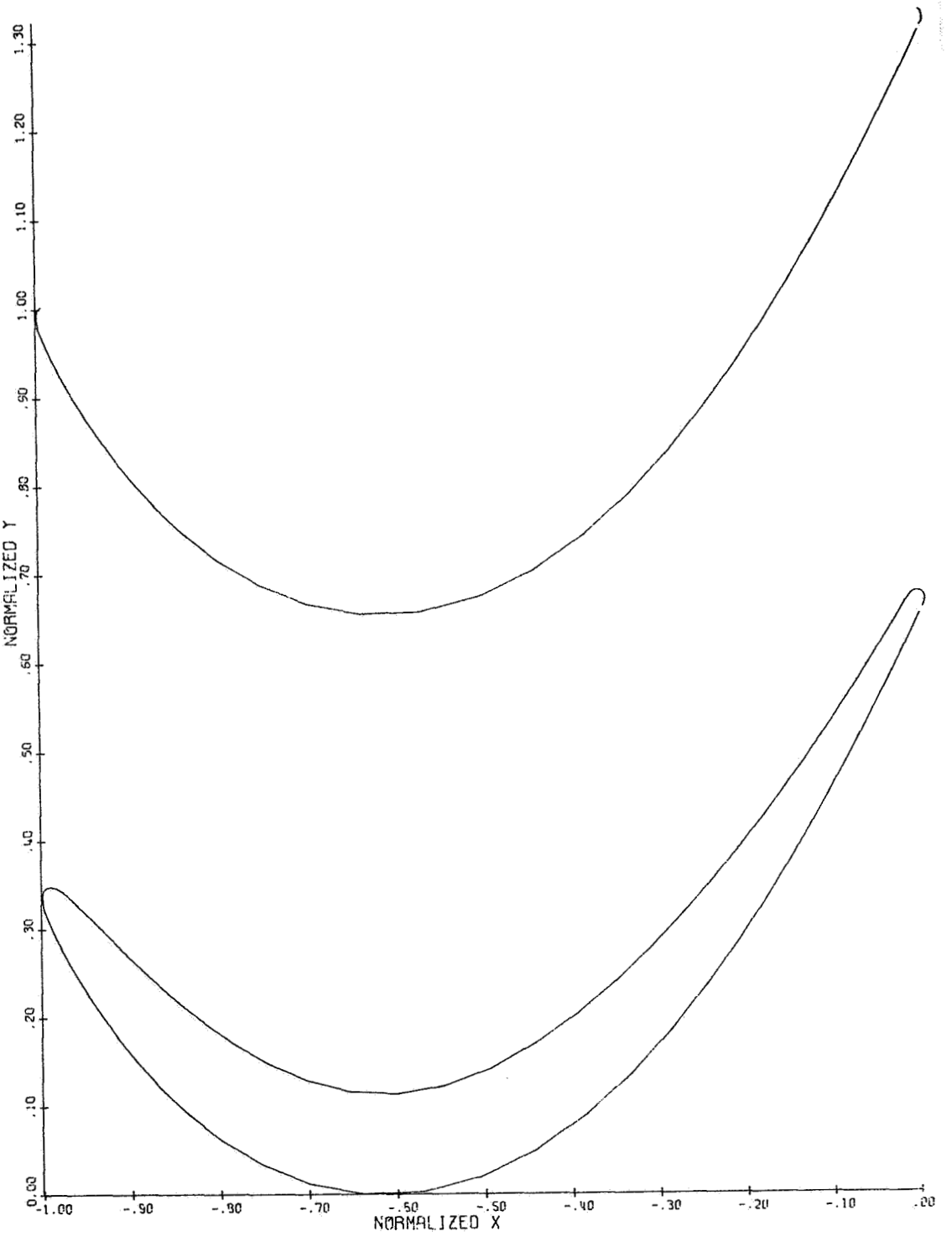

Figure 21. Stage Two Vane Hub Airfoil Flowpath.

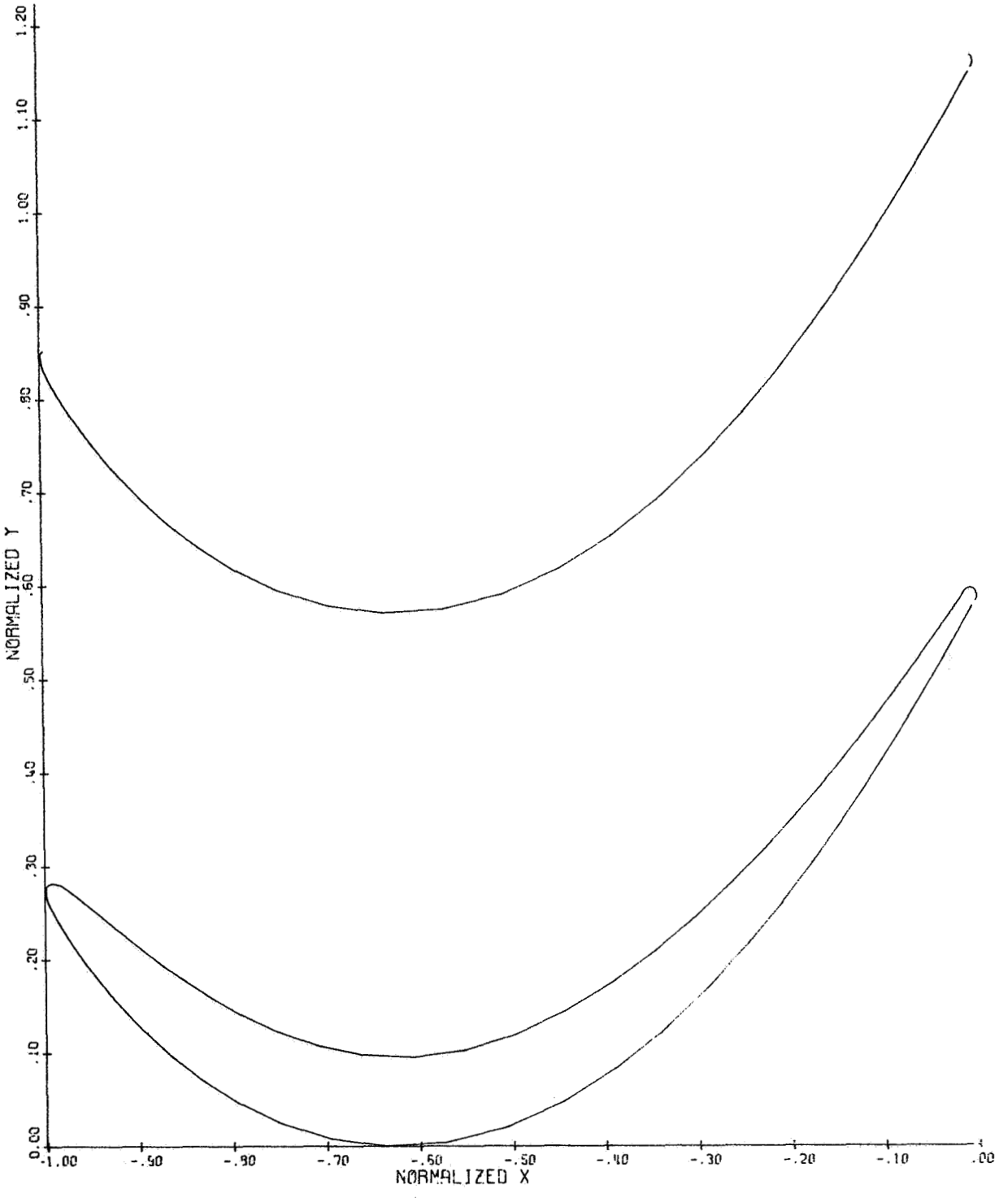

Figure 22. Stage Two Vane Pitch Airfoil Flowpath.

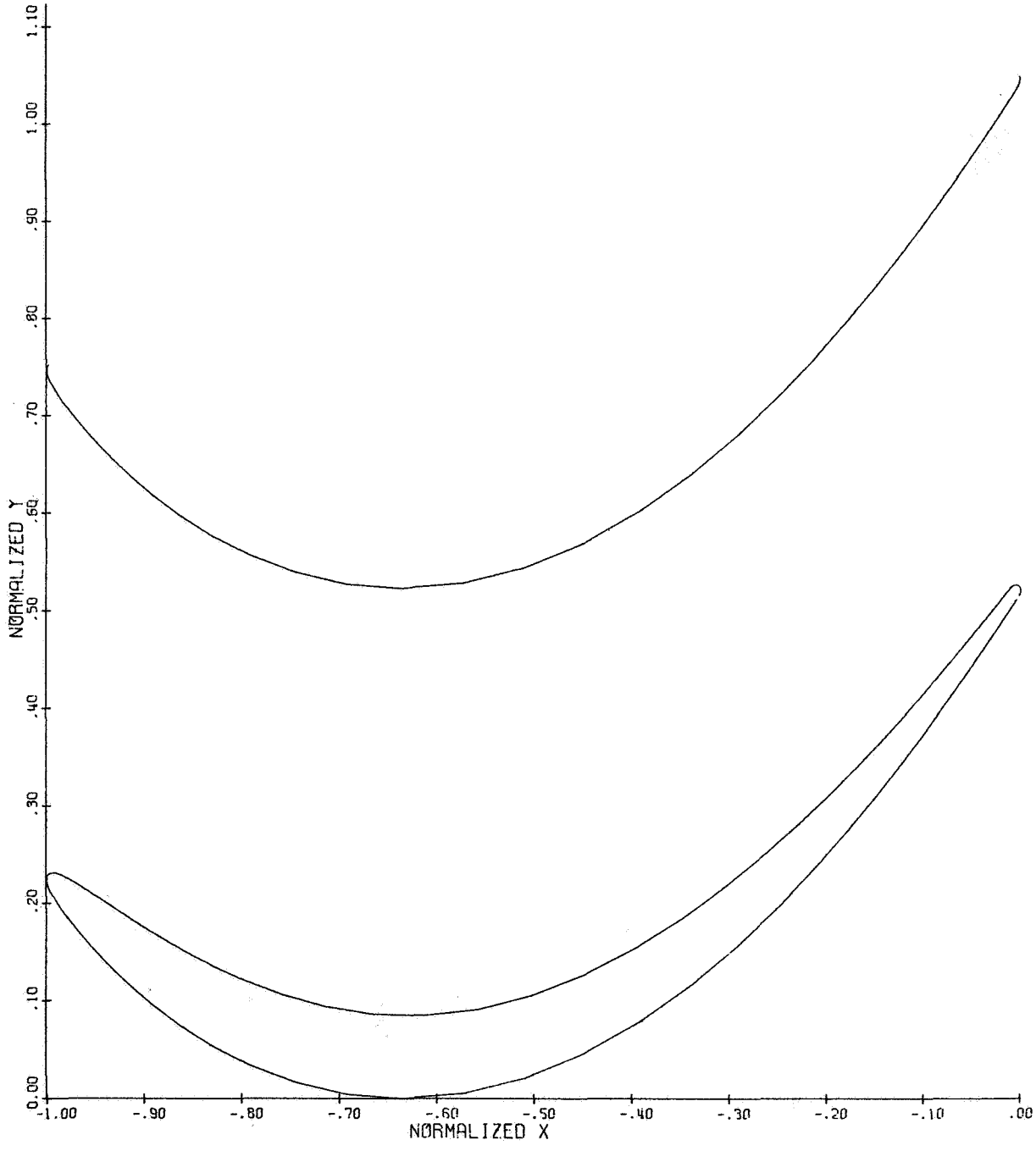

Figure 23. Stage Two Vane Tip Airfoil Flowpath.

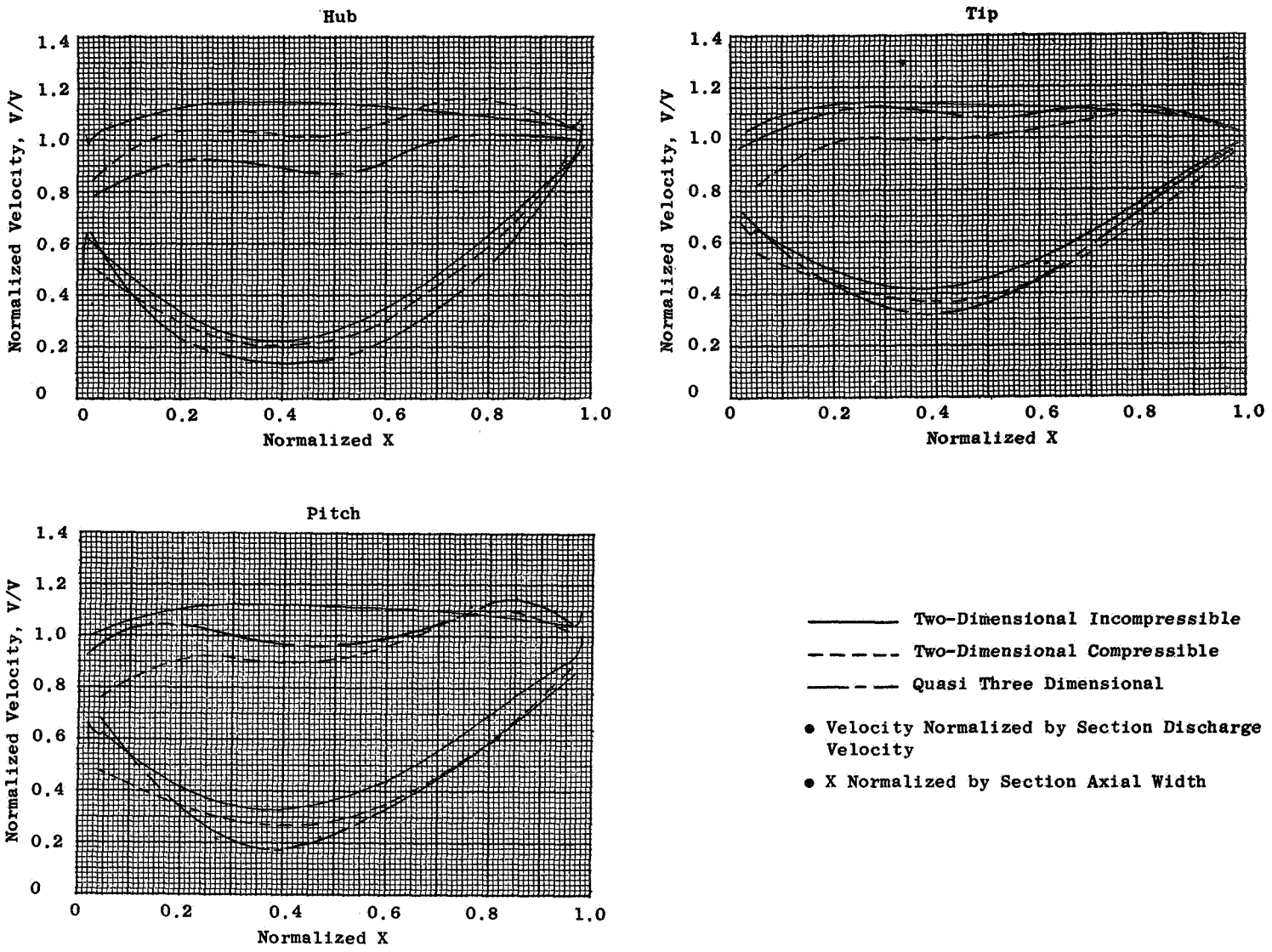

Figure 24. Stage Two Vane Velocity Distribution.

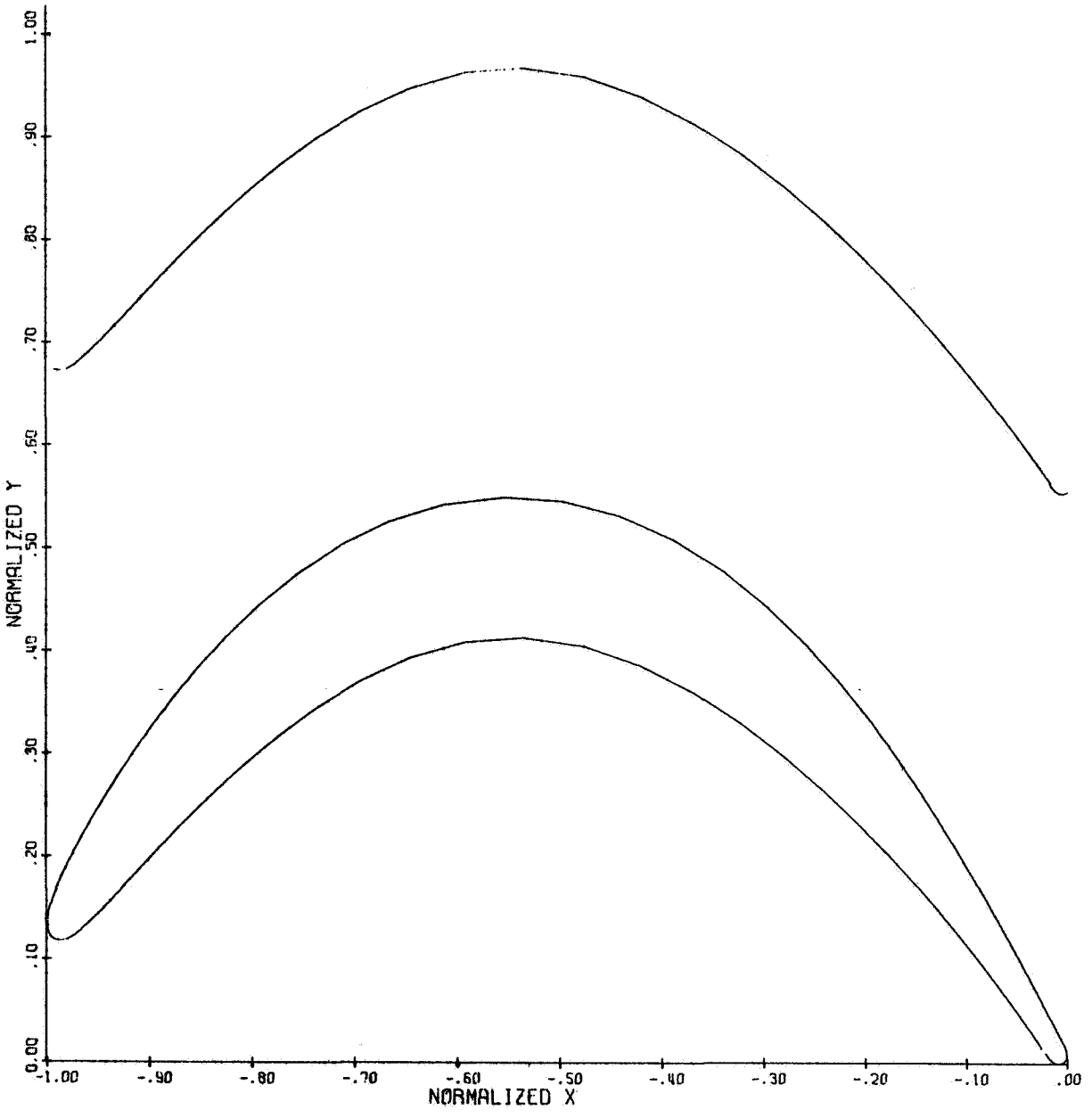

Figure 25. Stage Two Rotor Hub Airfoil Flowpath.

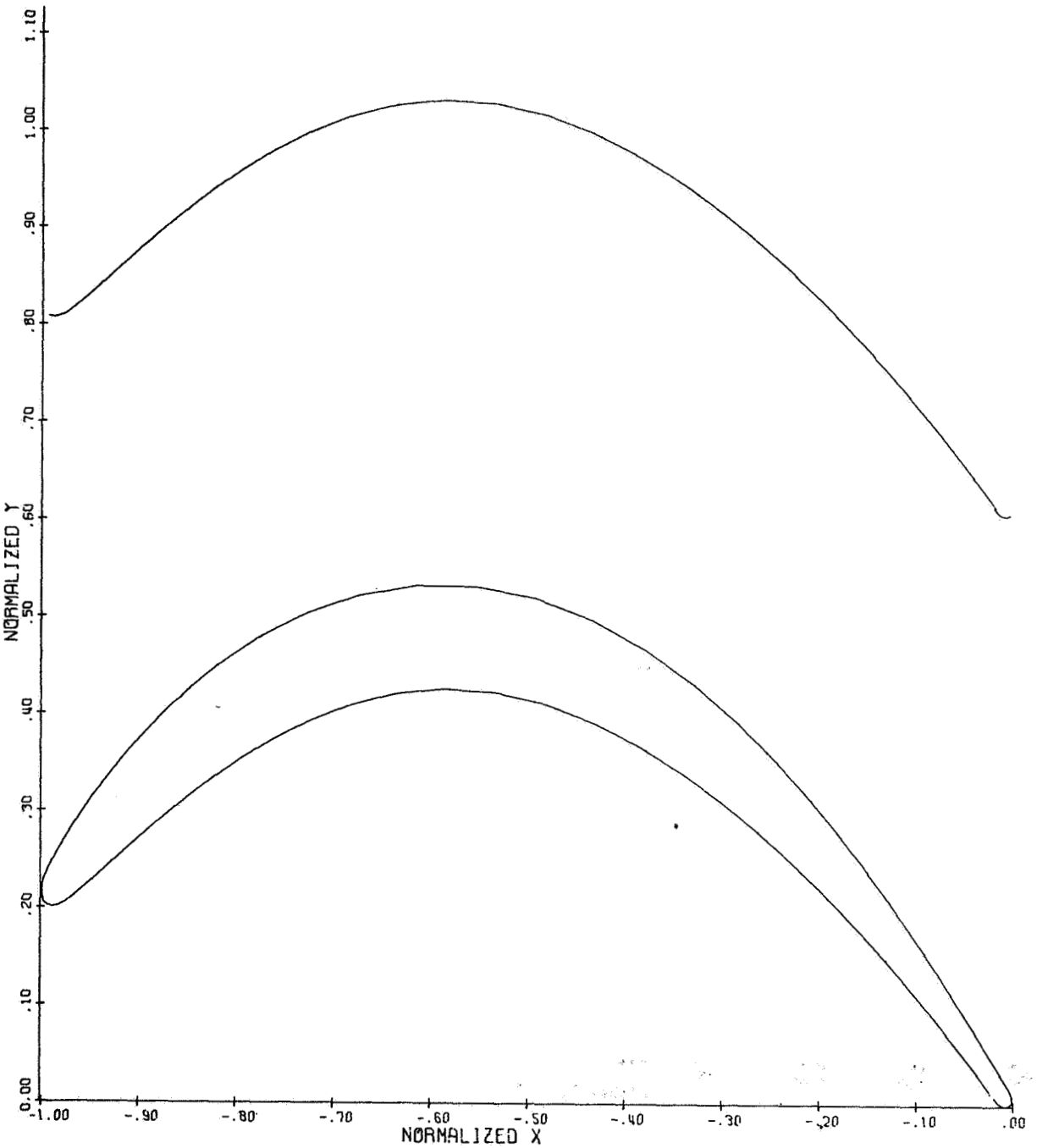

Figure 26. Stage Two Rotor Pitch Airfoil Flowpath.

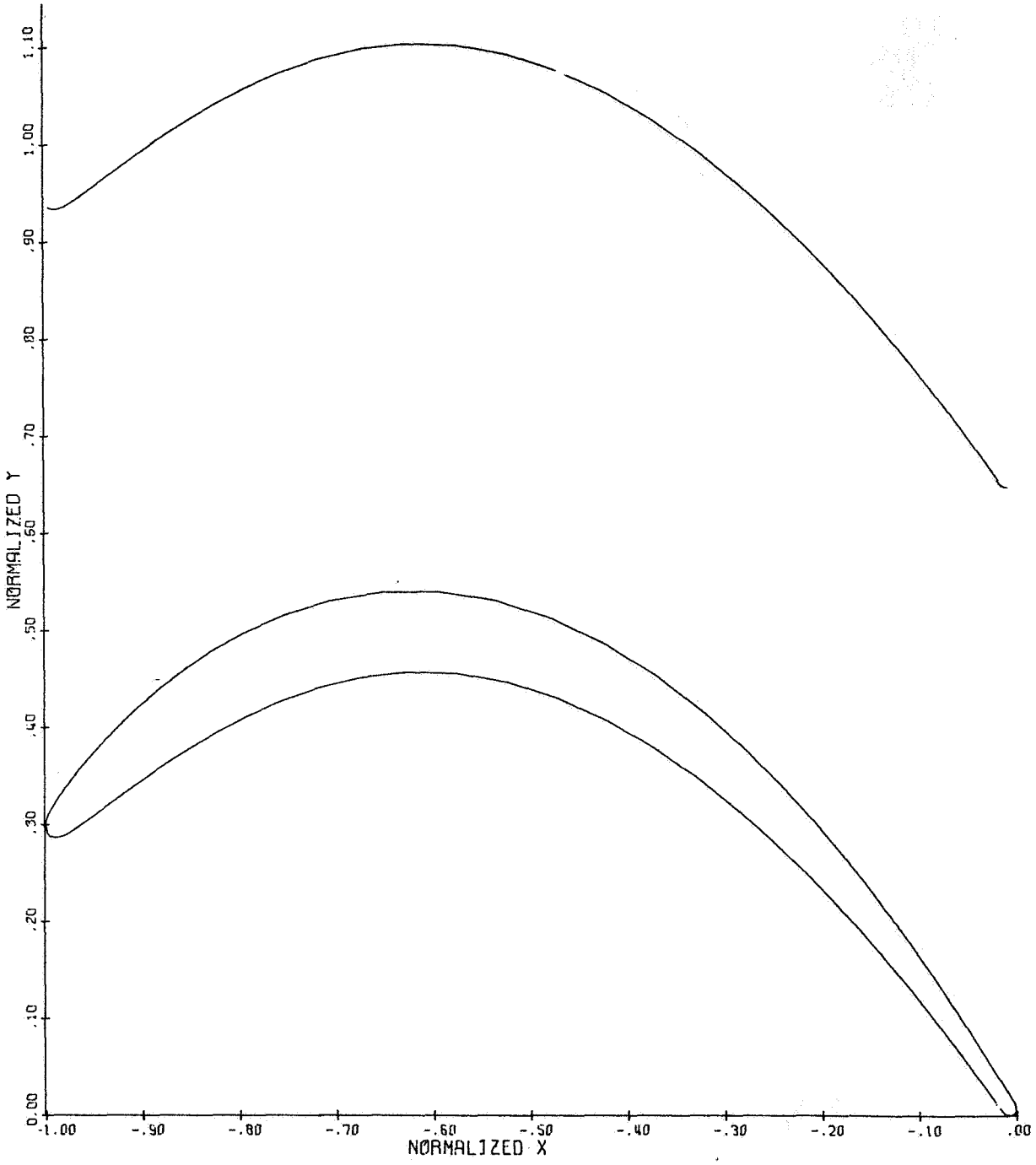

Figure 27. Stage Two Rotor Tip Airfoil Flowpath.

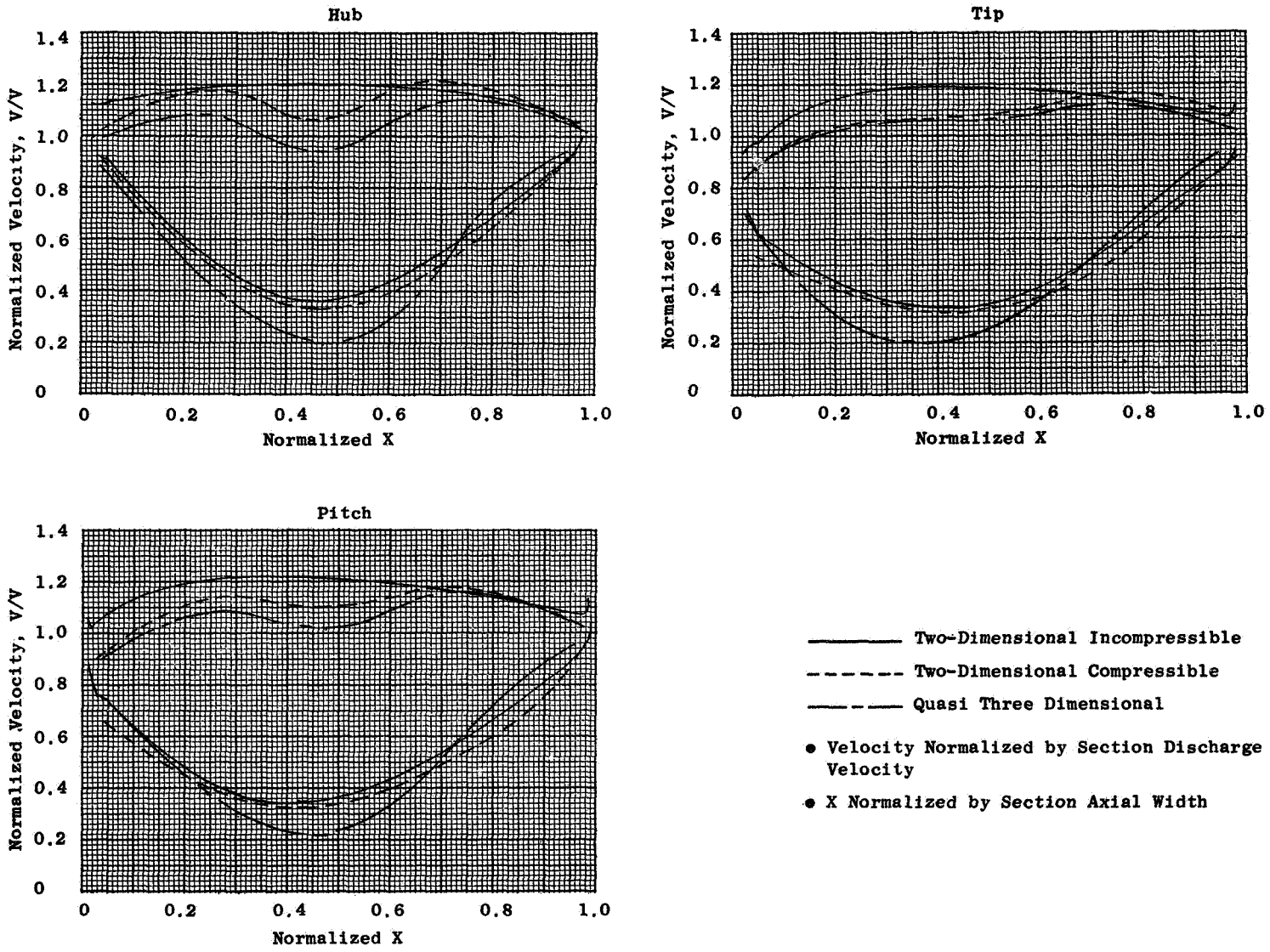

Figure 28. Stage Two Rotor Velocity Distribution.

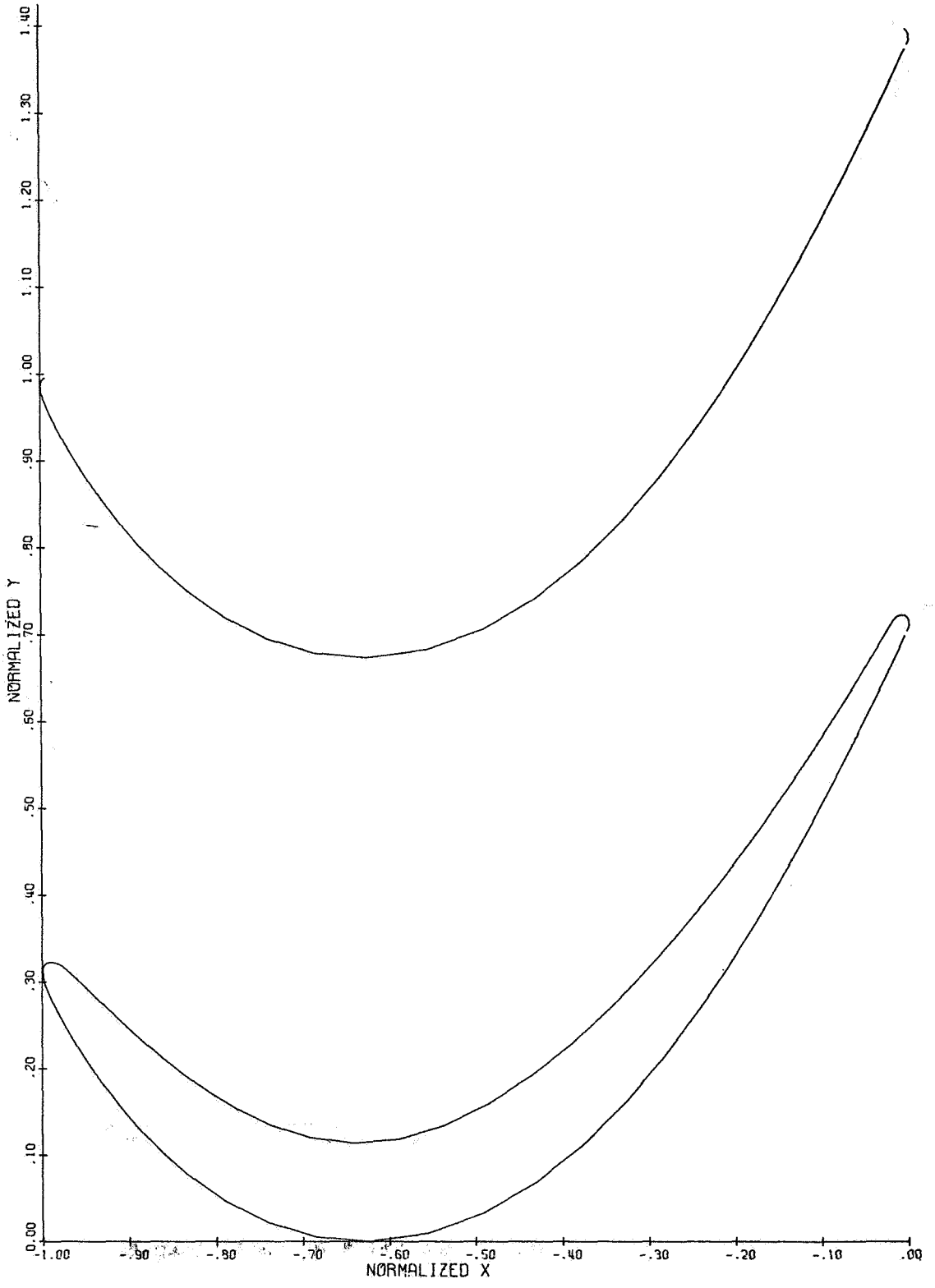

Figure 29. Stage Three Vane Hub Airfoil Flowpath.

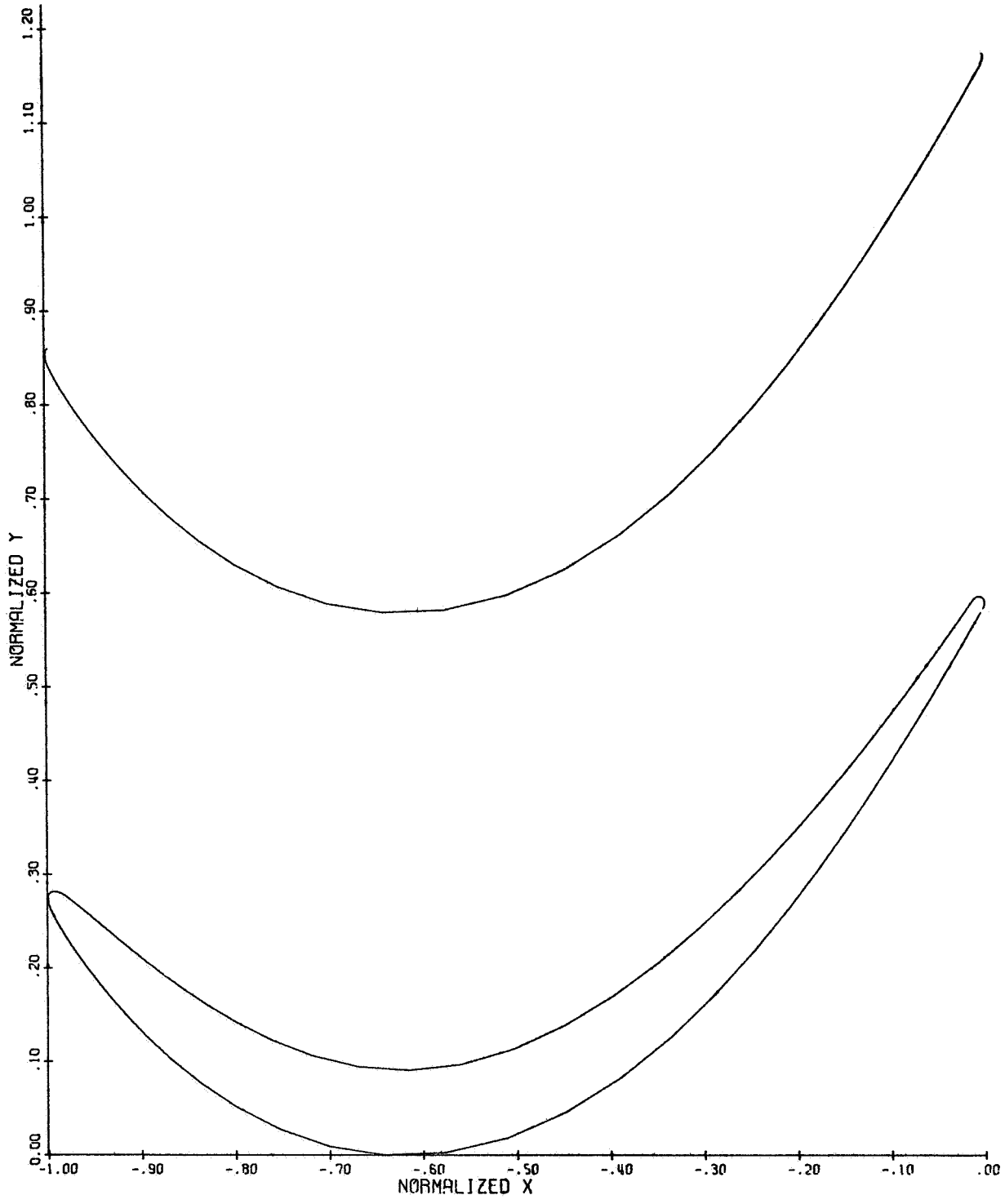

Figure 30. Stage Three Vane Pitch Airfoil Flowpath.

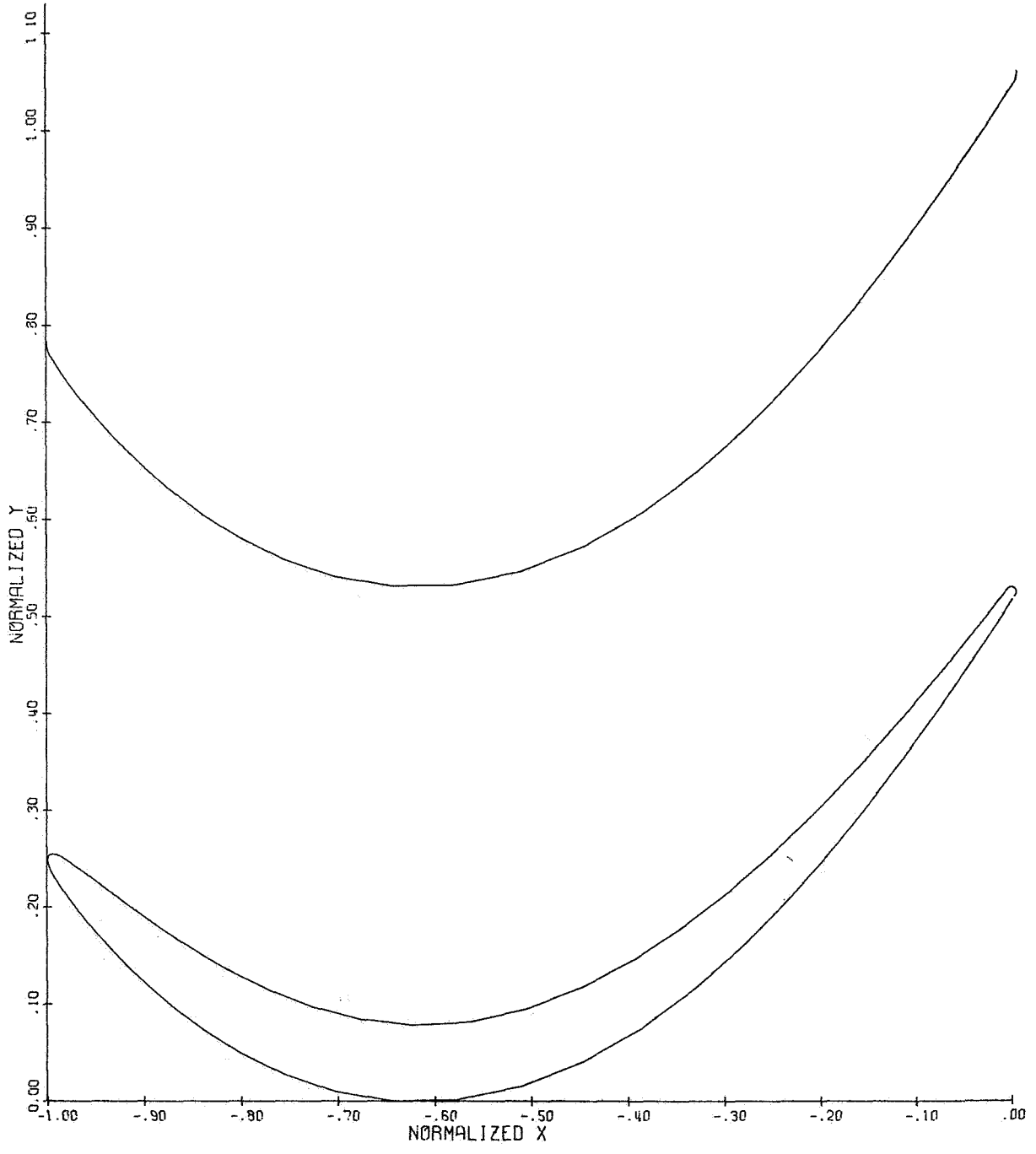

Figure 31. Stage Three Vane Tip Airfoil Flowpath.

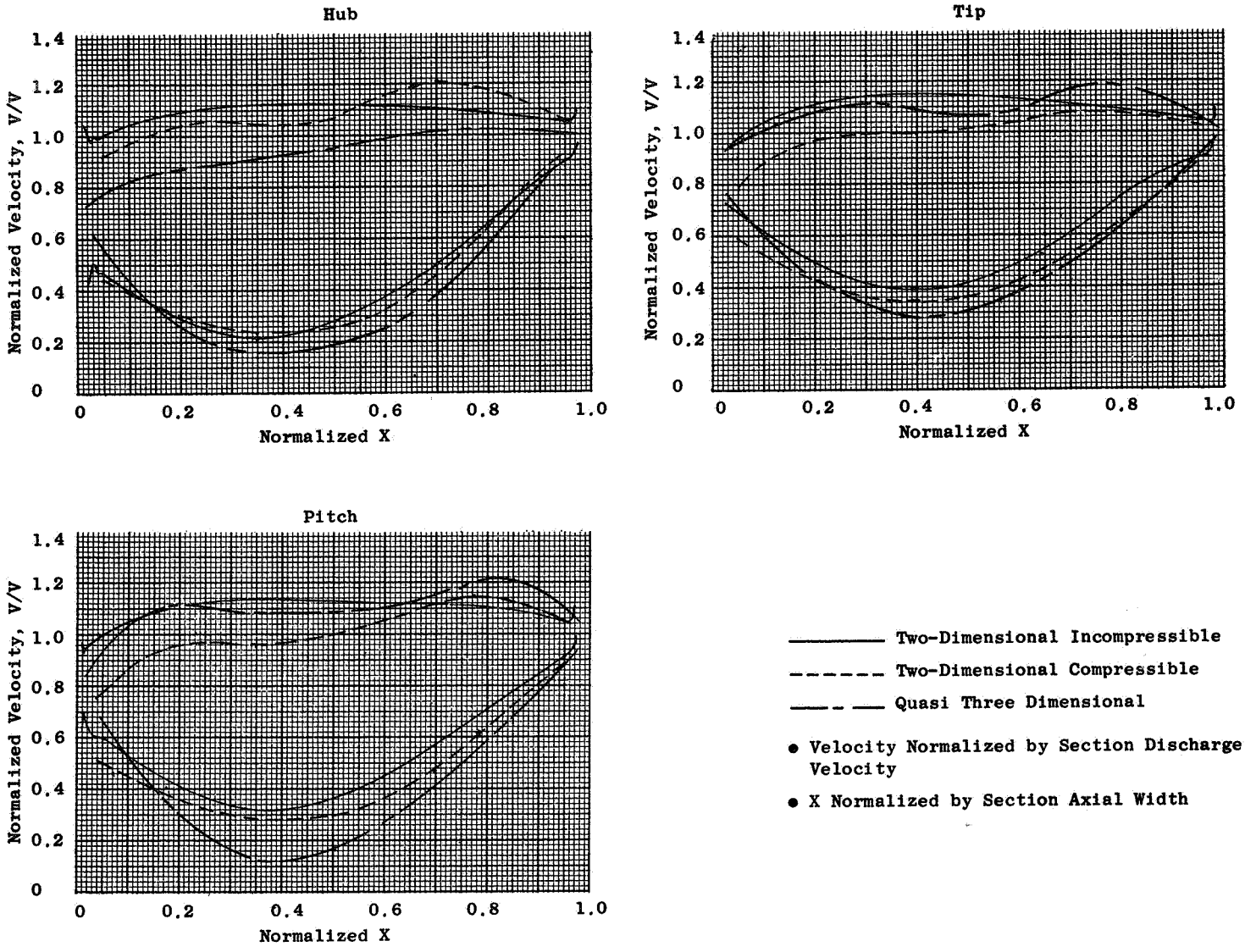

Figure 32. Stage Three Vane Velocity Distribution.

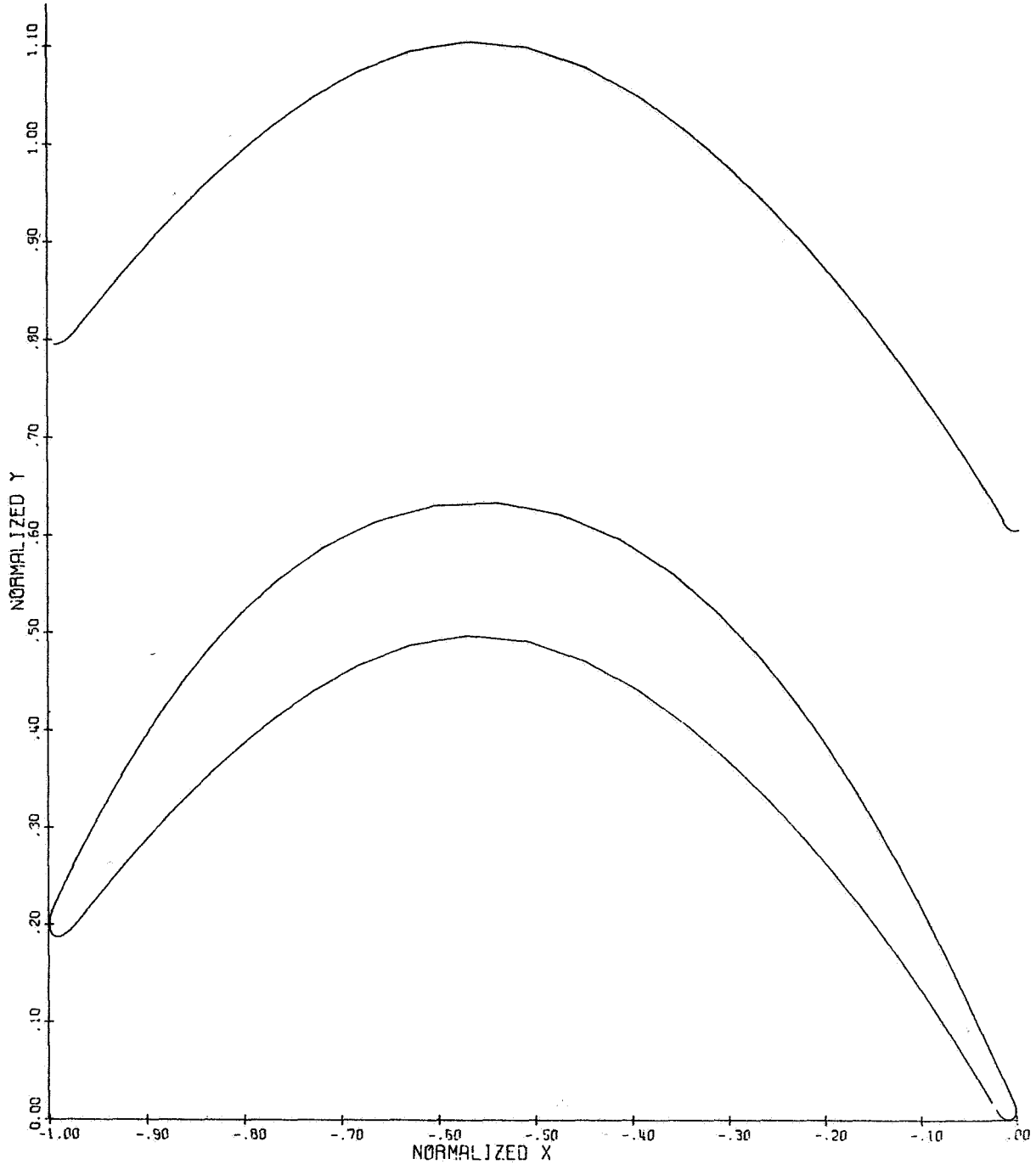

Figure 33. Stage Three Rotor Hub Airfoil Flowpath.

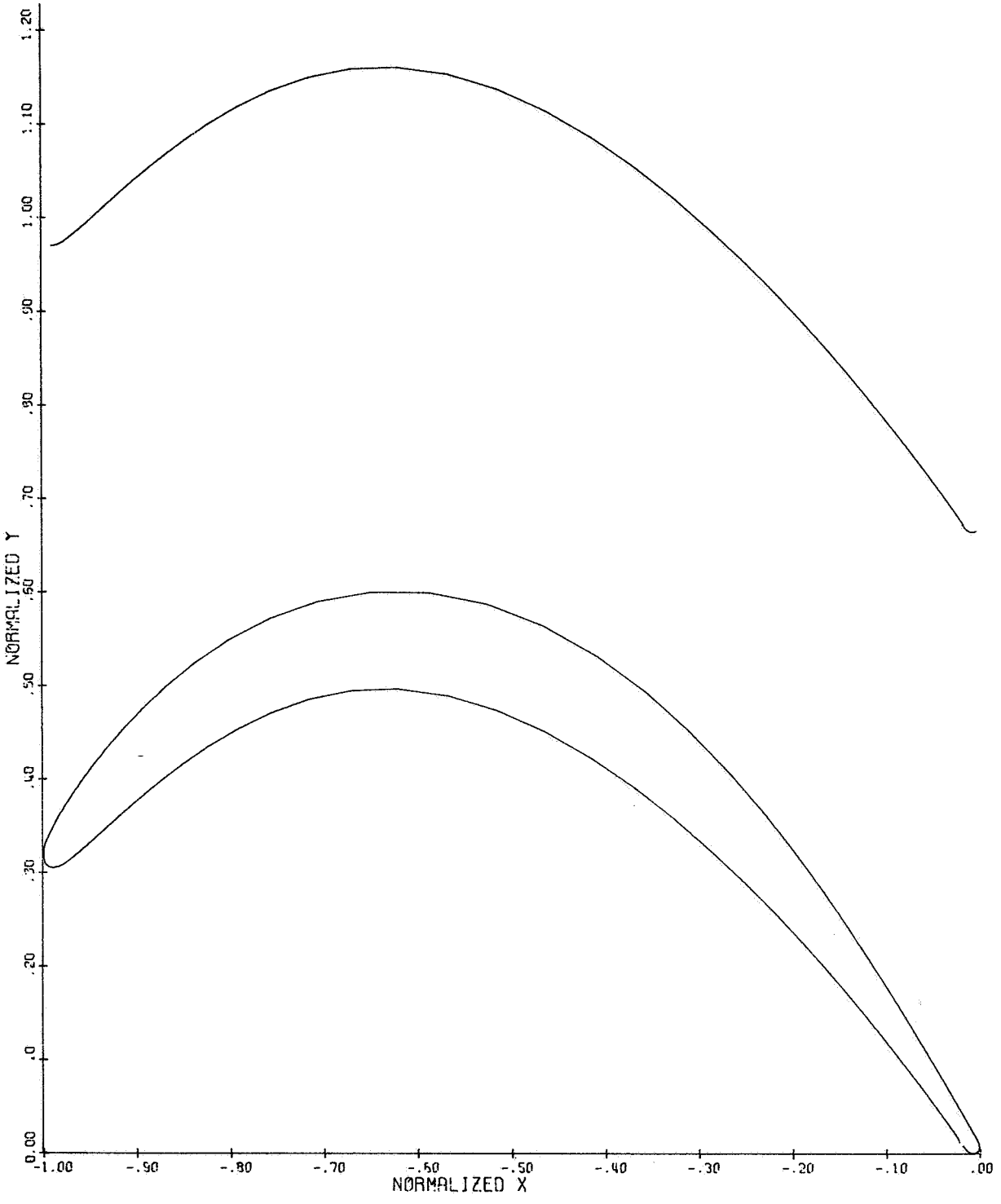

Figure 34. Stage Three Rotor Pitch Airfoil Flowpath.

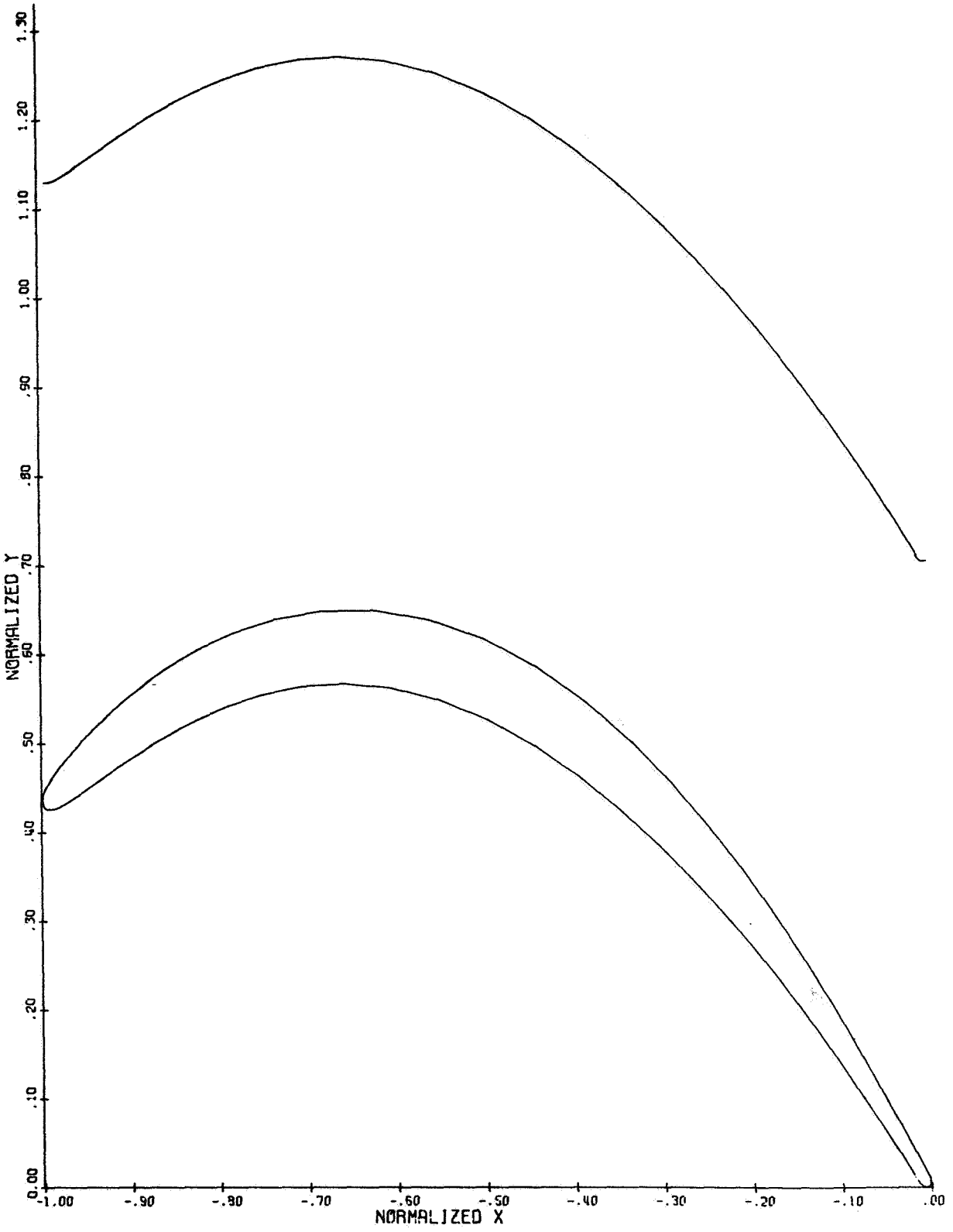

Figure 35. Stage Three Rotor Tip Airfoil Flowpath.

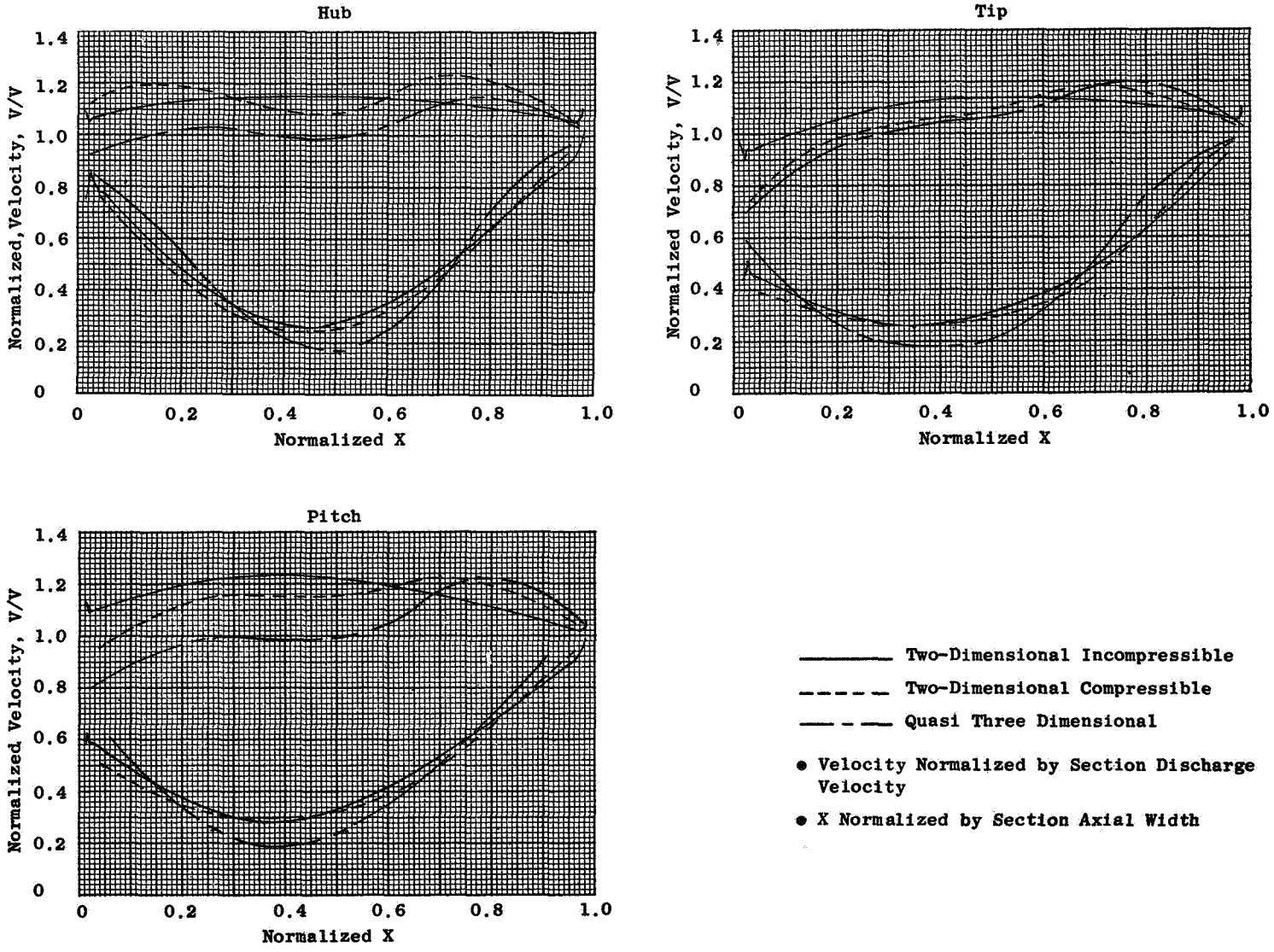

Figure 36. Stage Three Rotor Velocity Distribution.

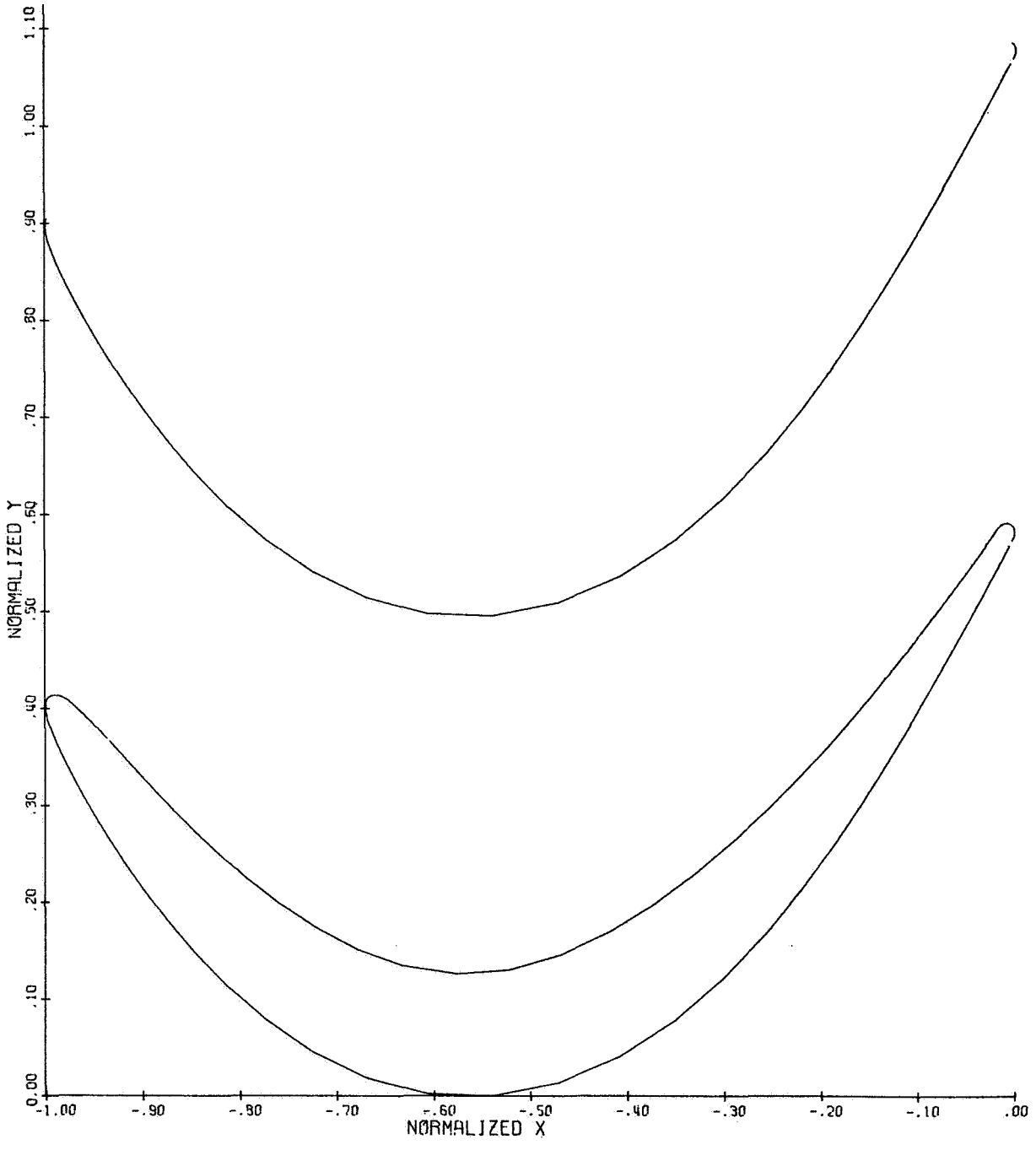

Figure 37. Stage Four Vane Hub Airfoil Flowpath.

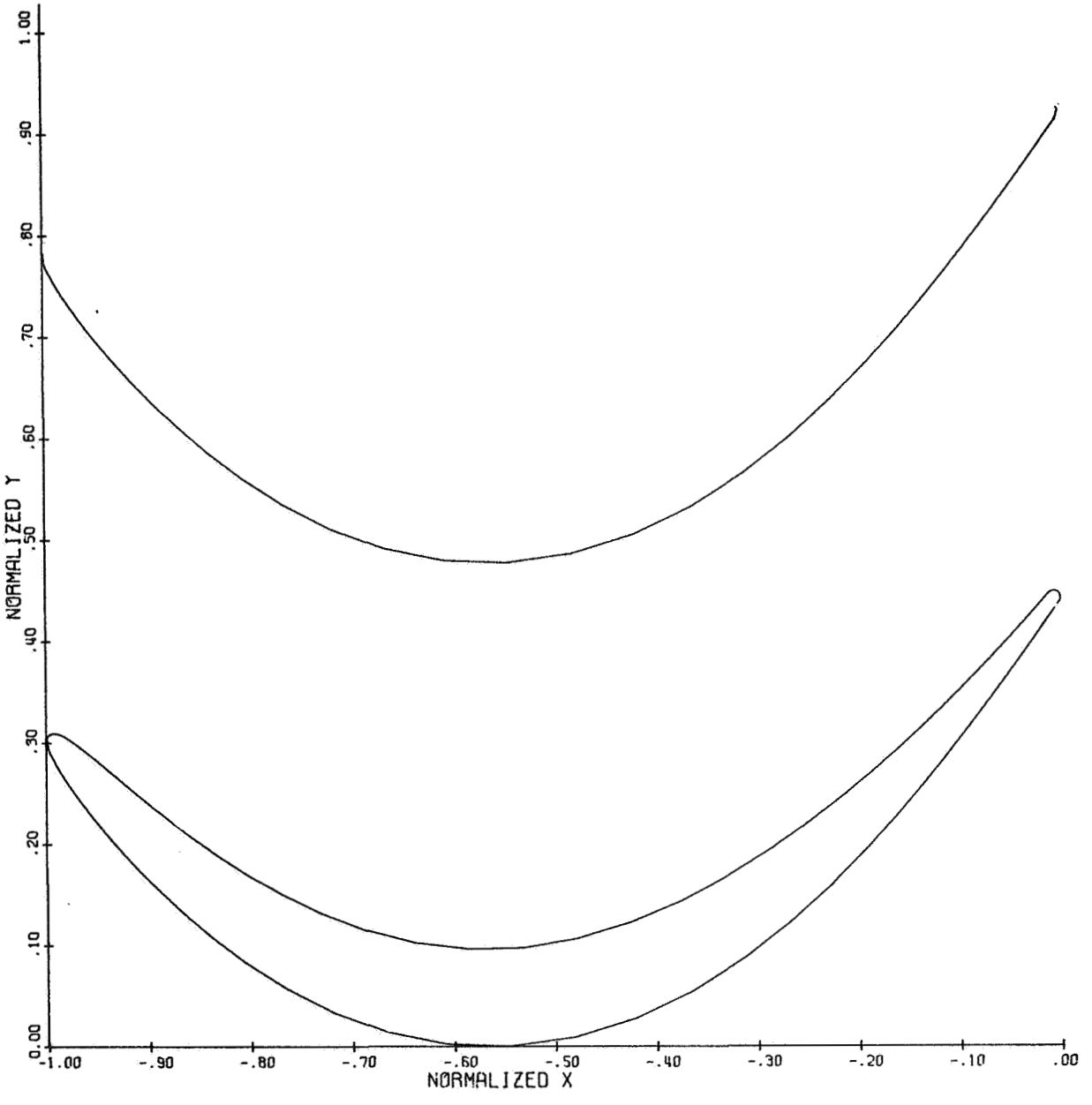

Figure 38. Stage Four Vane Pitch Airfoil Flowpath.

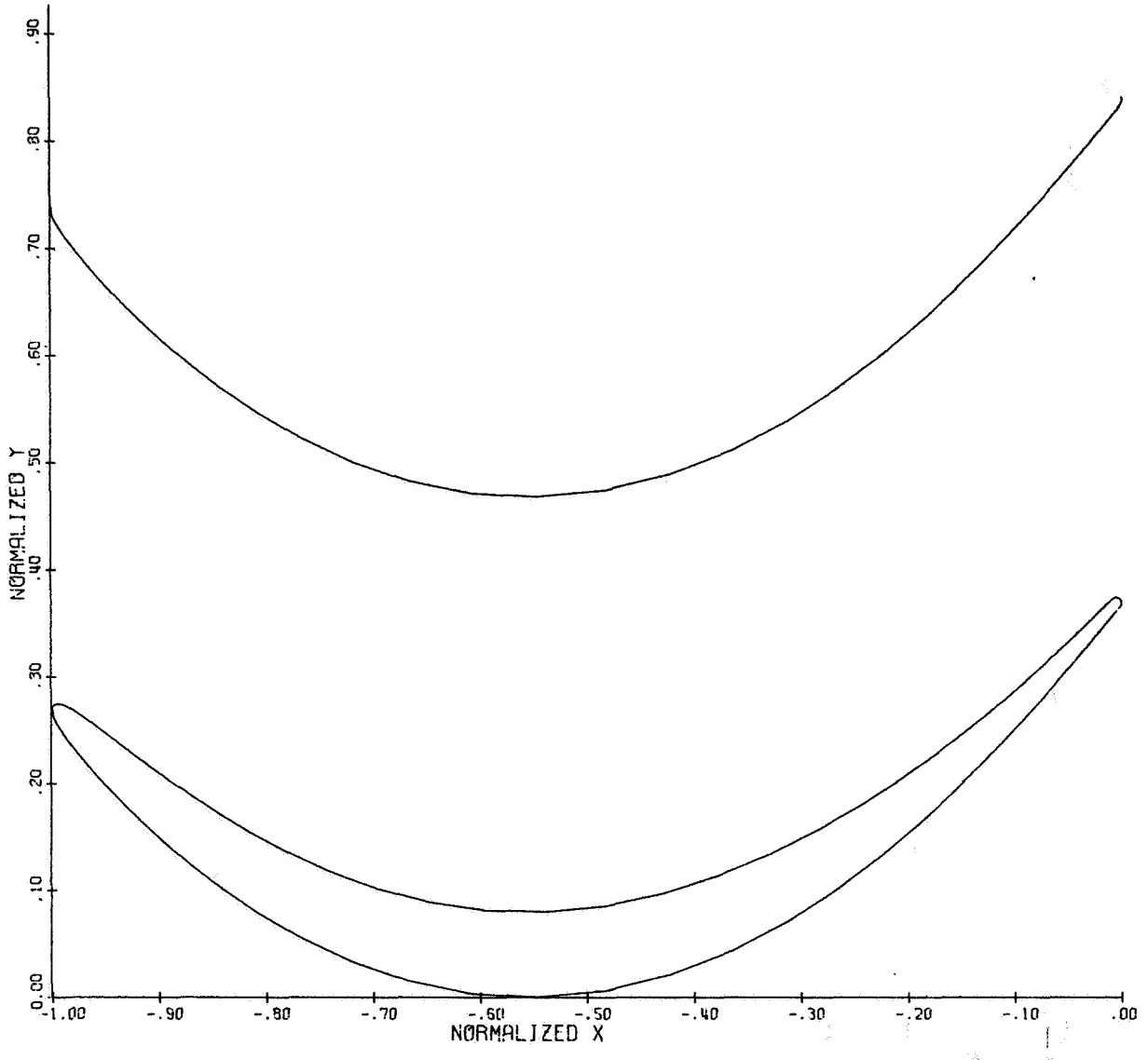

Figure 39. Stage Four Vane Tip Airfoil Flowpath.

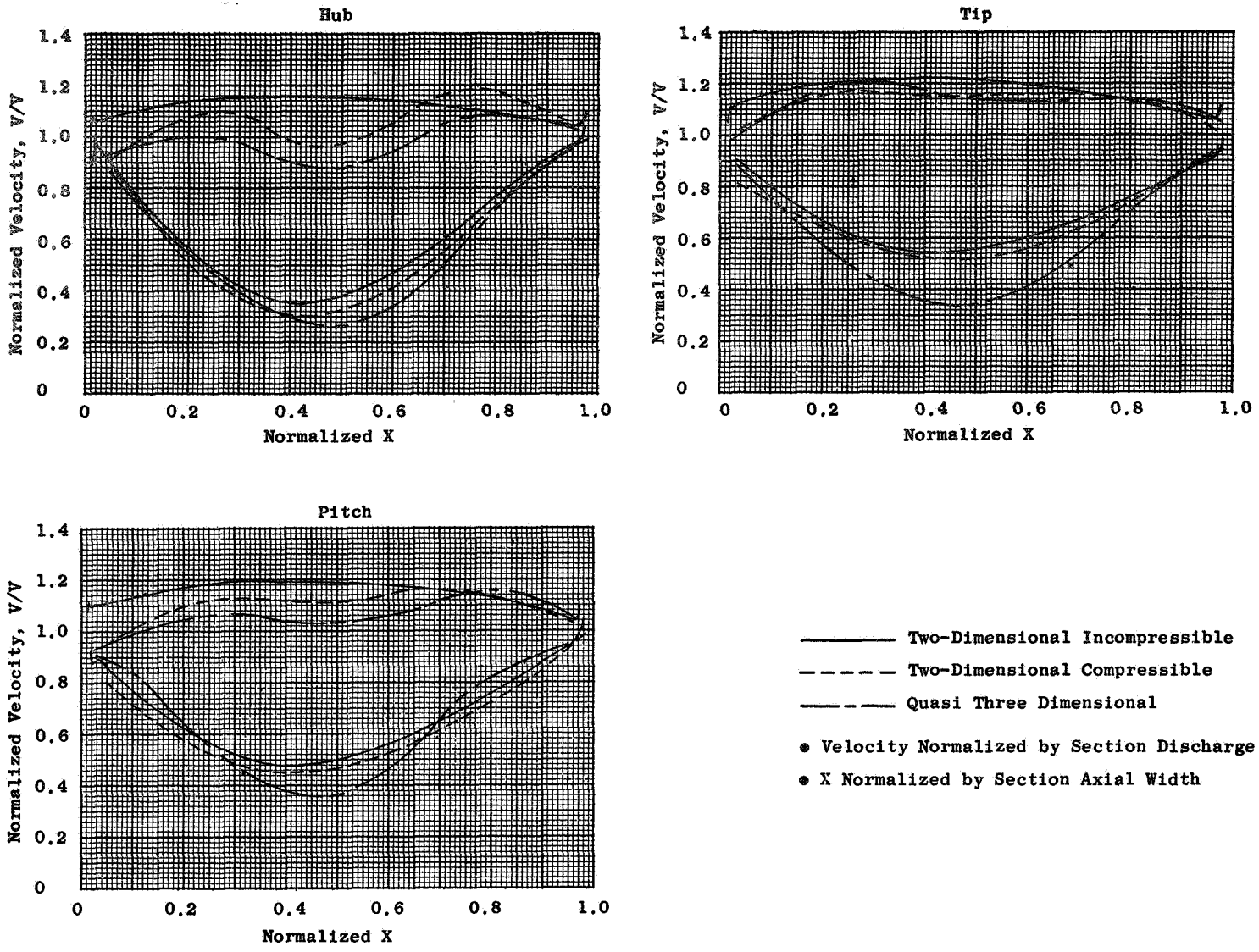

Figure 40. Stage Four Vane Velocity Distribution.

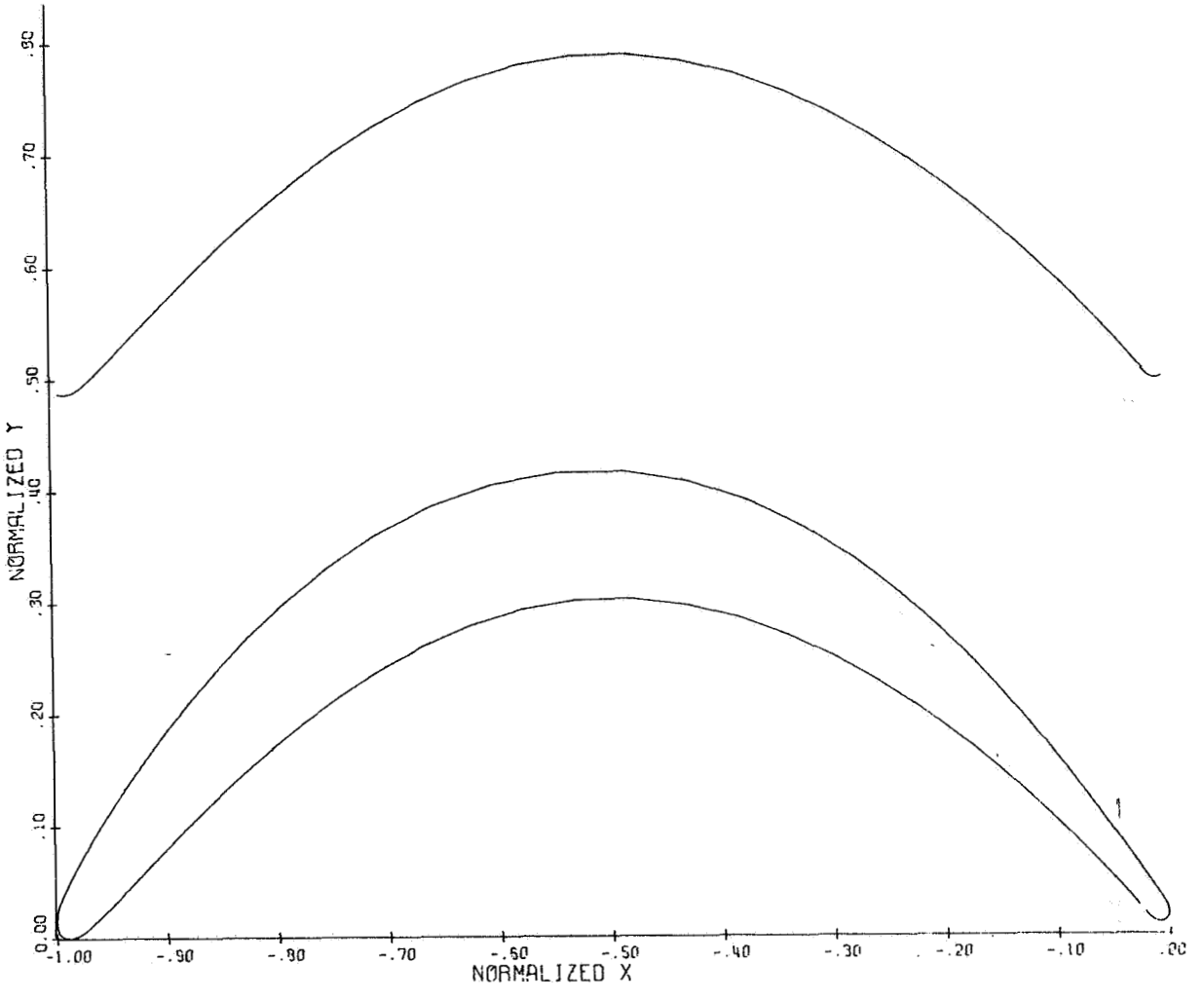

Figure 41. Stage Four Rotor Hub Airfoil Flowpath.

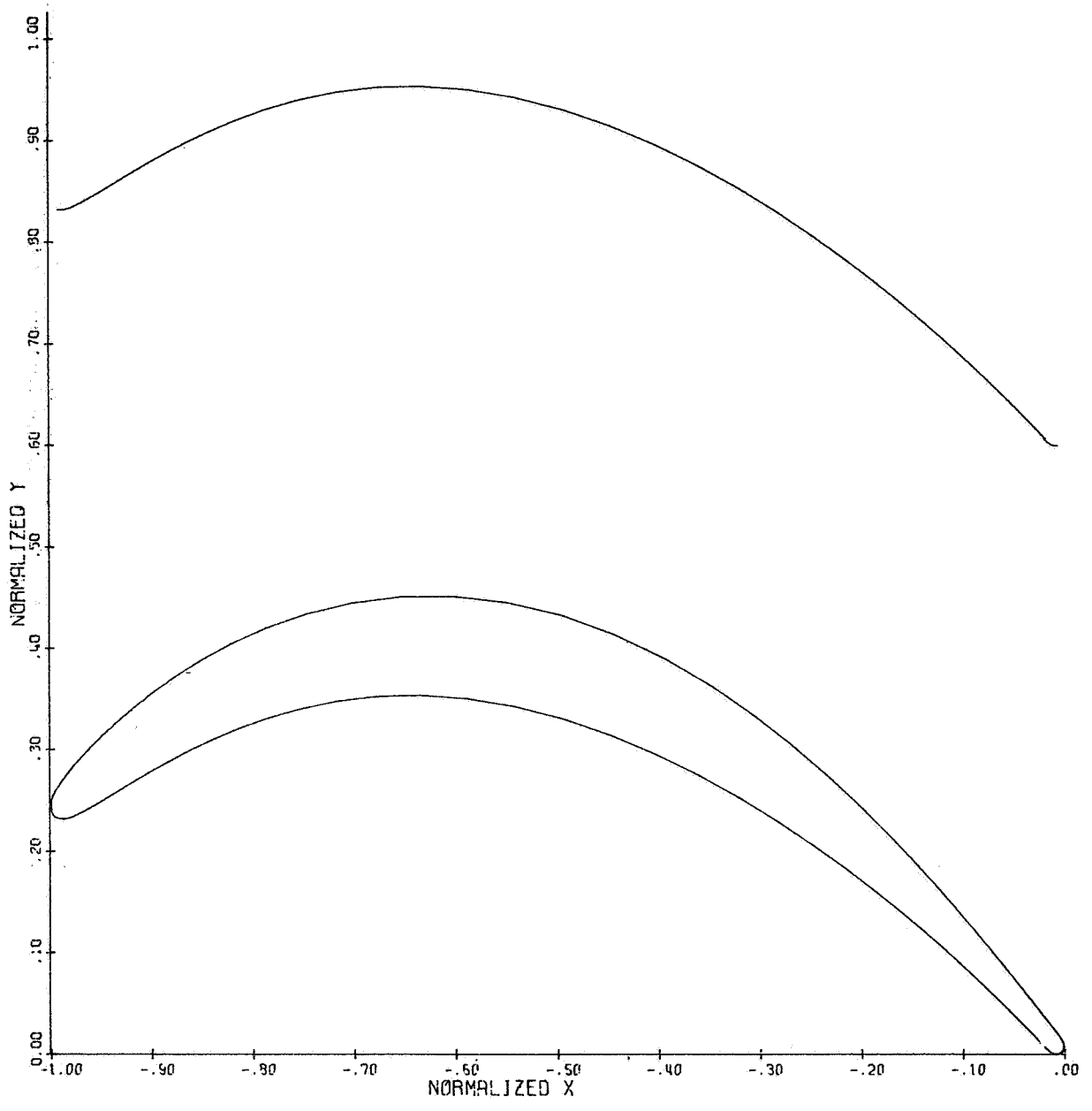

Figure 42. Stage Four Rotor Pitch Airfoil Flowpath.

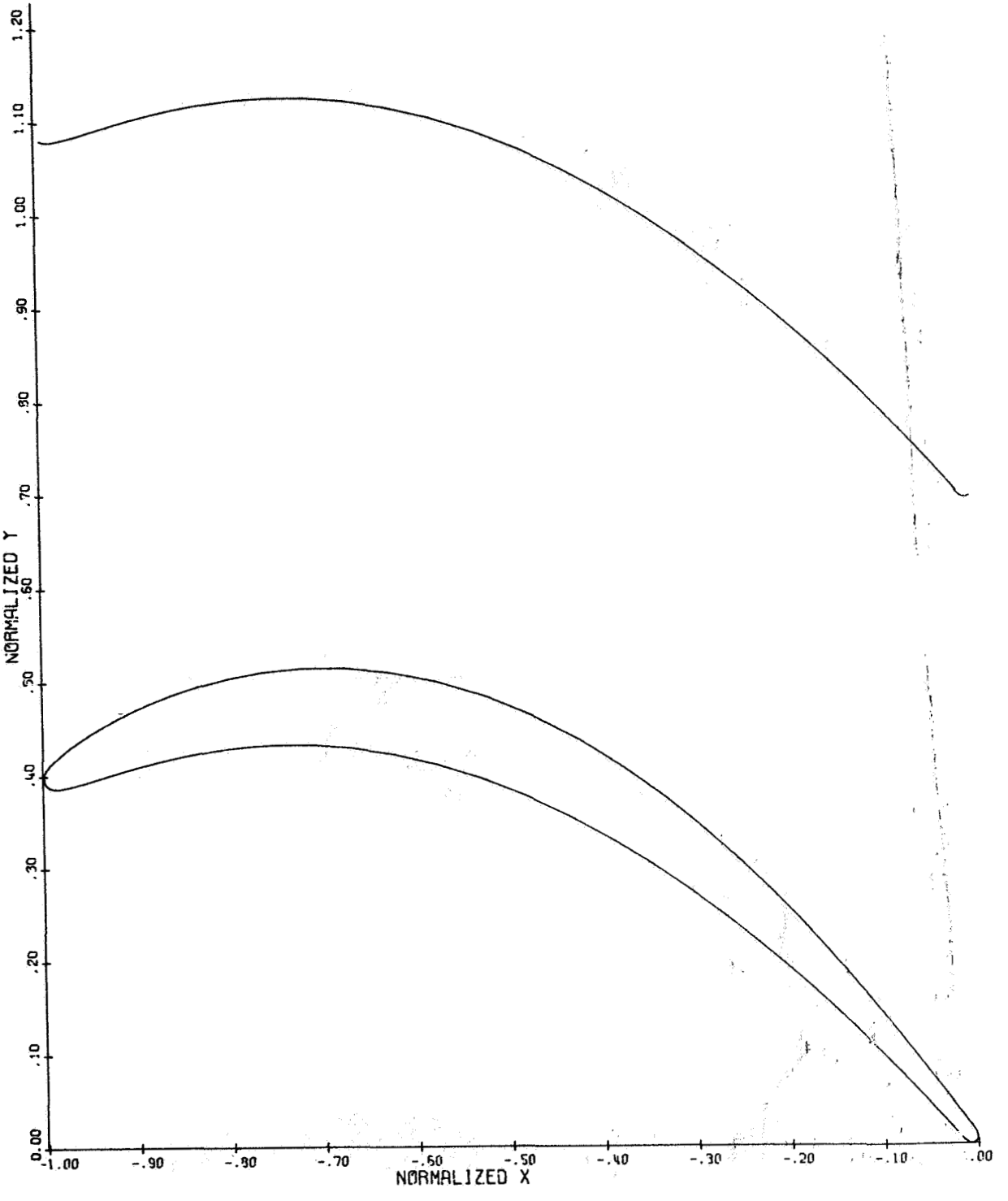

Figure 43. Stage Four Rotor Tip Airfoil Flowpath.

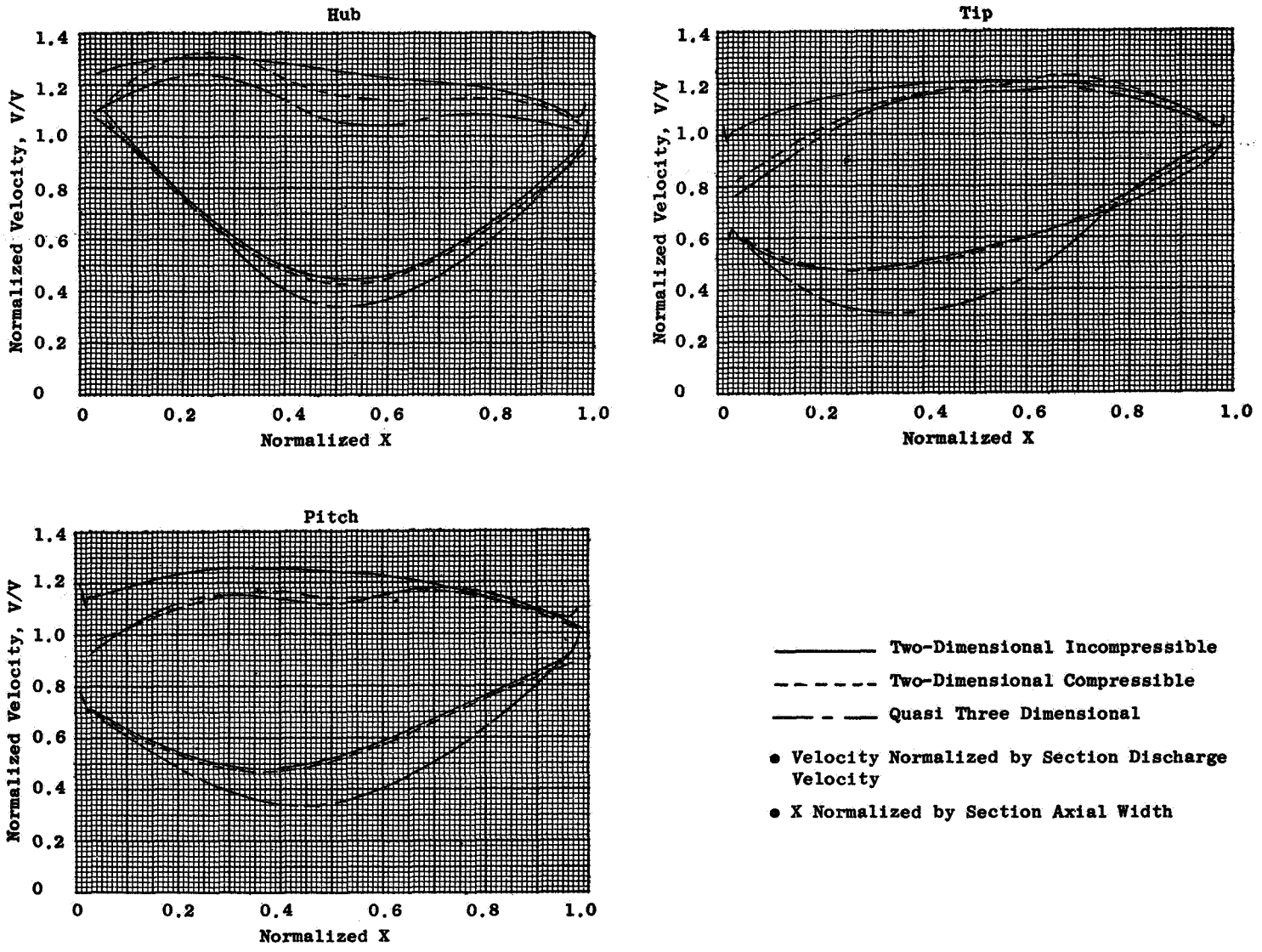

Figure 44. Stage Four Rotor Velocity Distribution.

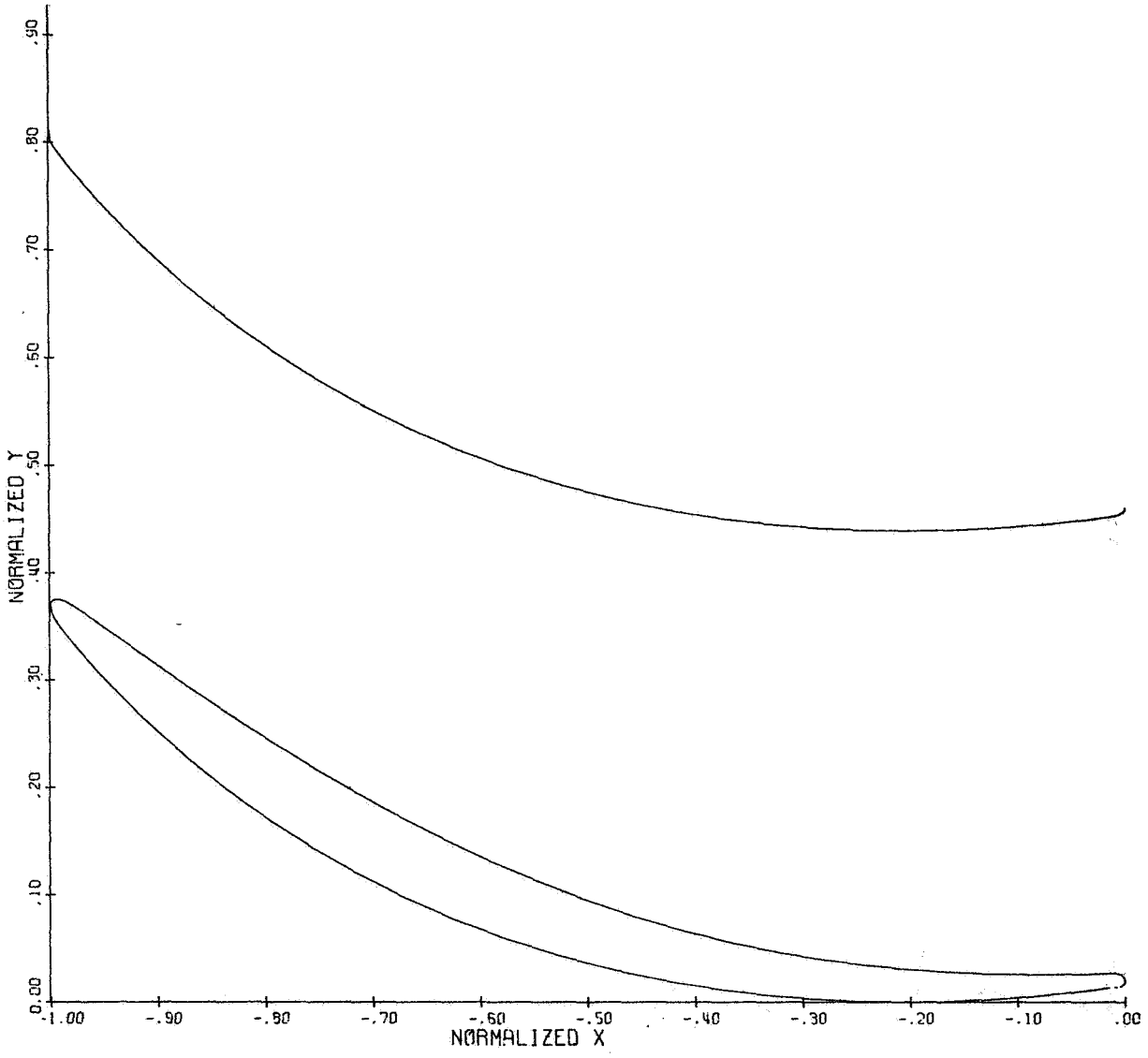

Figure 45. Outlet Turning Vane Hub Airfoil Flowpath.

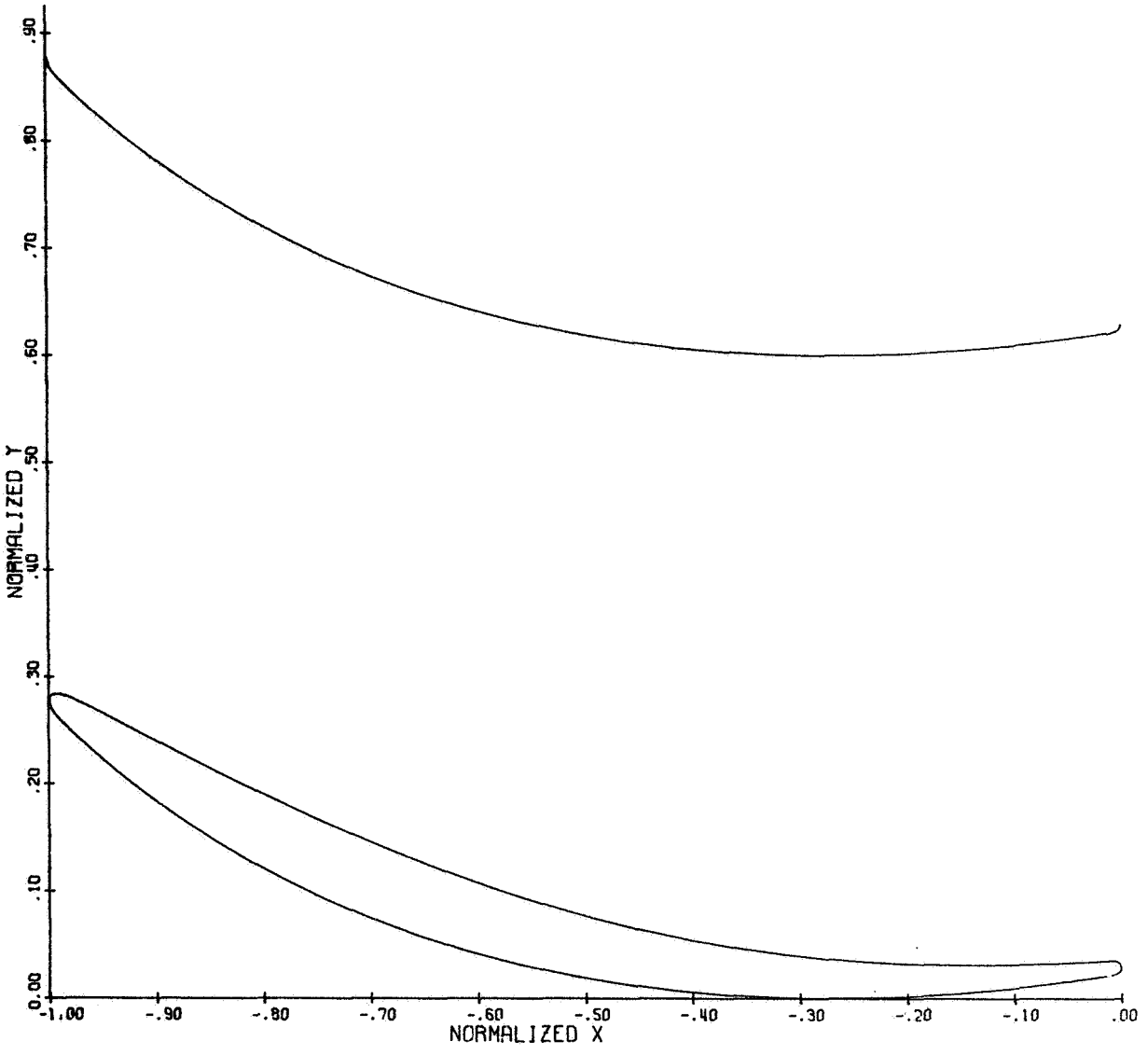

Figure 46. Outlet Turning Vane Pitch Airfoil Flowpath.

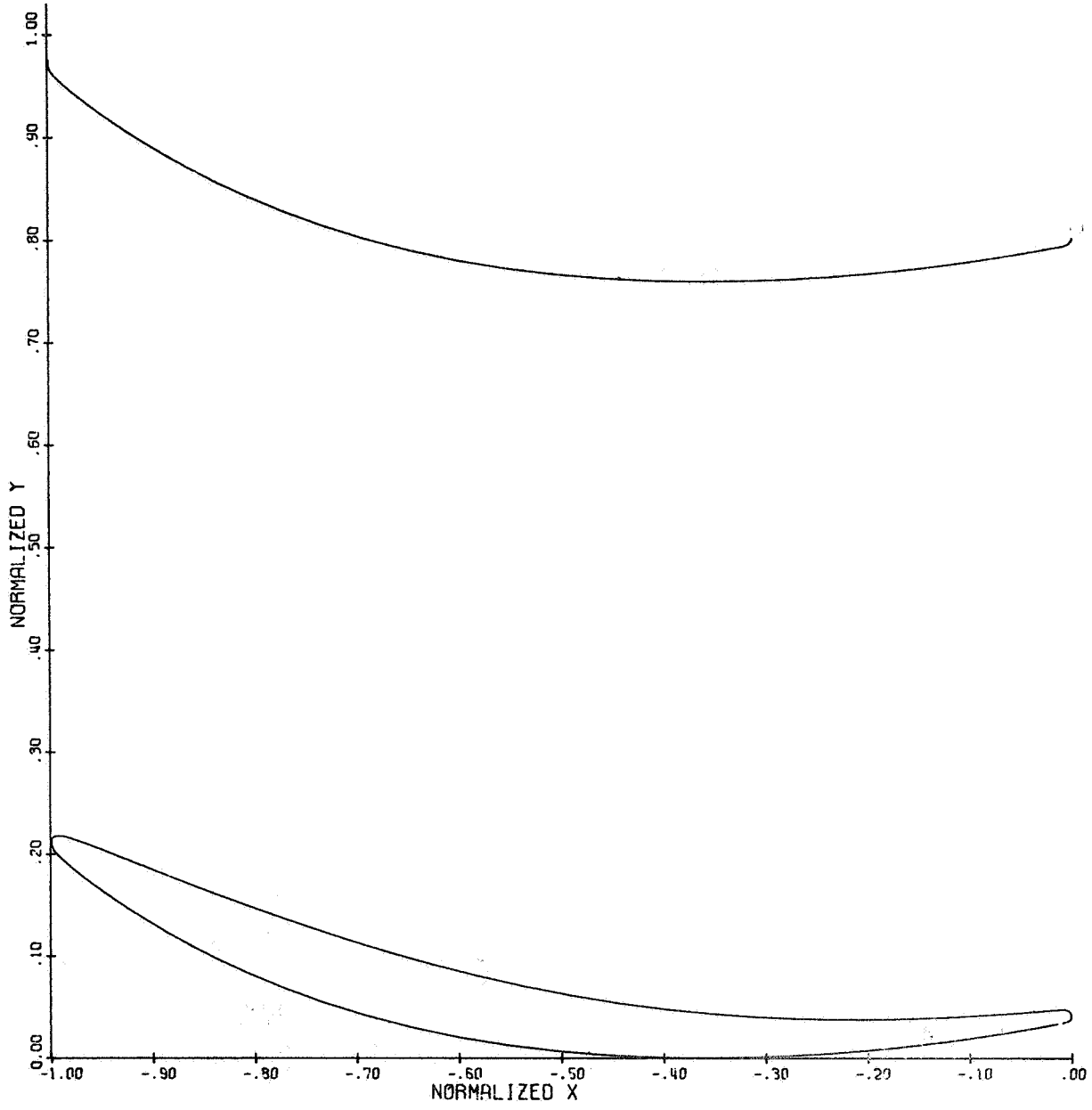

Figure 47. Outlet Turning Vane Tip Airfoil Flowpath.

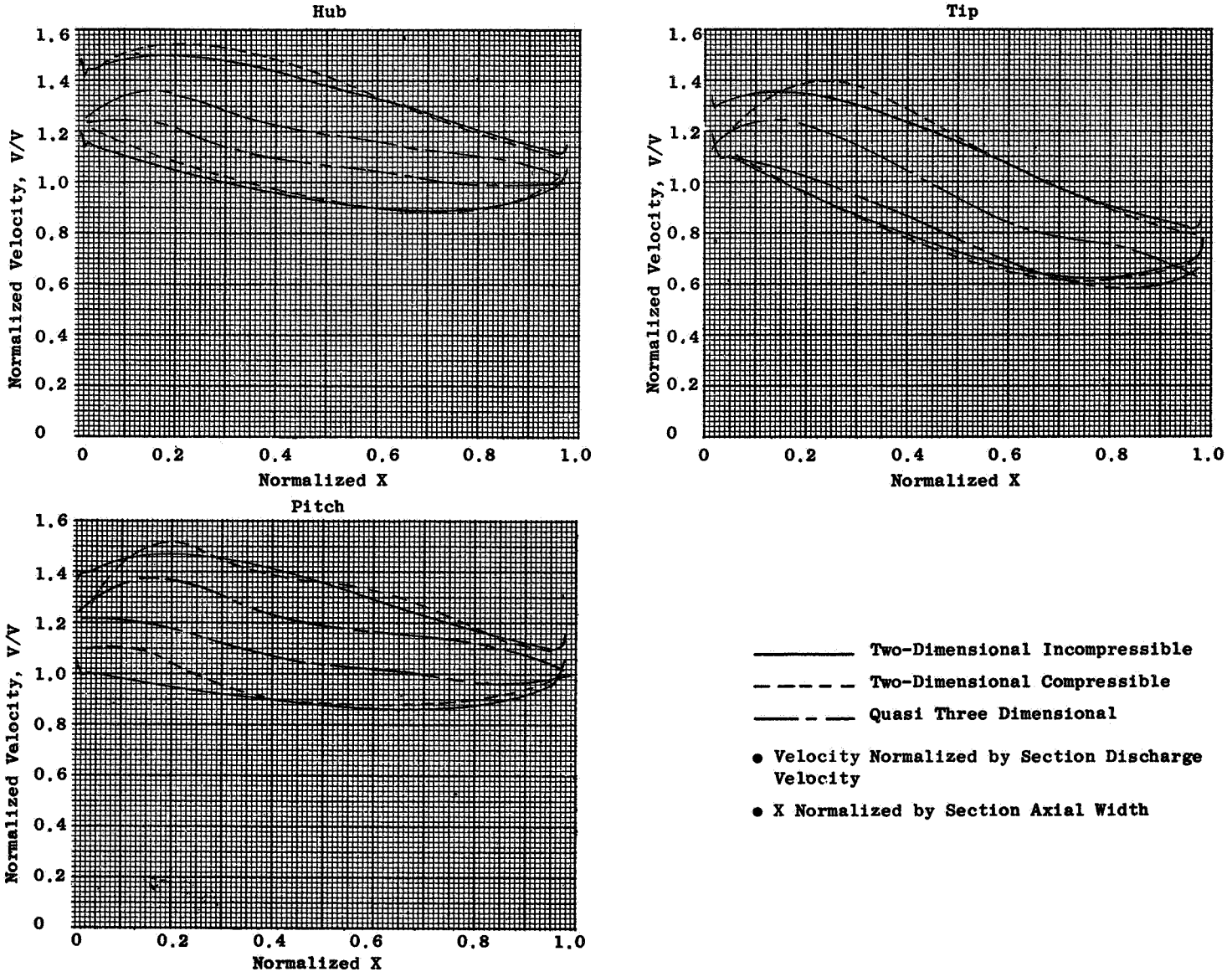

Figure 48. Outlet Turning Vane Velocity Distribution.

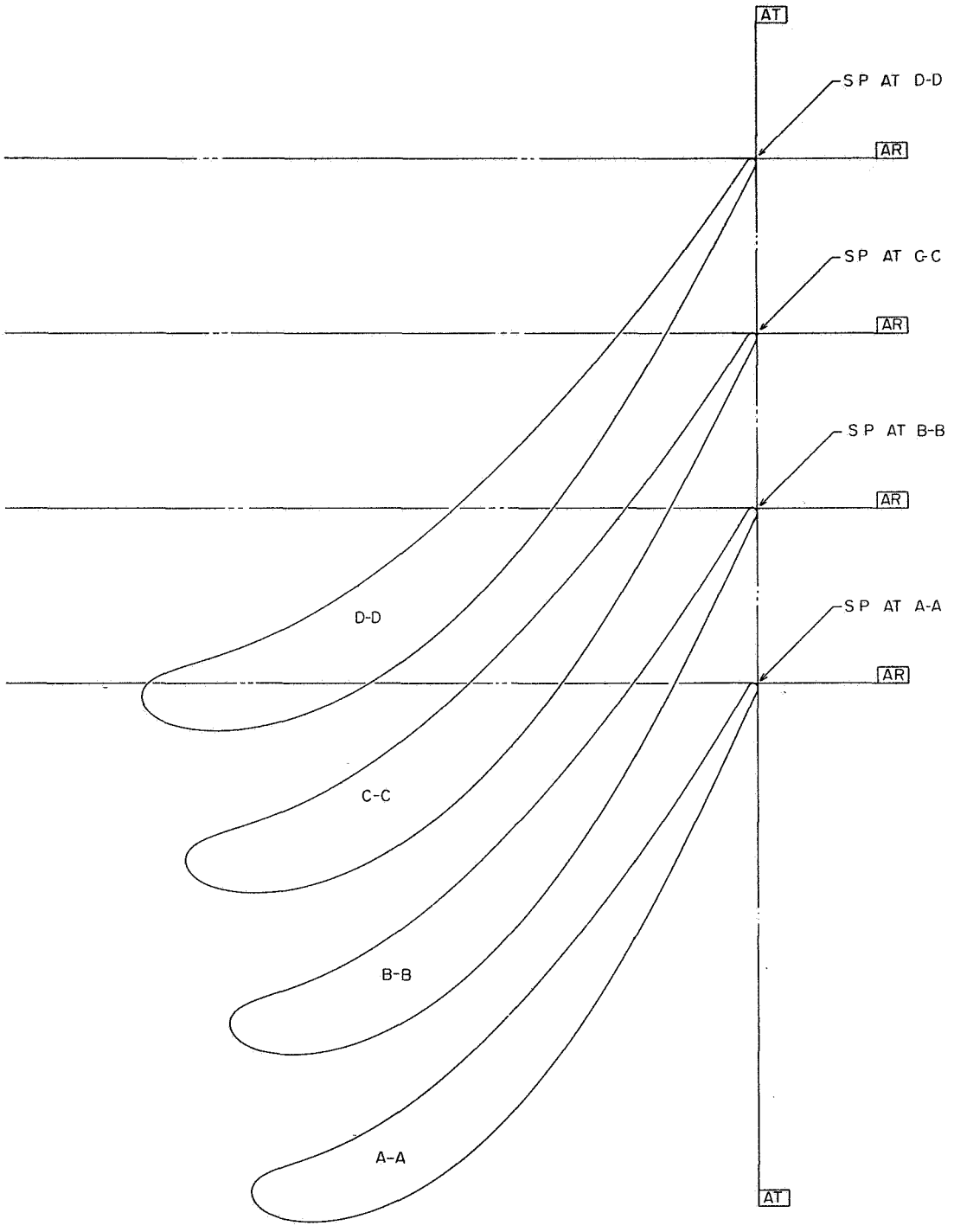

Figure 49. Stage One Vane Precision Master (4013164-009).

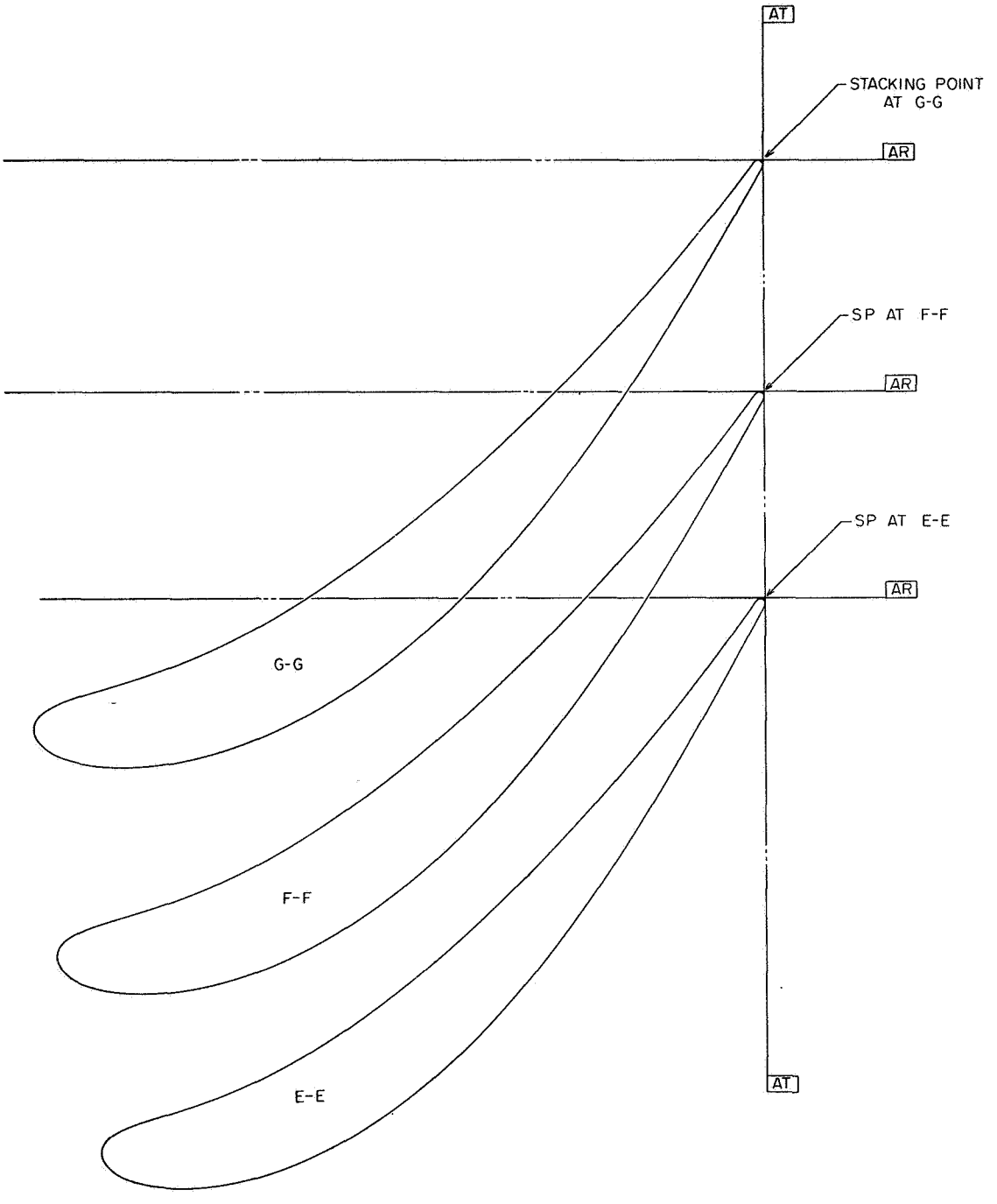

Figure 49. Stage One Vane Precision Master (Concluded).

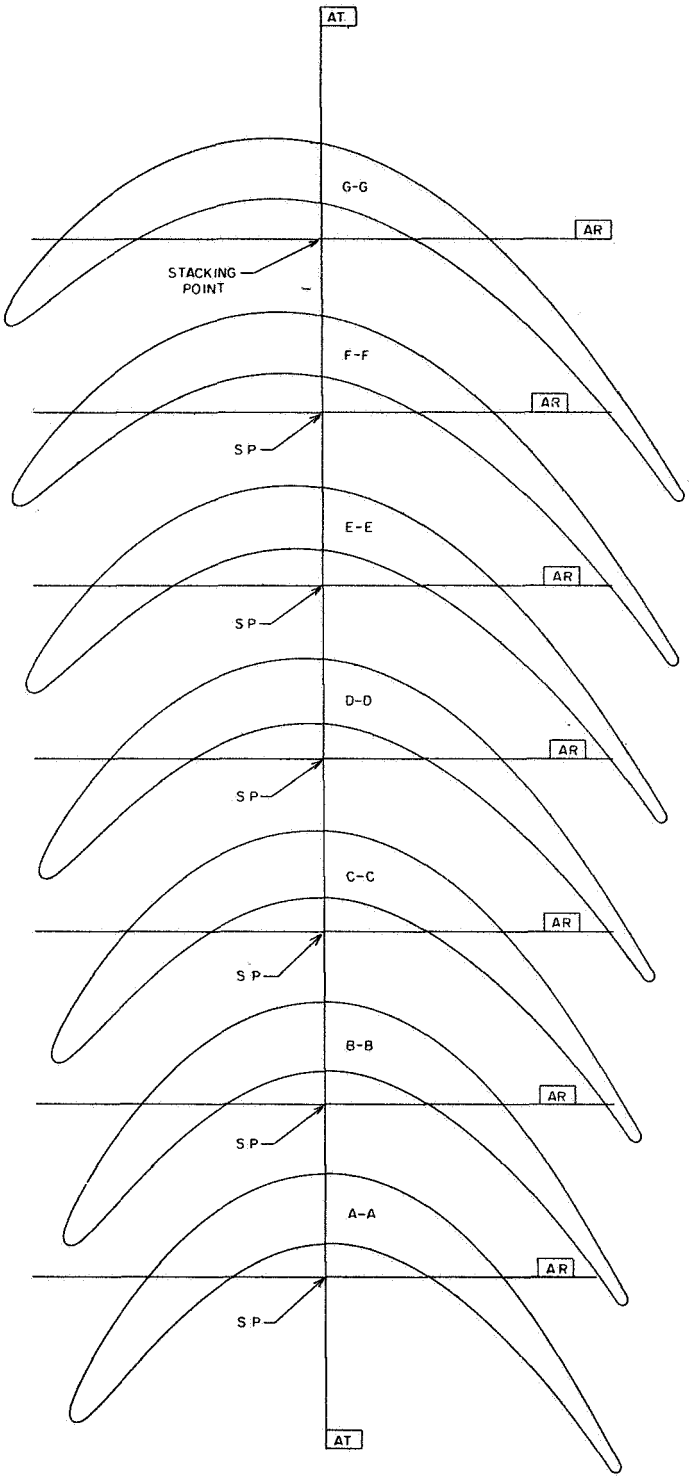

Figure 50. Stage One Rotor Precision Master (4013164-001).

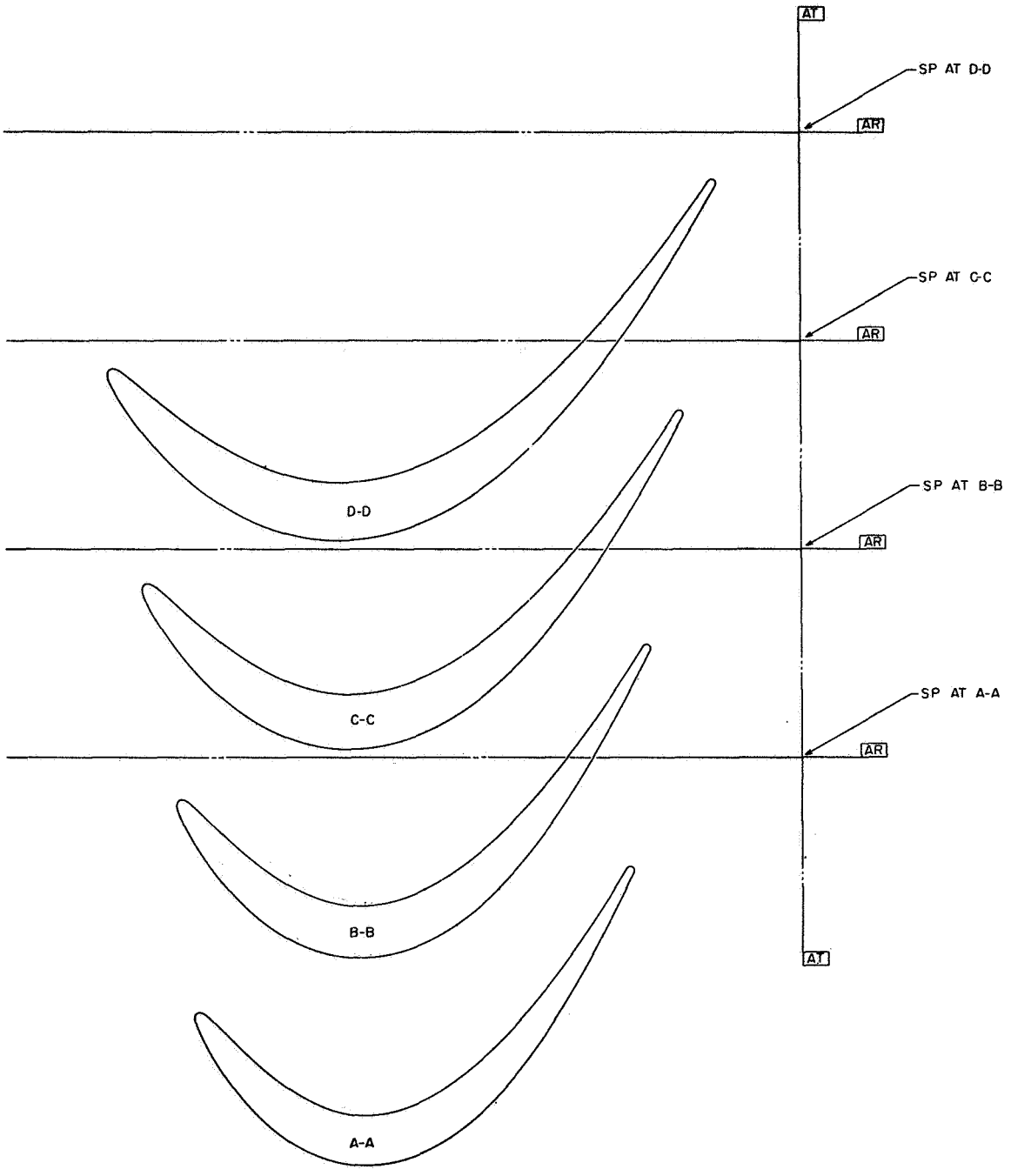

Figure 51. Stage Two Vane Precision Master (4013164-011).

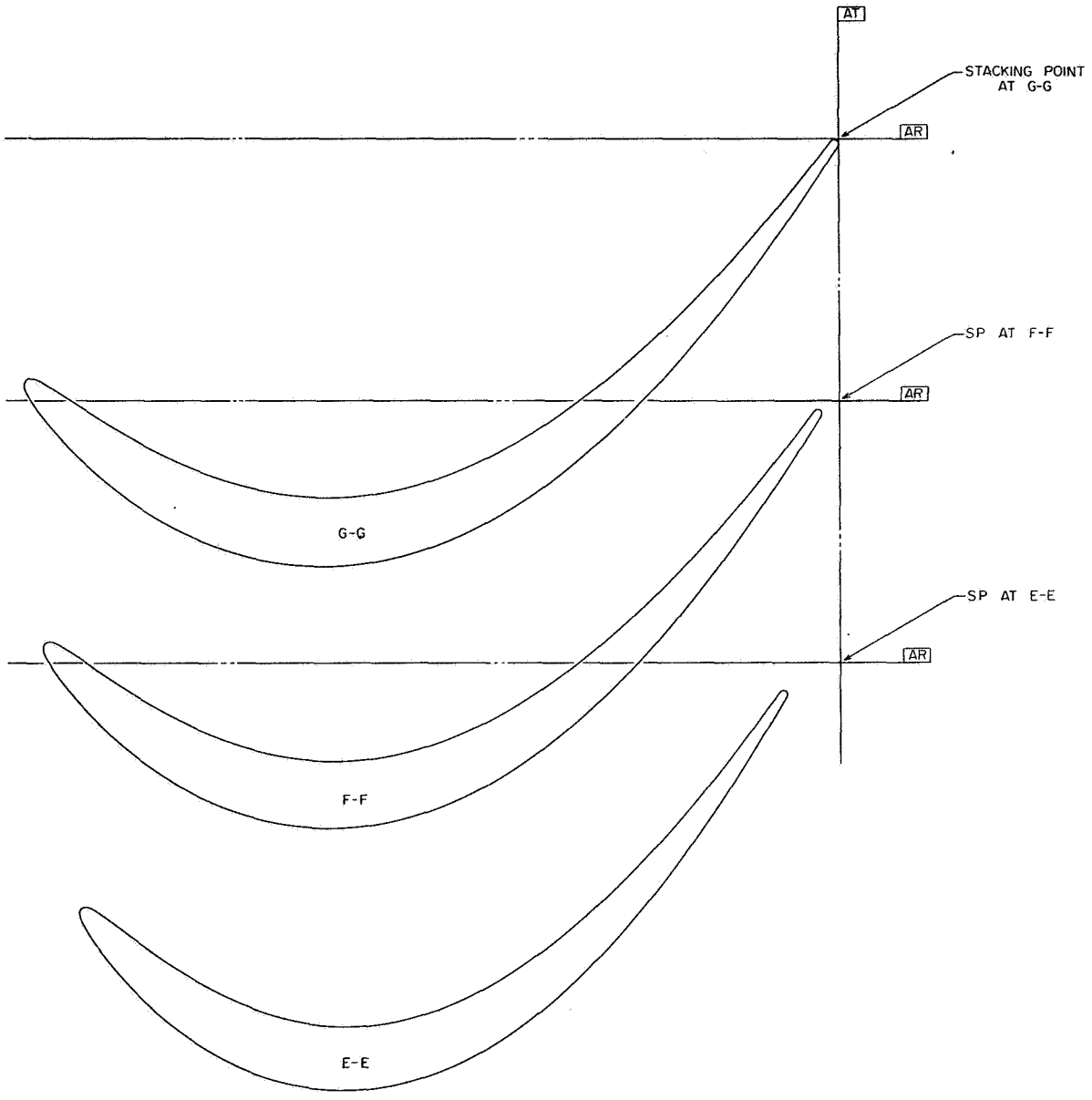

Figure 51. Stage Two Vane Precision Master (Concluded).

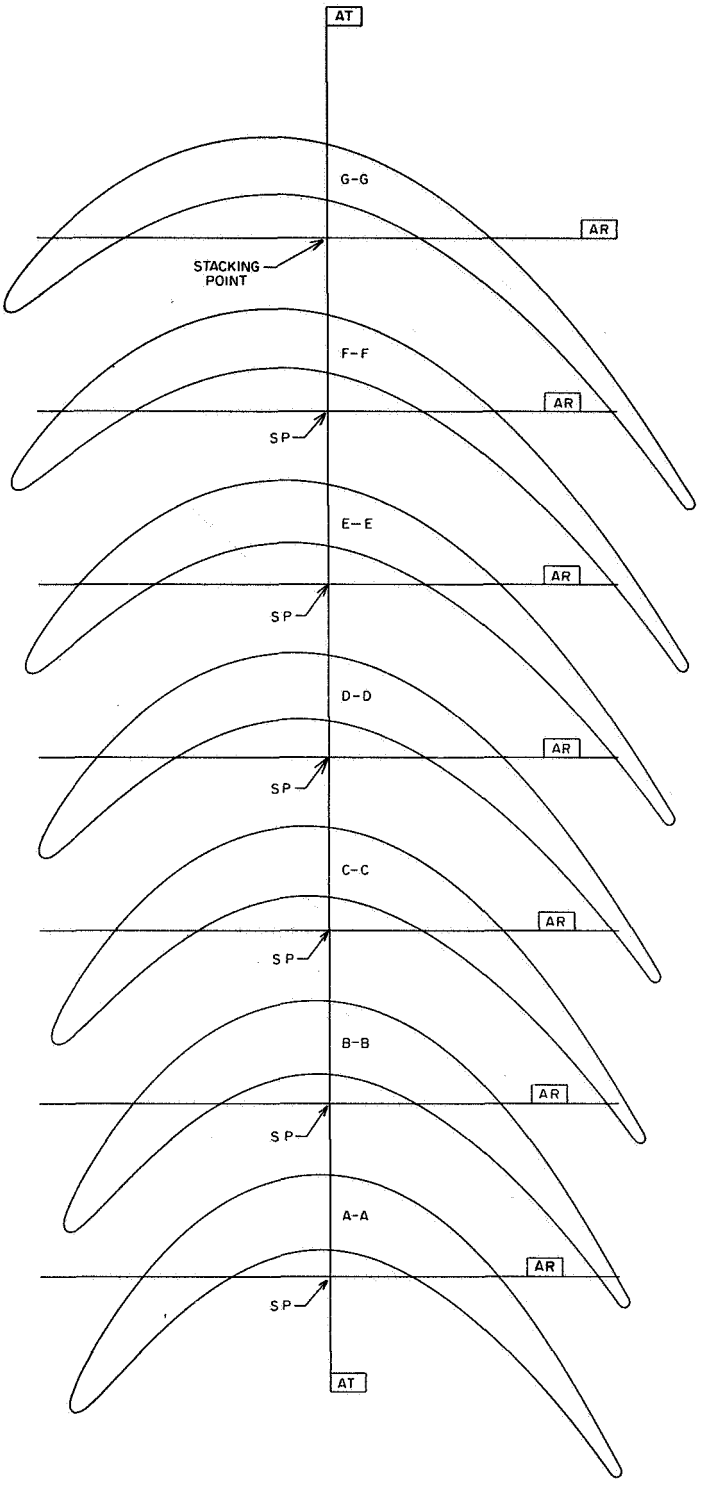

Figure 52. Stage Two Rotor Precision Master (4013164-003).

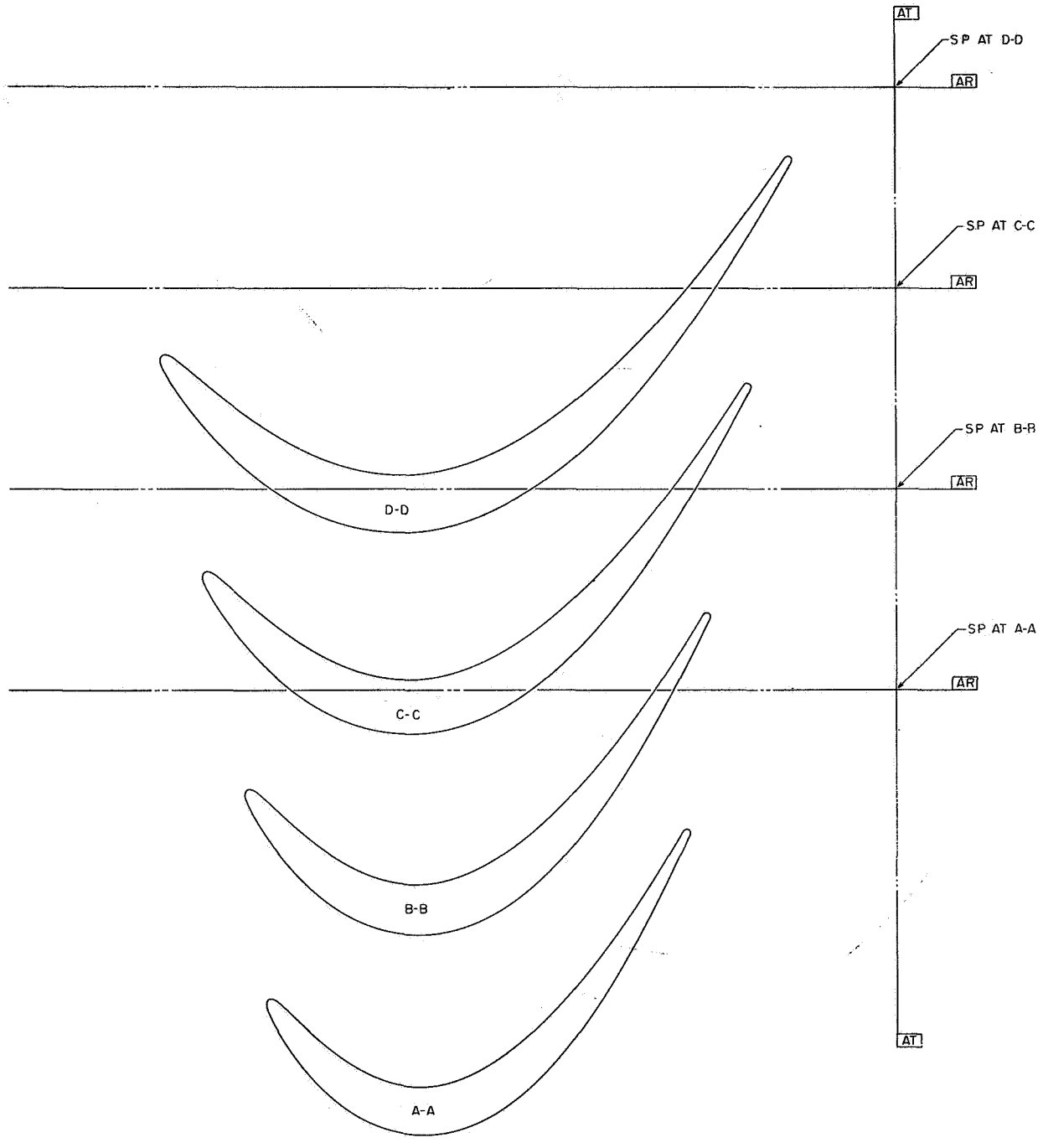

Figure 53. Stage Three Vane Precision Master (4013164-013).

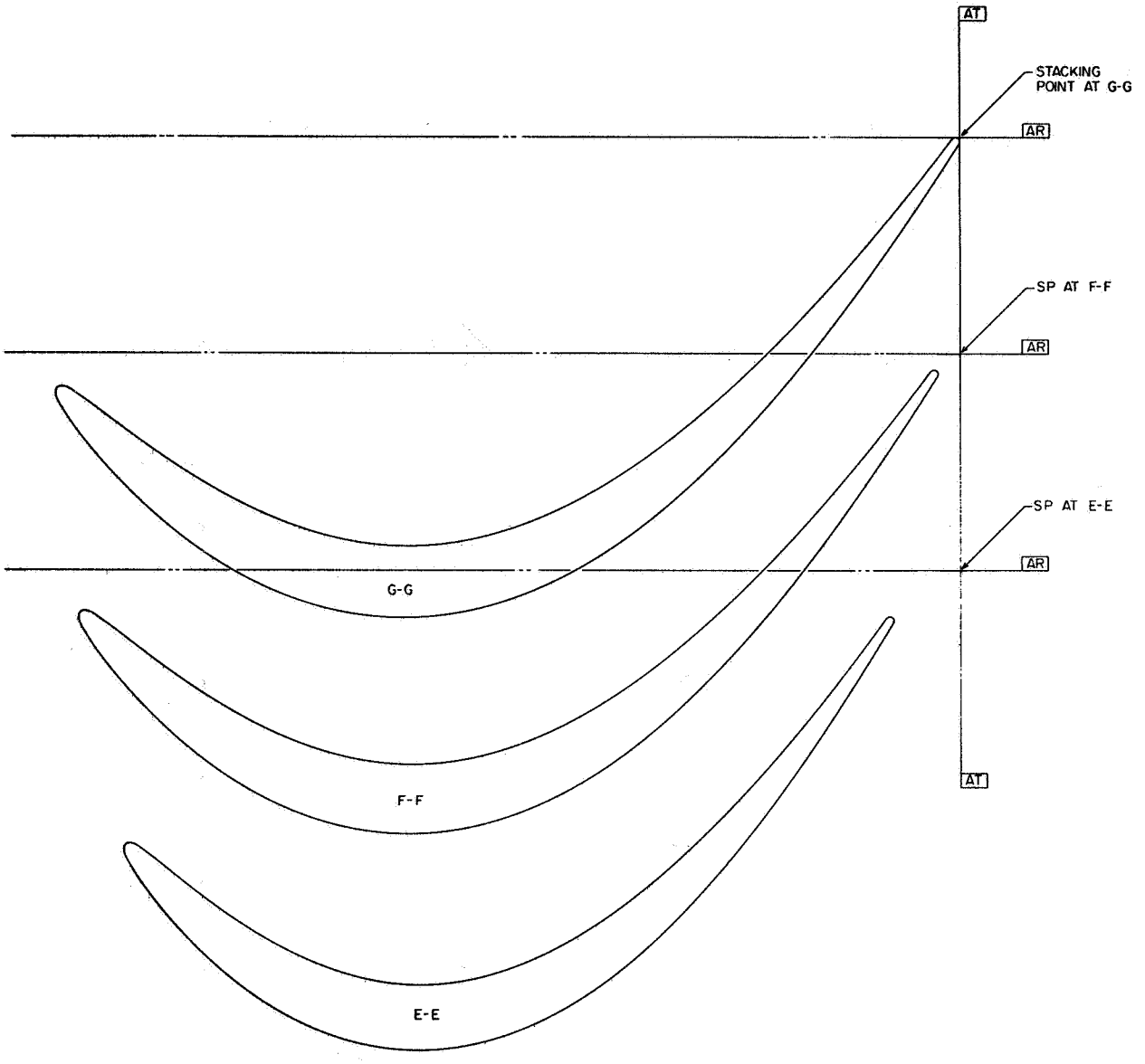

Figure 53. Stage Three Vane Precision Master (Concluded).

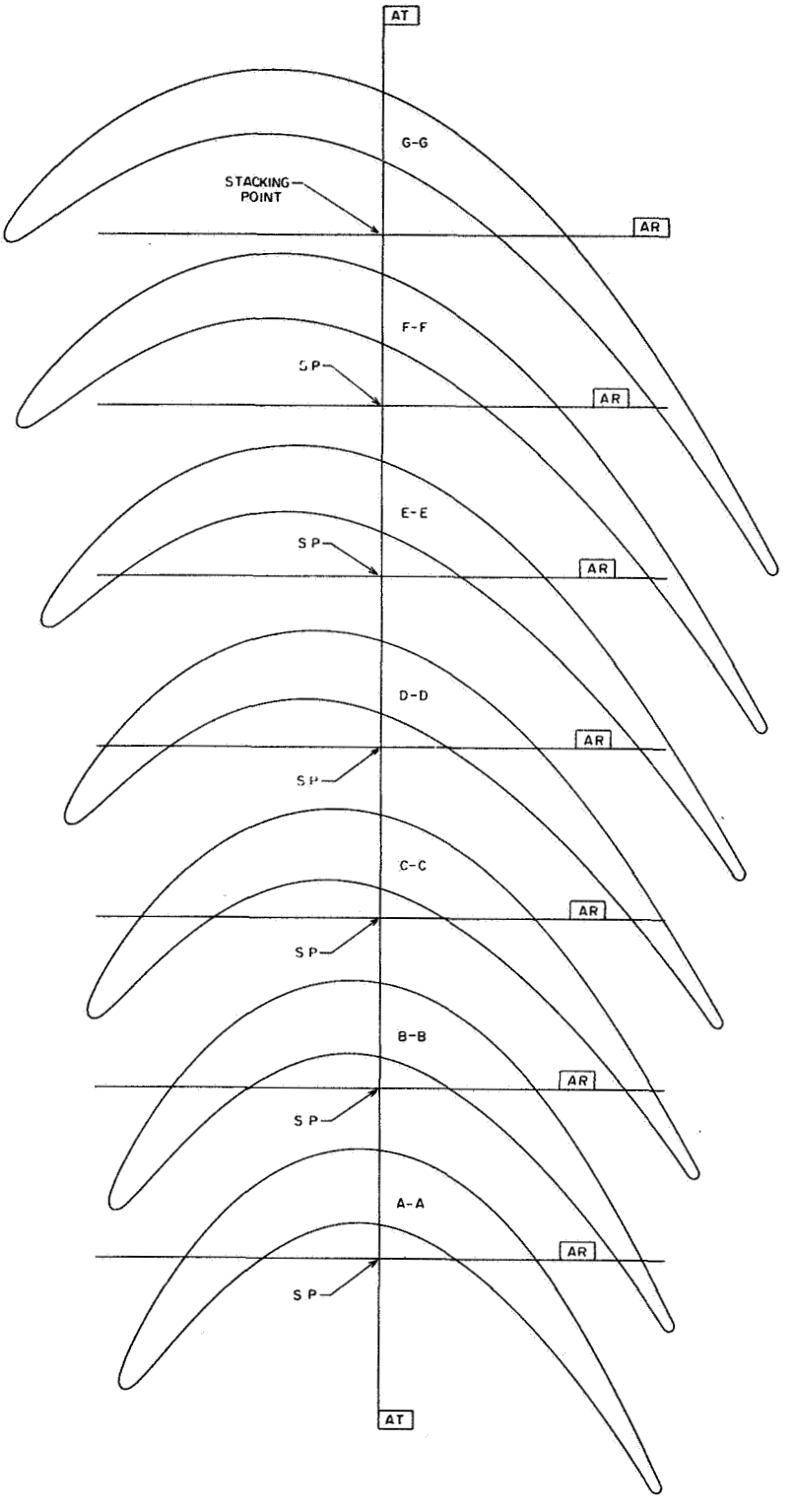

Figure 54. Stage Three Rotor Precision Master (4013164-005).

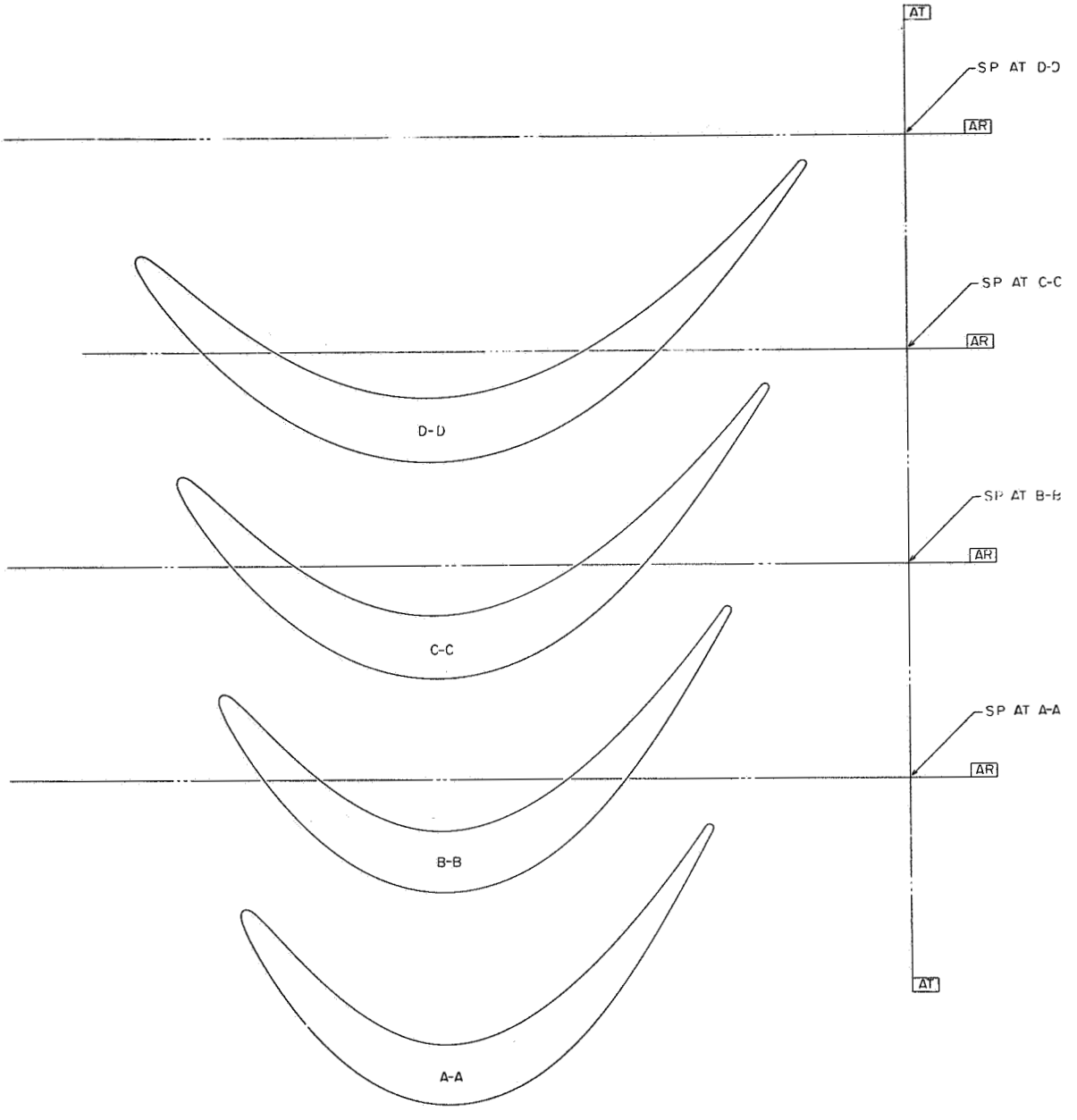

Figure 55. Stage Four Vane Precision Master (4013164-015).

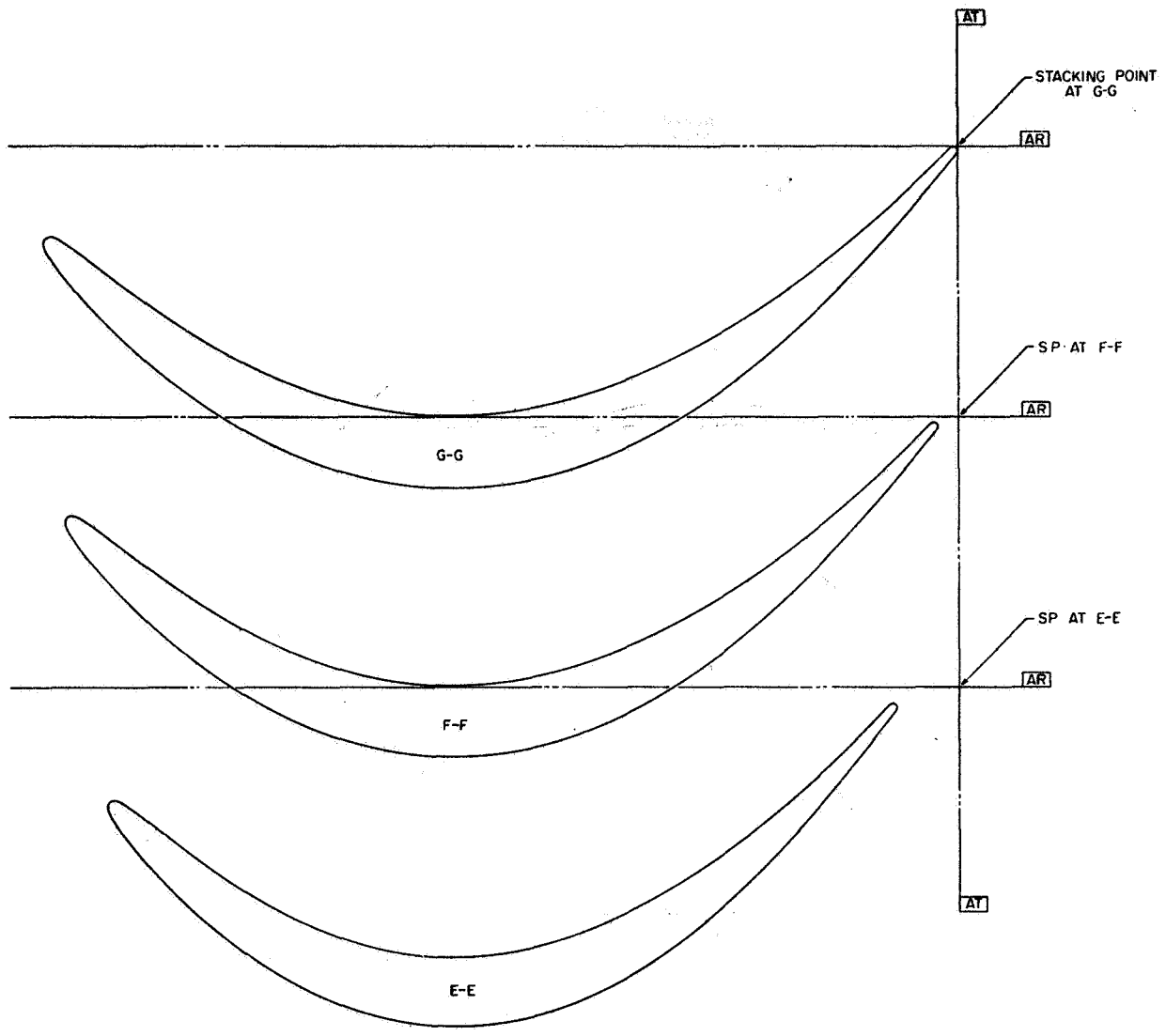

Figure 55. Stage Four Vane Precision Master (Concluded).

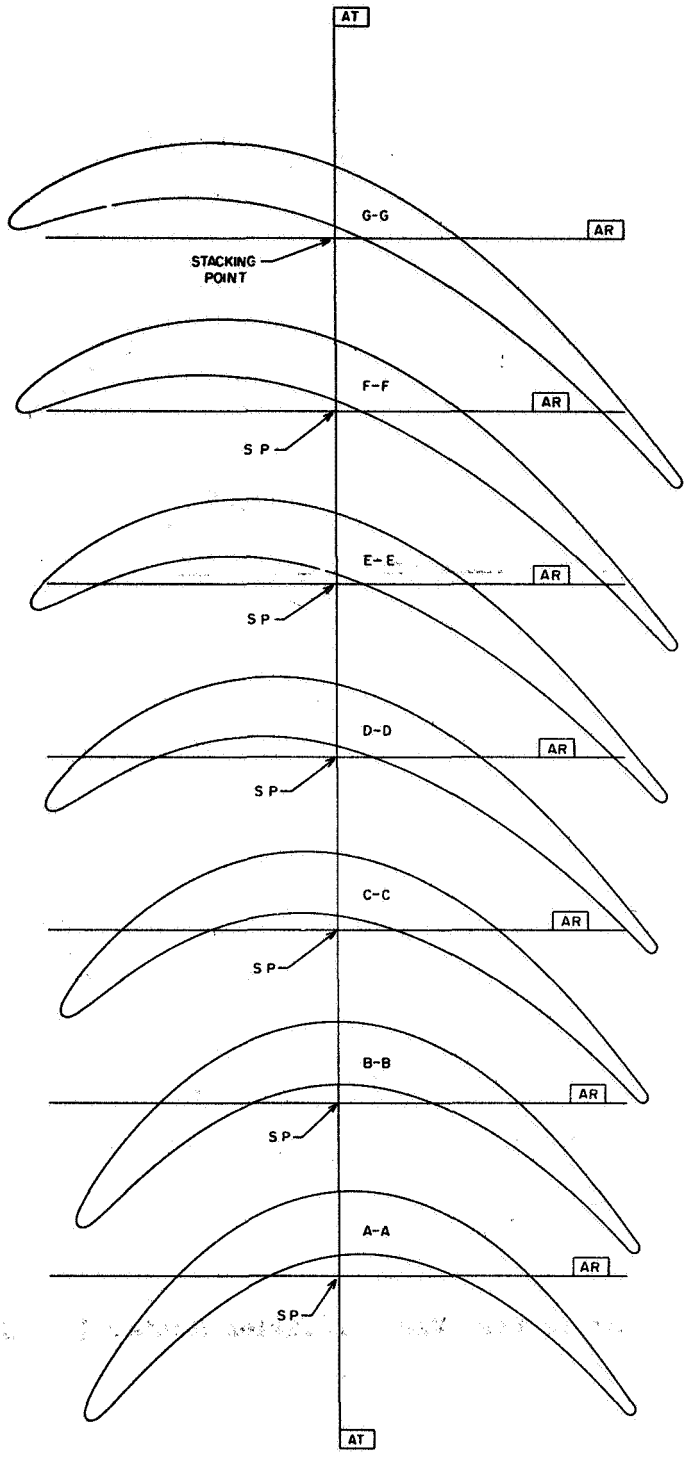

Figure 56. Stage Four Rotor Precision Master (4013164-007).

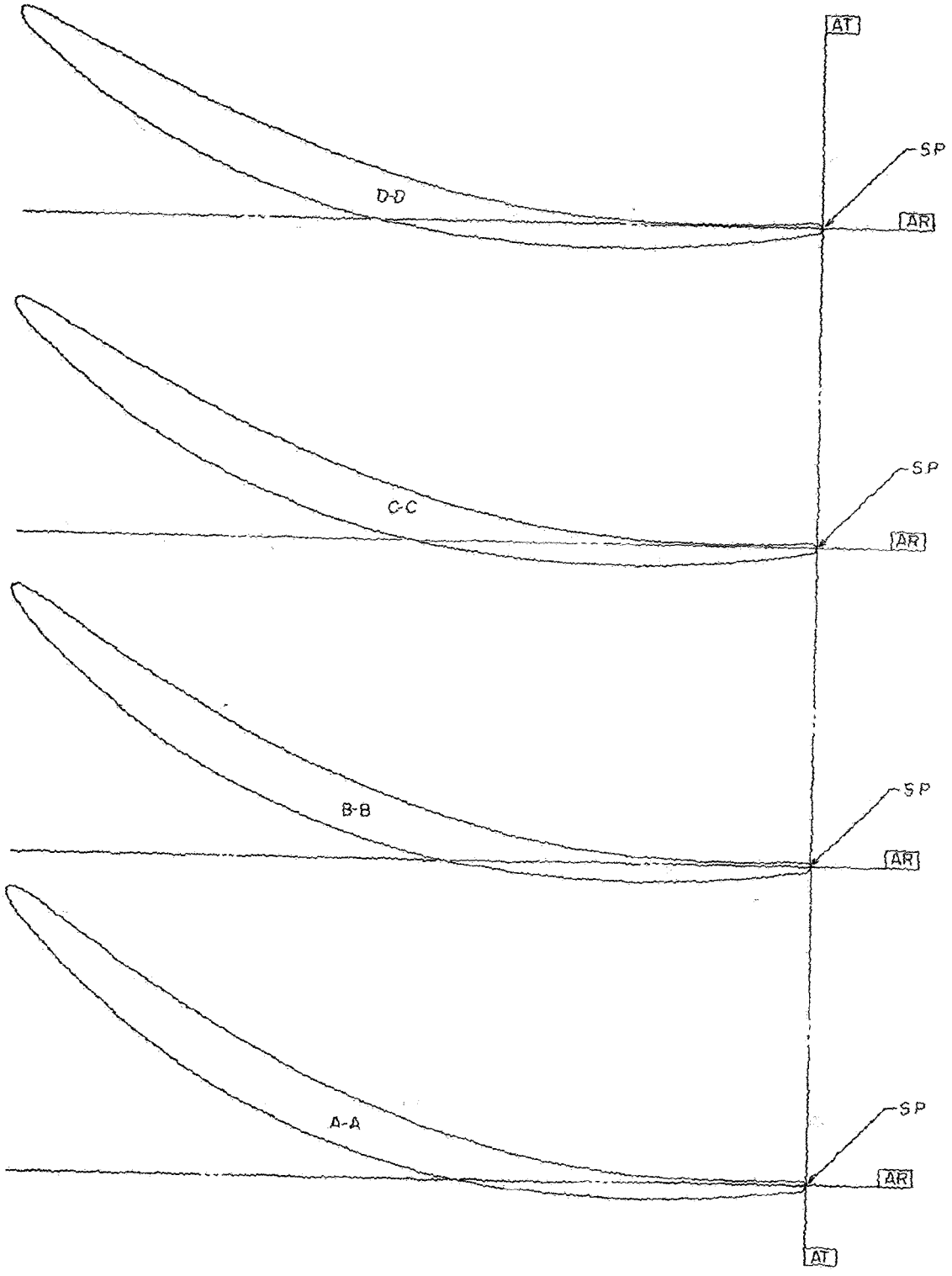

Figure 57. Outlet Turning Vane Precision Master (4013164-017).

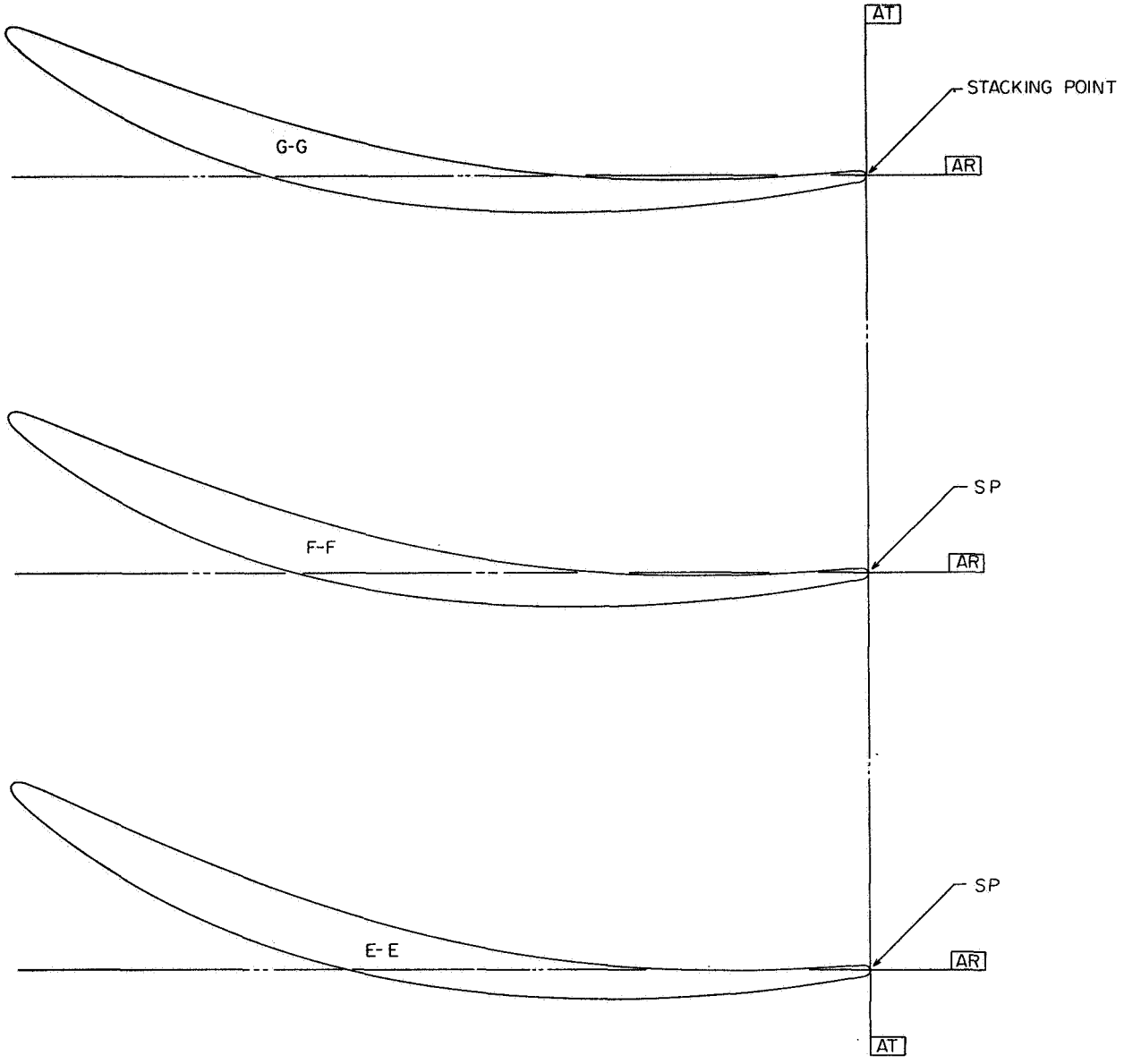

Figure 57. Outlet Turning Vane Precision Master (Concluded).

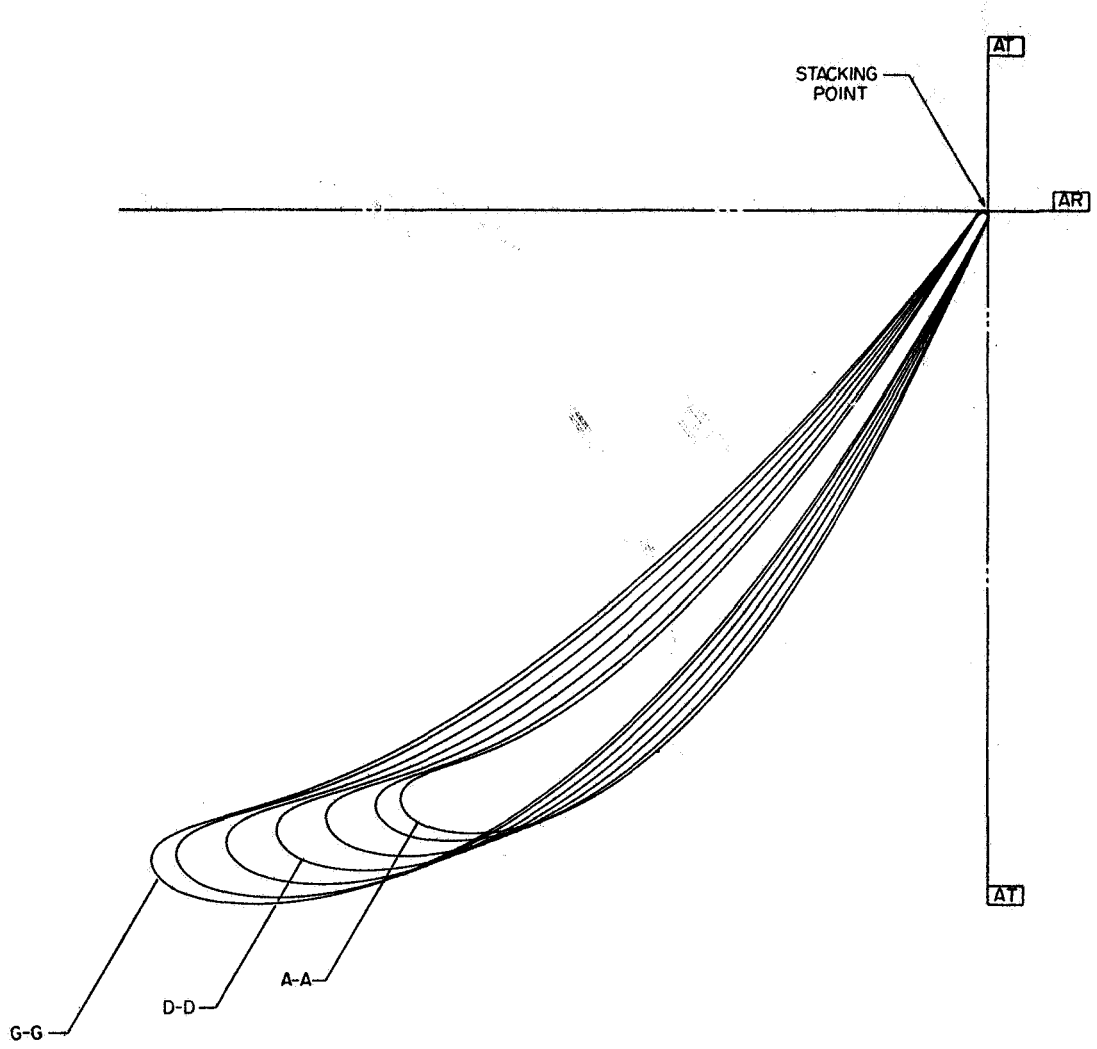

Figure 58. Stage One Vane Stackup (4013164-010).

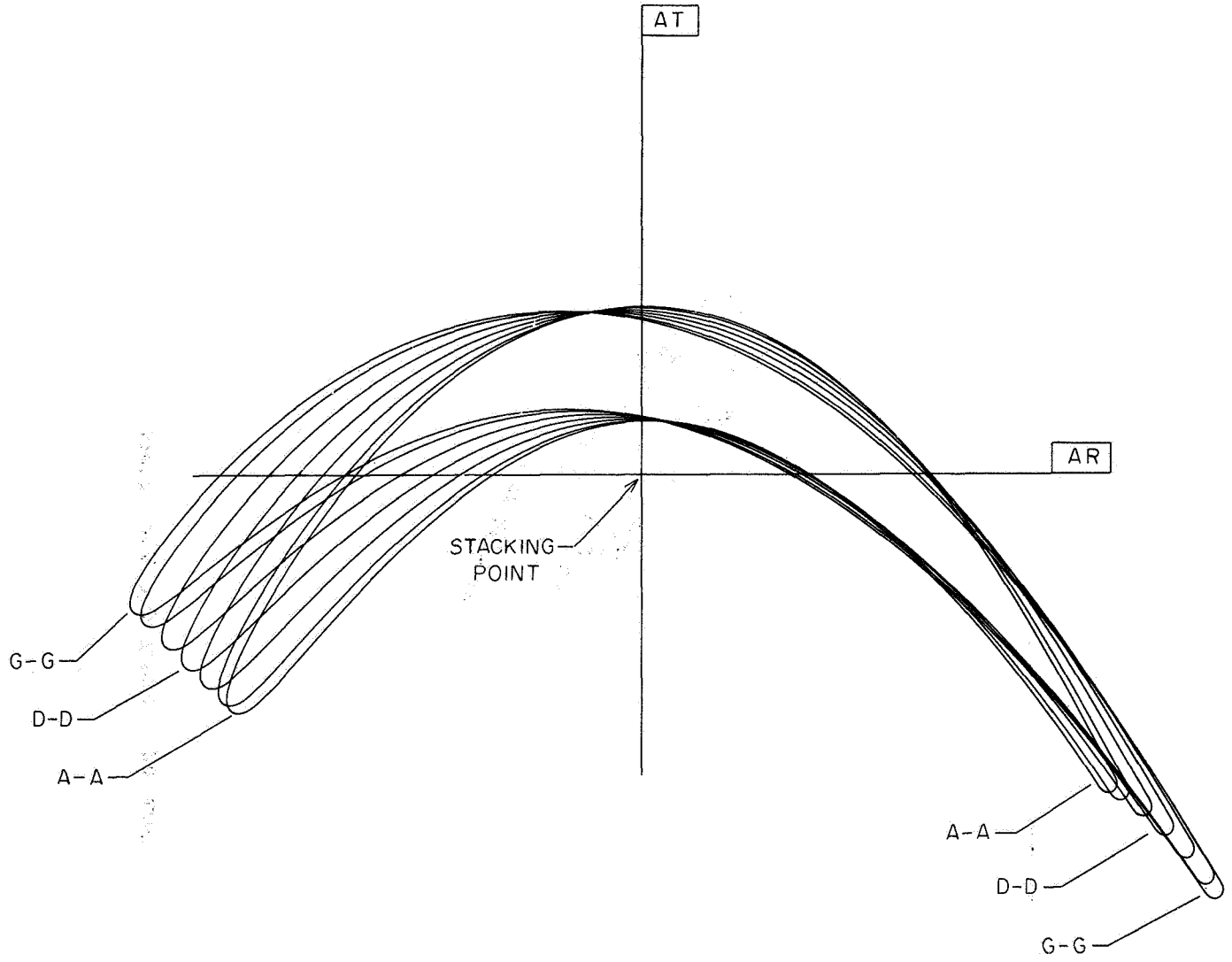

Figure 59. Stage One Rotor Stackup (4013164-002).

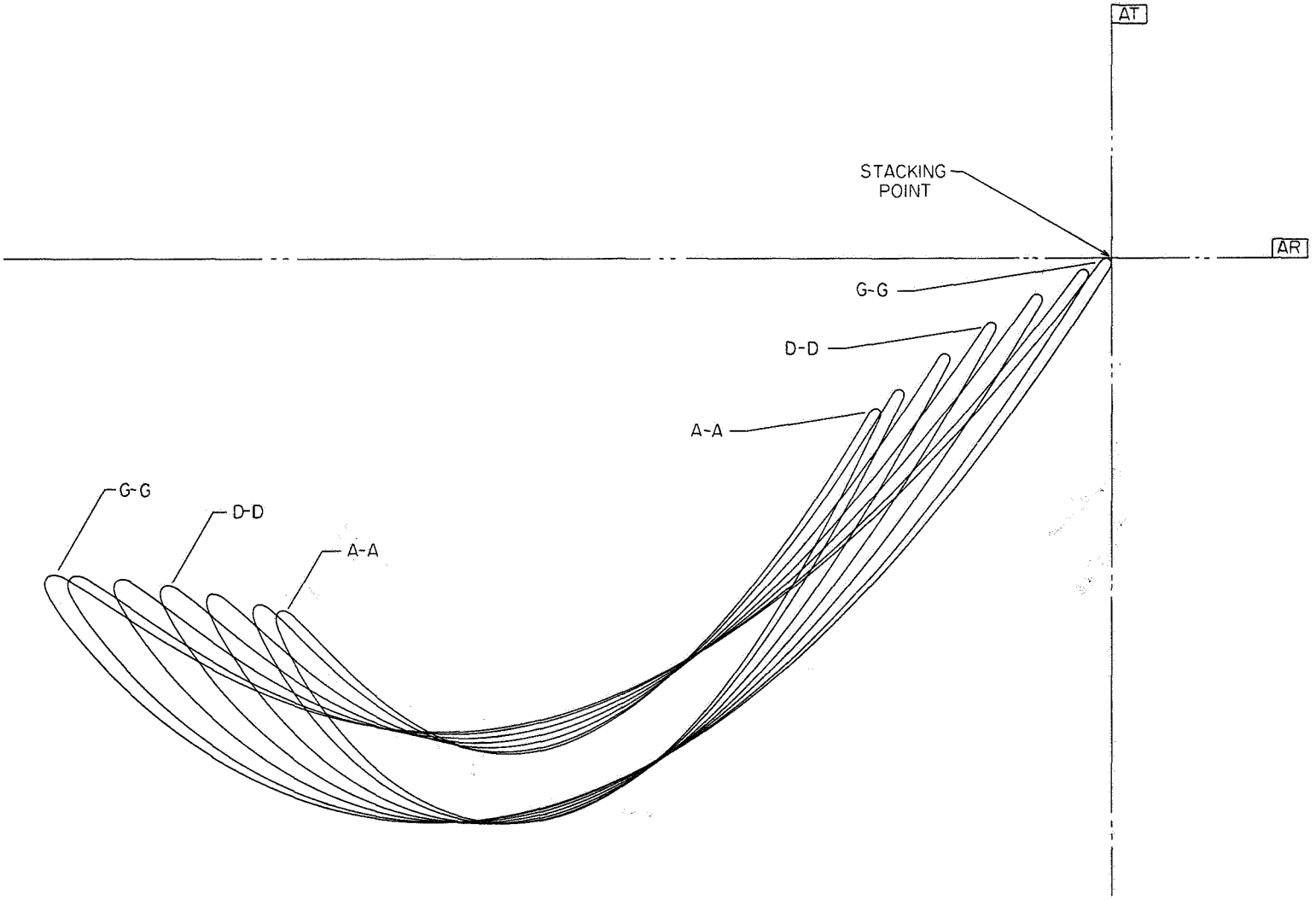

Figure 60. Stage Two Vane Stackup (4013164-012).

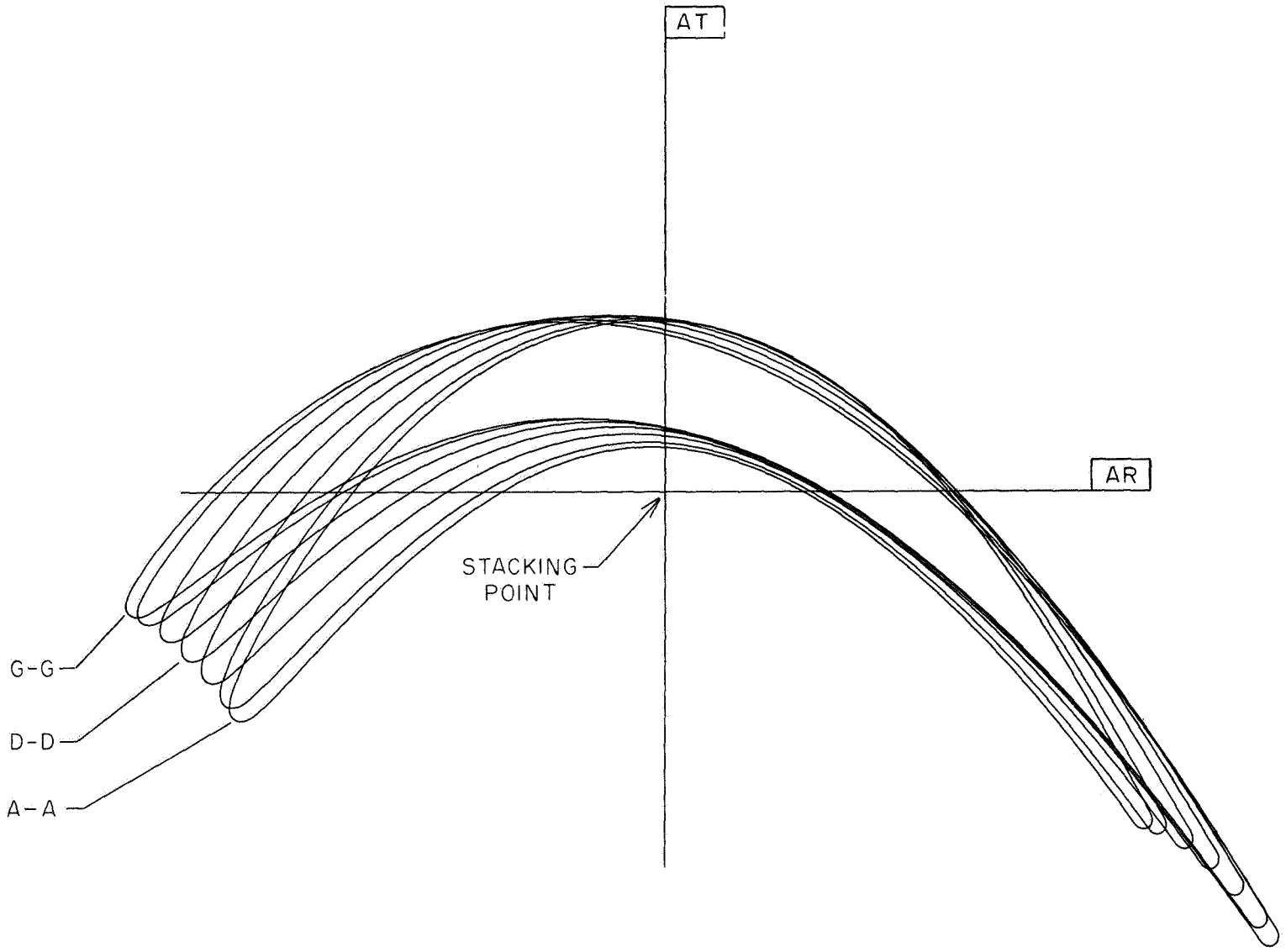

Figure 61. Stage Two Rotor Stackup (4013164-004).

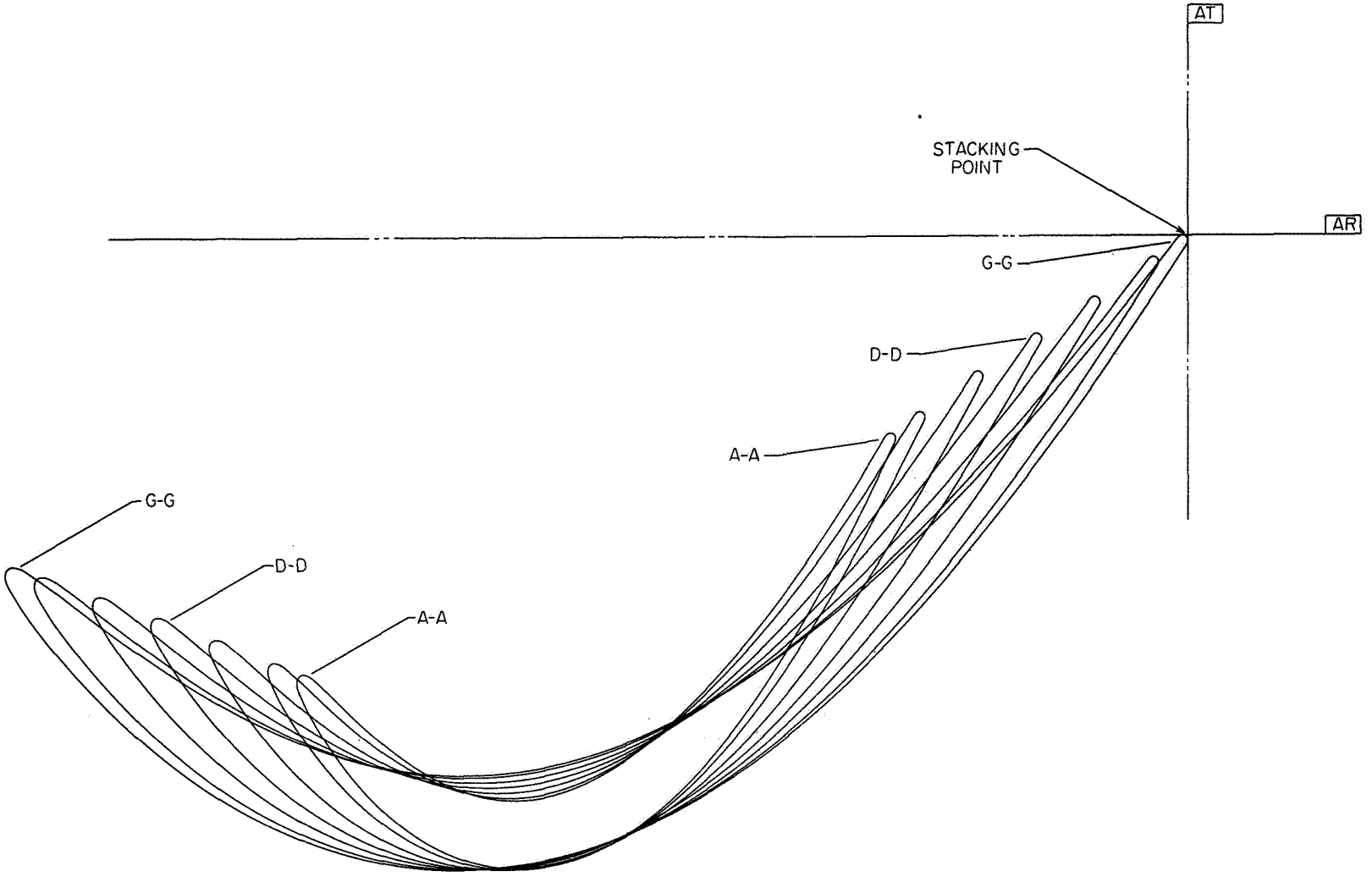

Figure 62. Stage Three Vane Stackup (4013164-014).

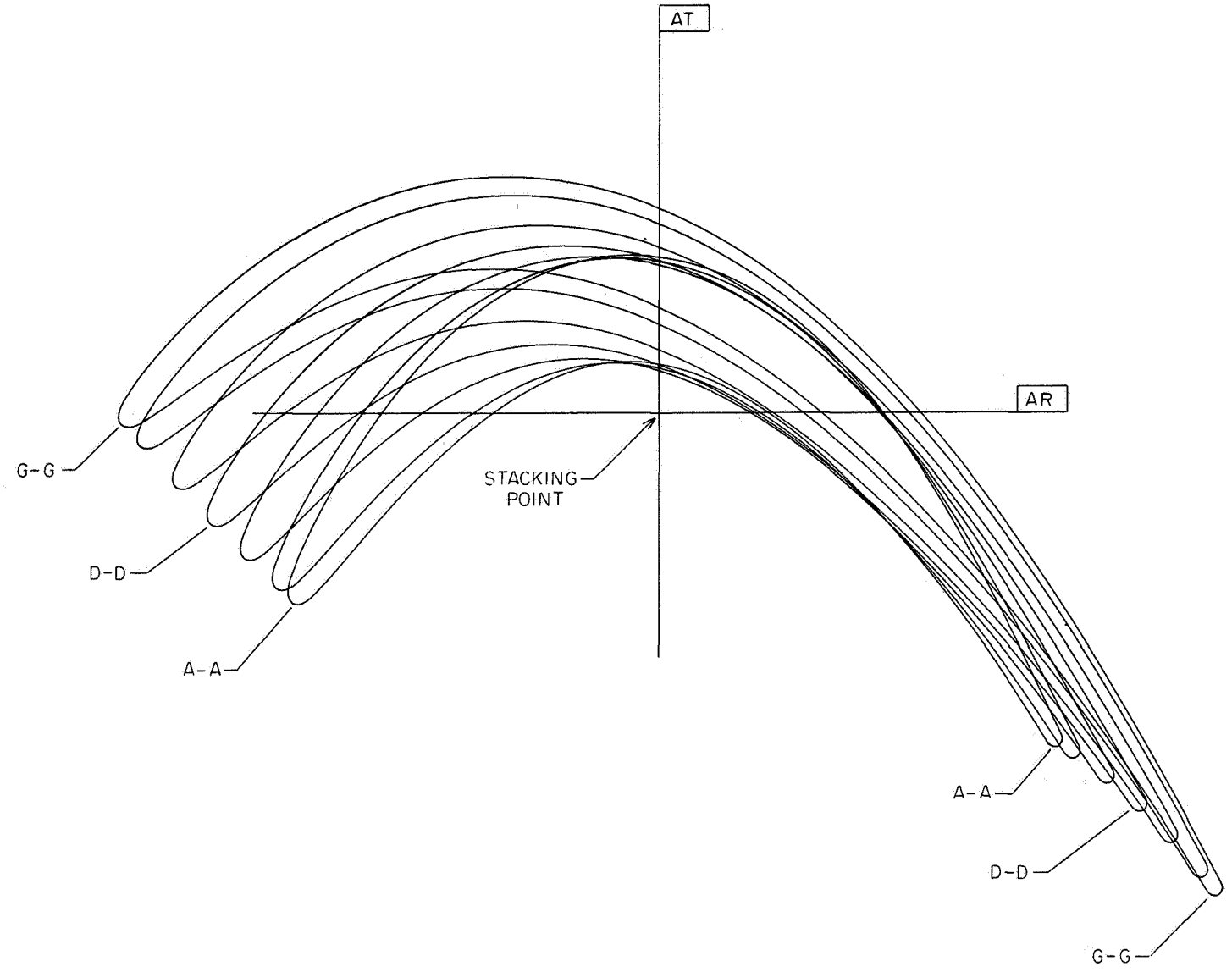

Figure 63. Stage Three Rotor Stackup (4013164-006).

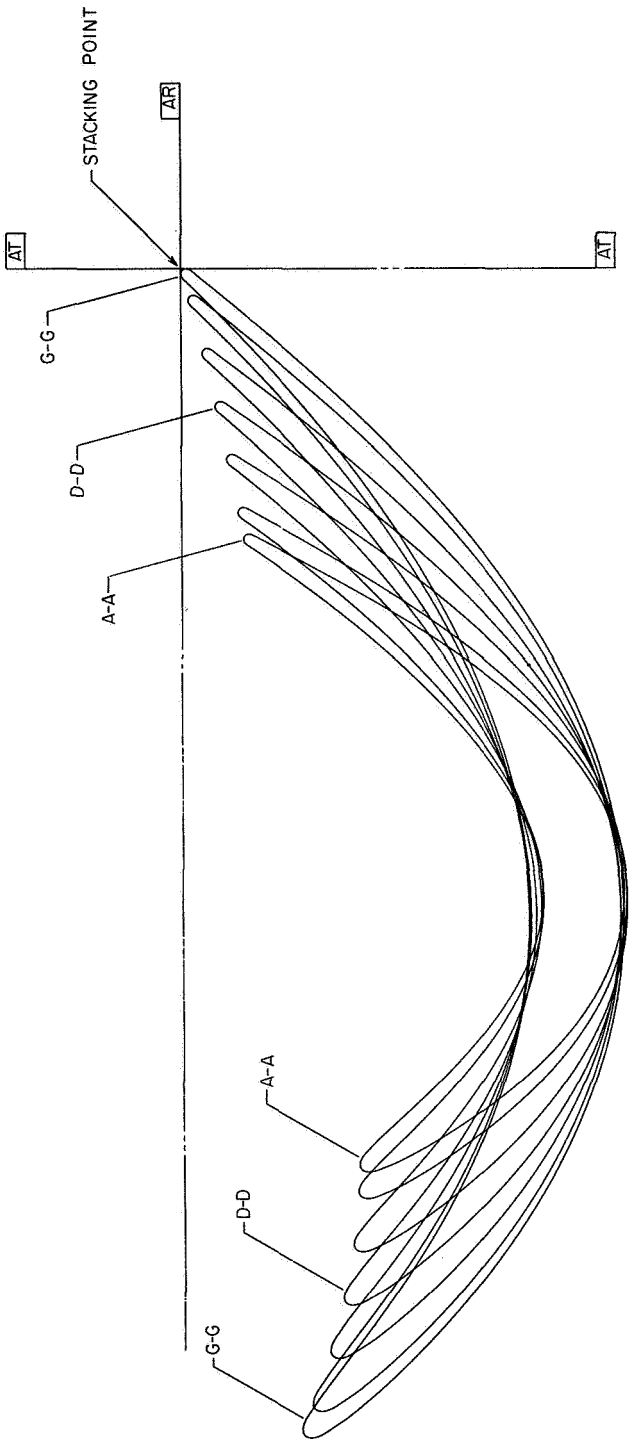

Figure 64. Stage Four Vane Stackup (4013164-016).

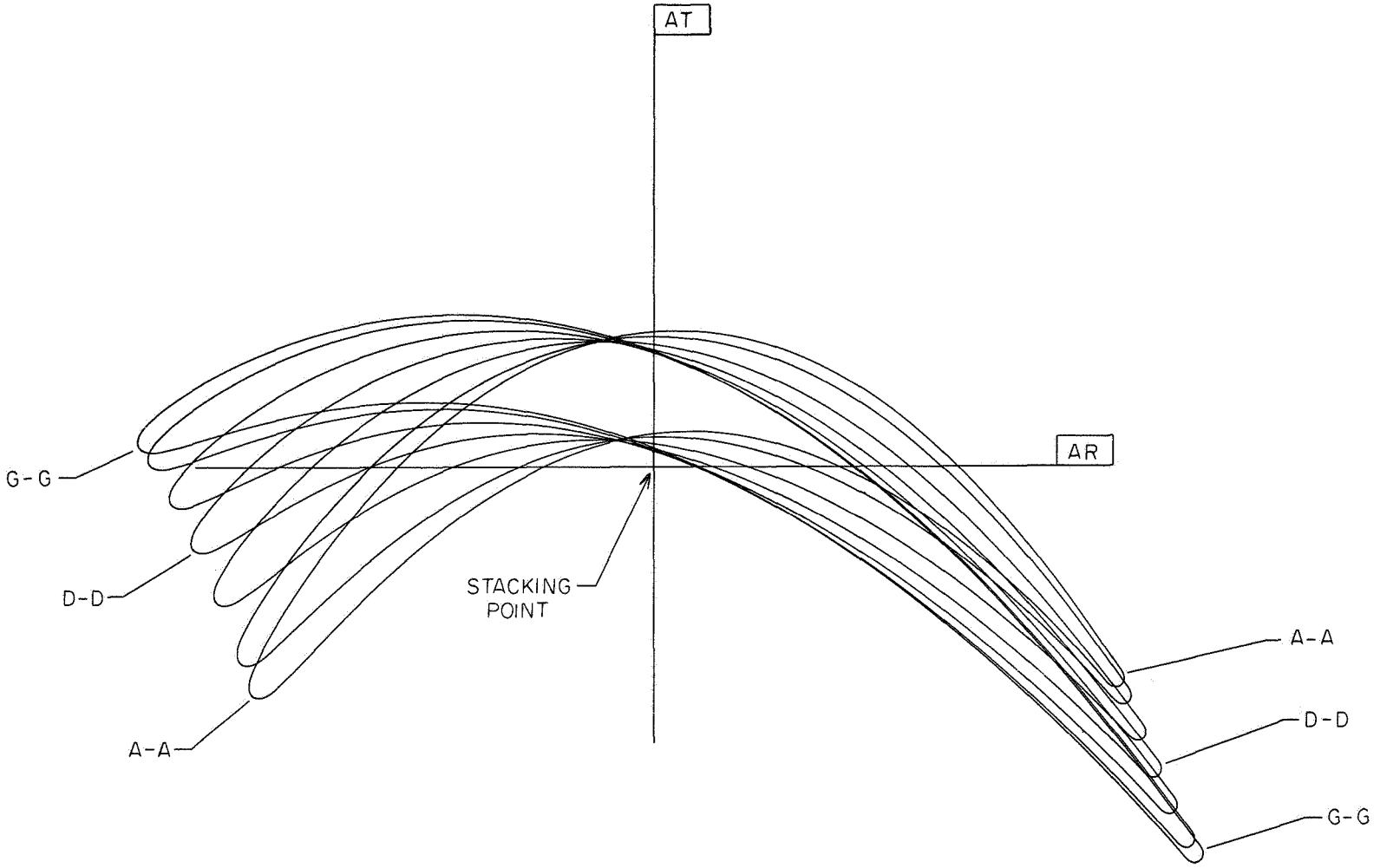

Figure 65. Stage Four Rotor Stackup (4013164-008).

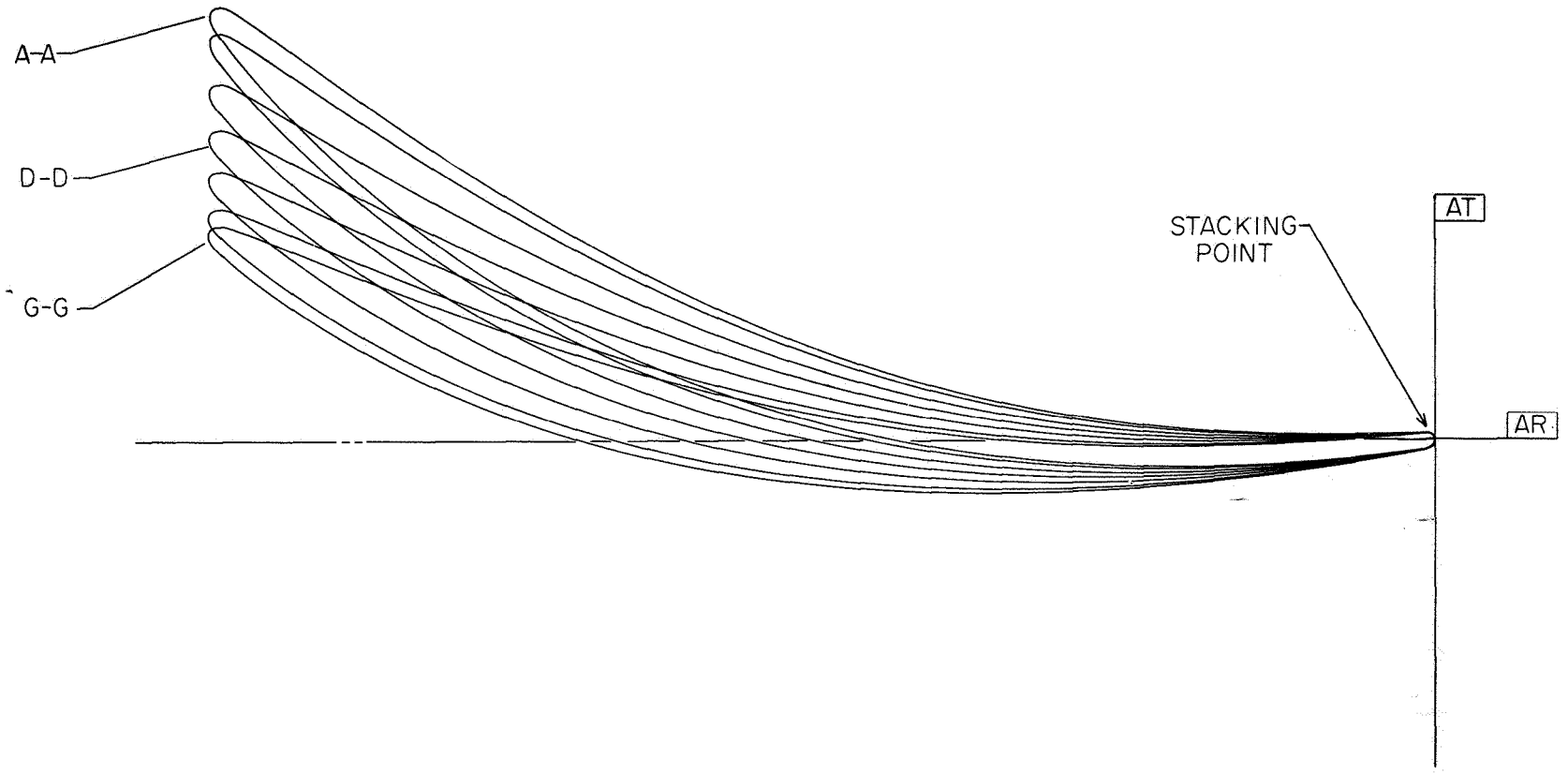

Figure 66. Outlet Turning Vane Stackup (4013164-018).

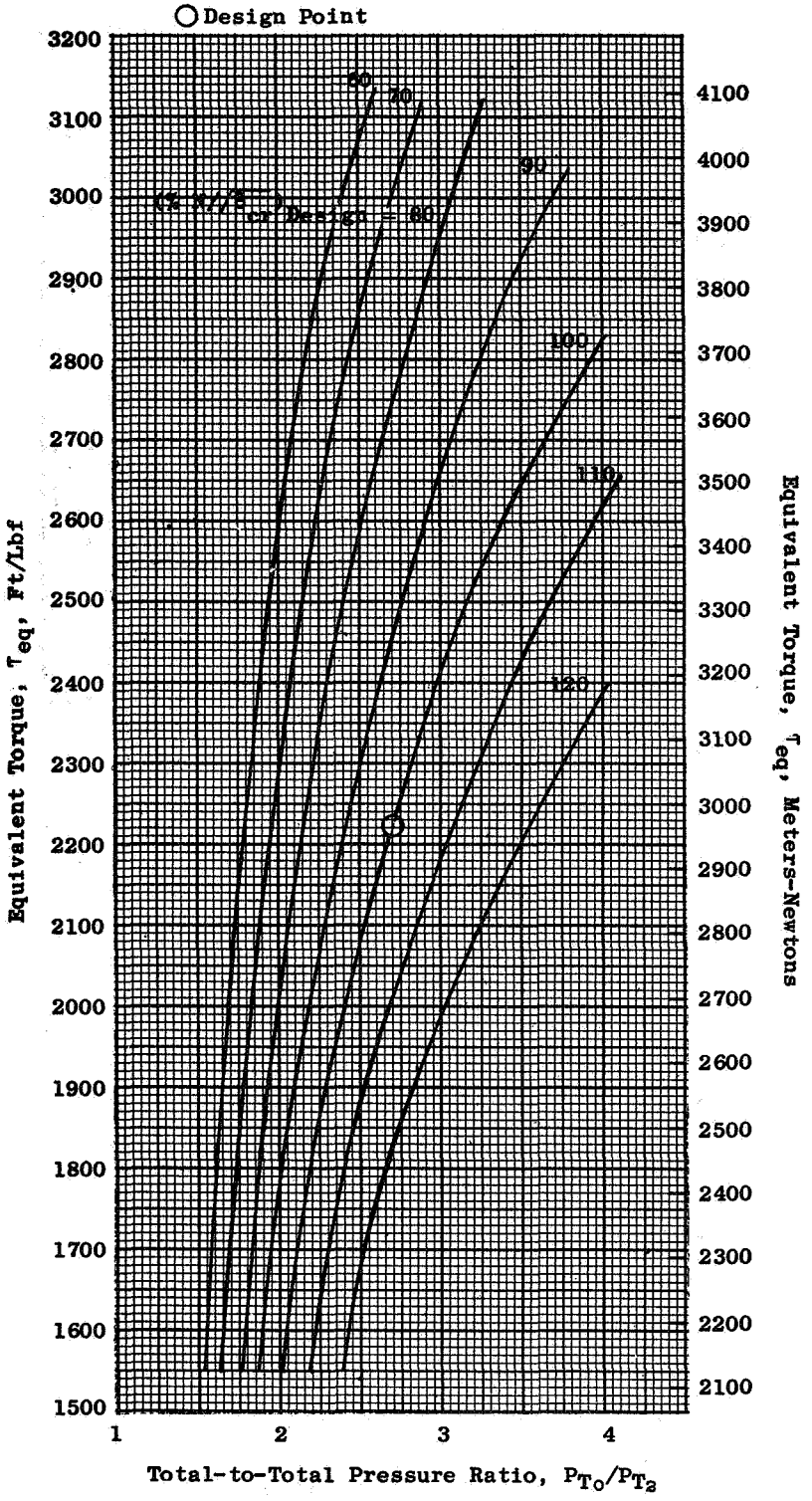

Figure 67. Equivalent Torque Vs. Total-to-Total Pressure Ratio.

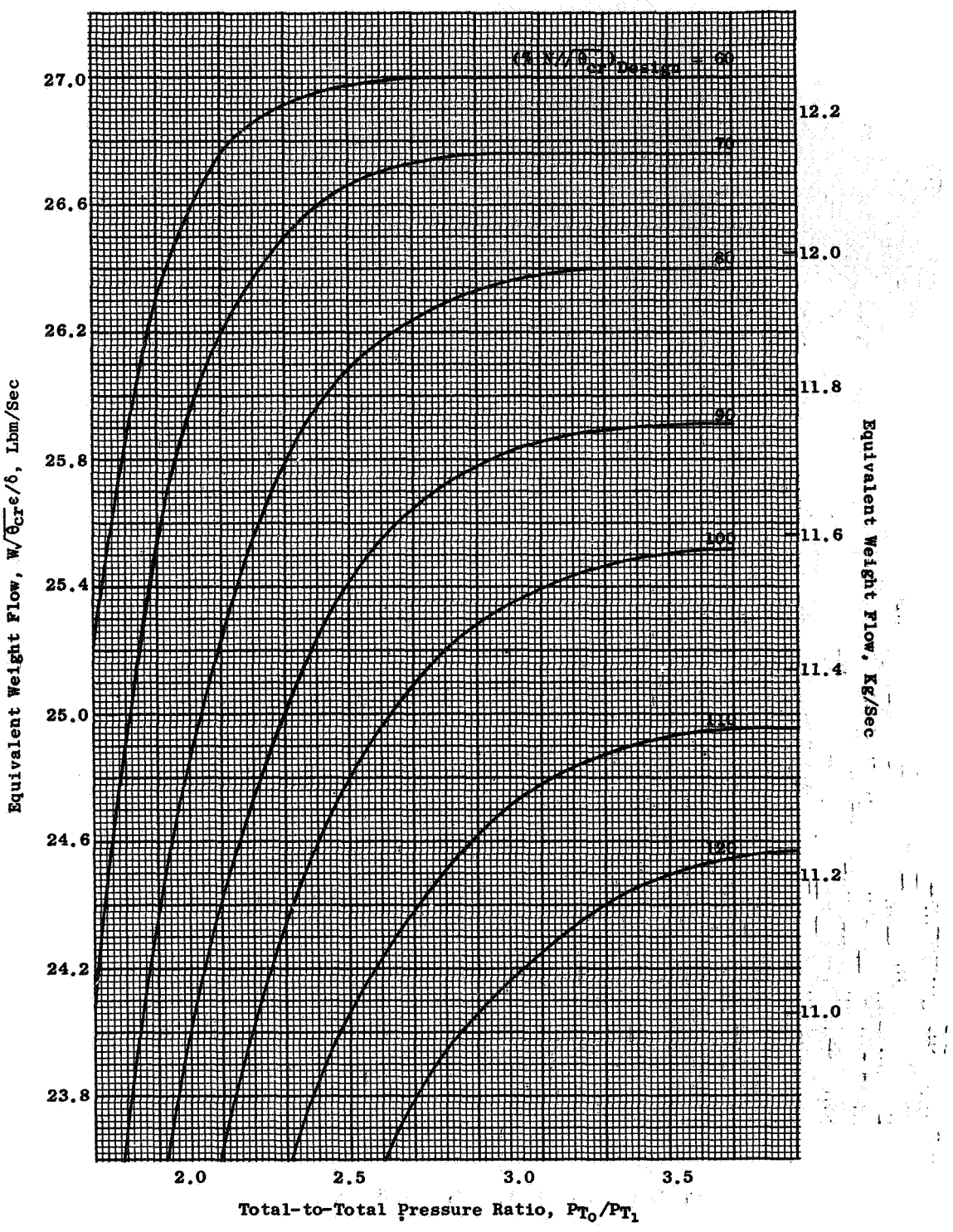

Figure 68. Equivalent Weight Flow Vs. Total-to-Total Pressure Ratio.

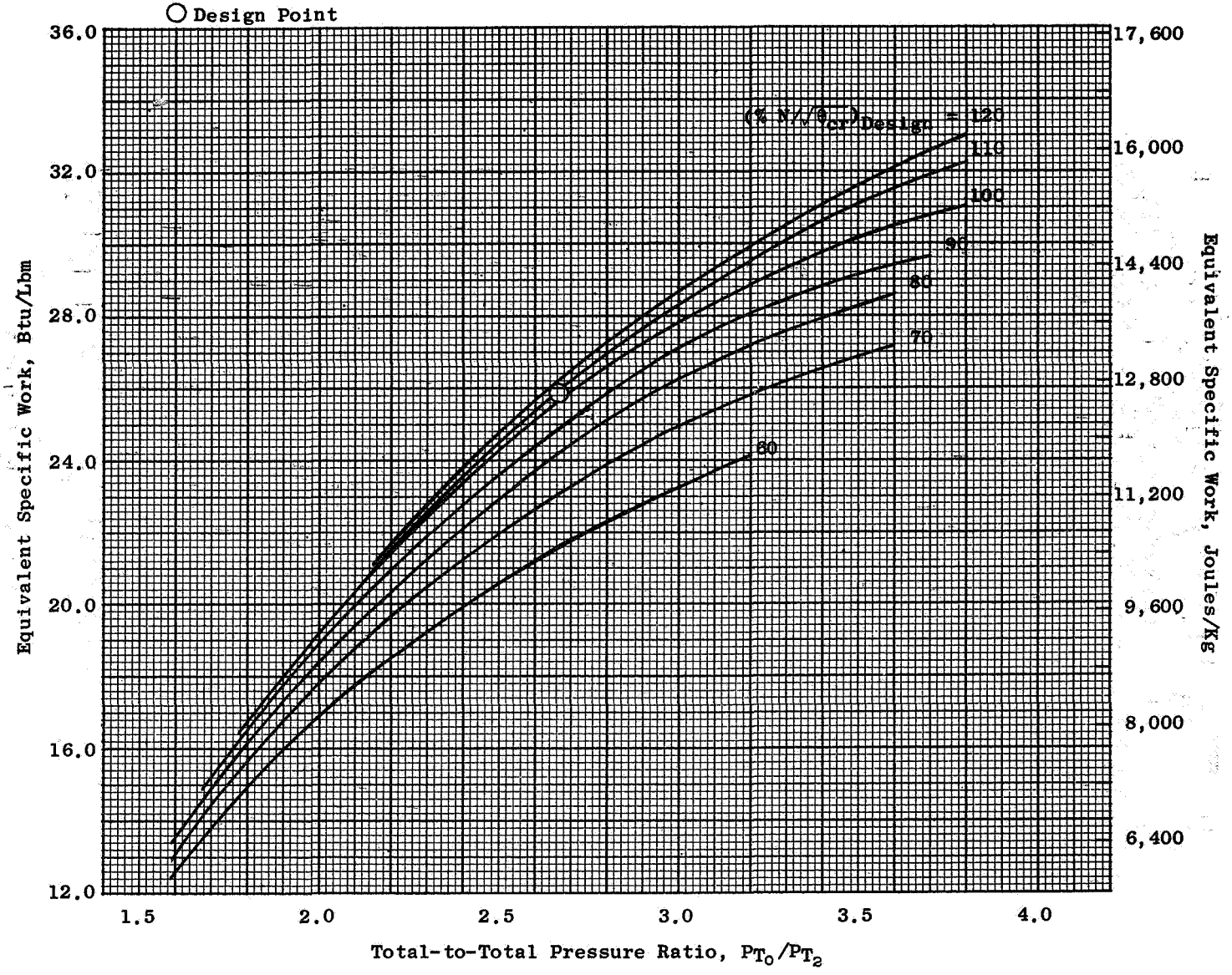

Figure 69. Equivalent Specific Work Vs. Total-to-Total Pressure Ratio.

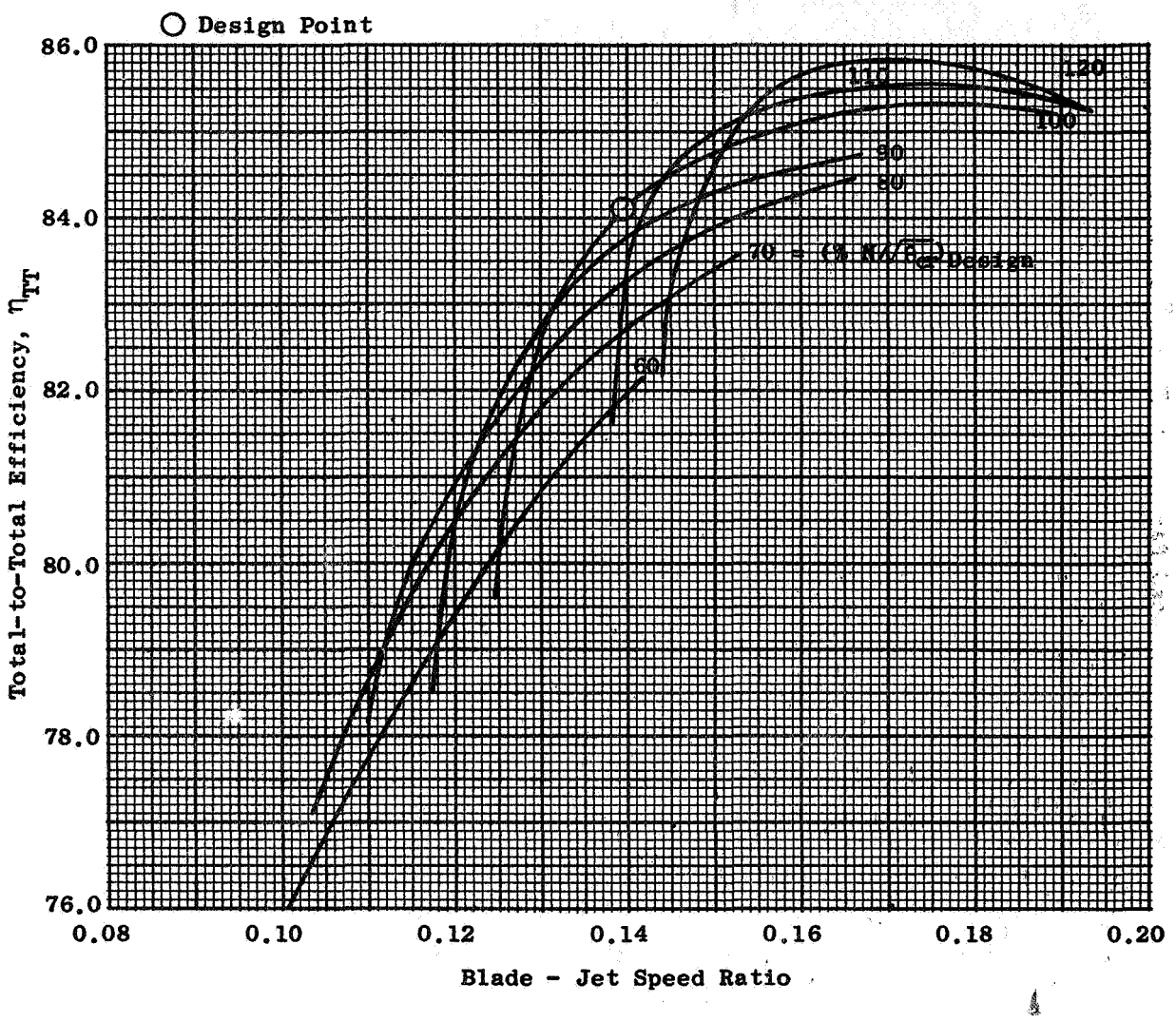

Figure 70. Total-to-Total Efficiency Vs. Blade-Jet Speed Ratio.

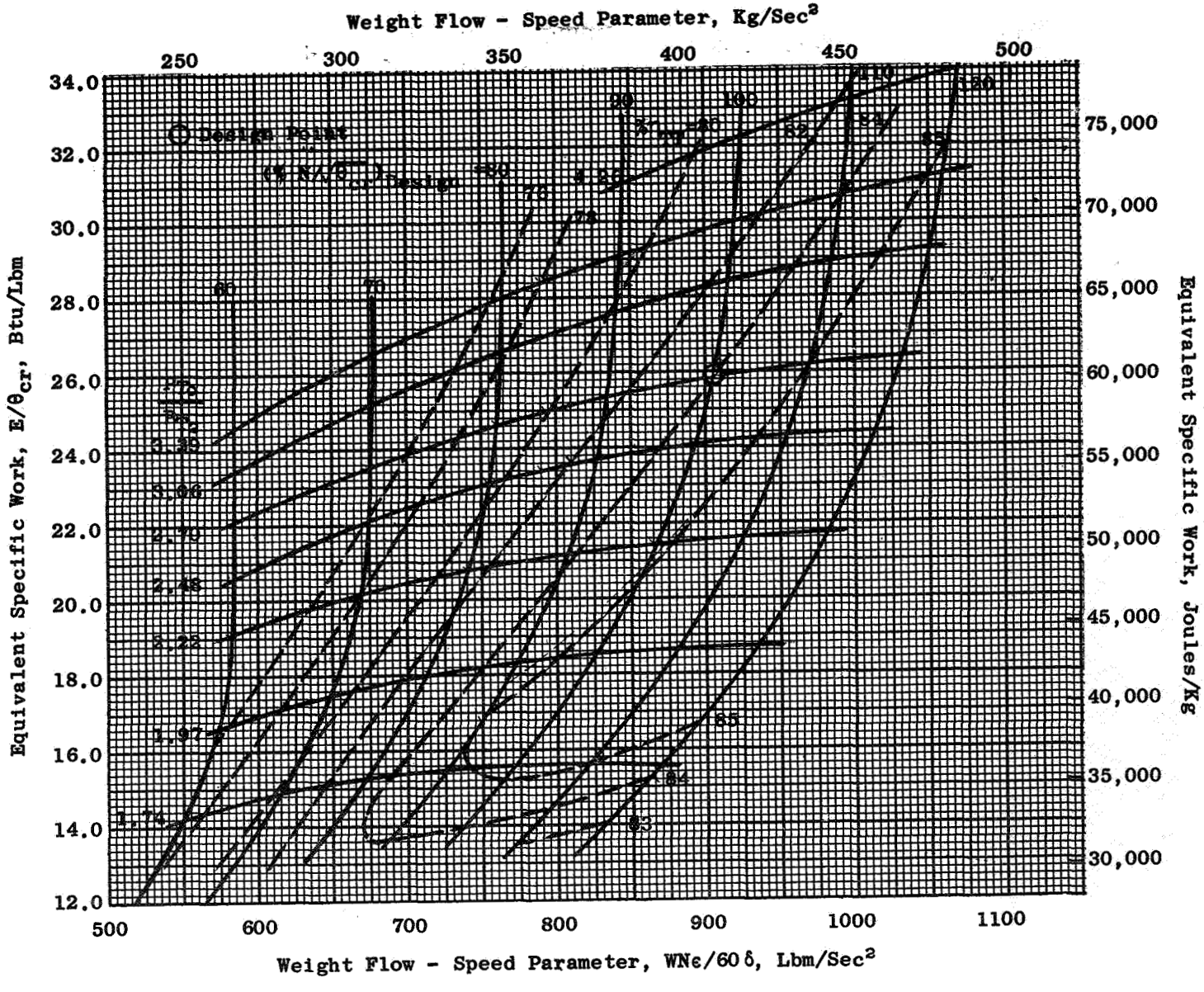

Figure 71. Equivalent Specific Work Vs. Weight Flow - Speed Parameter.

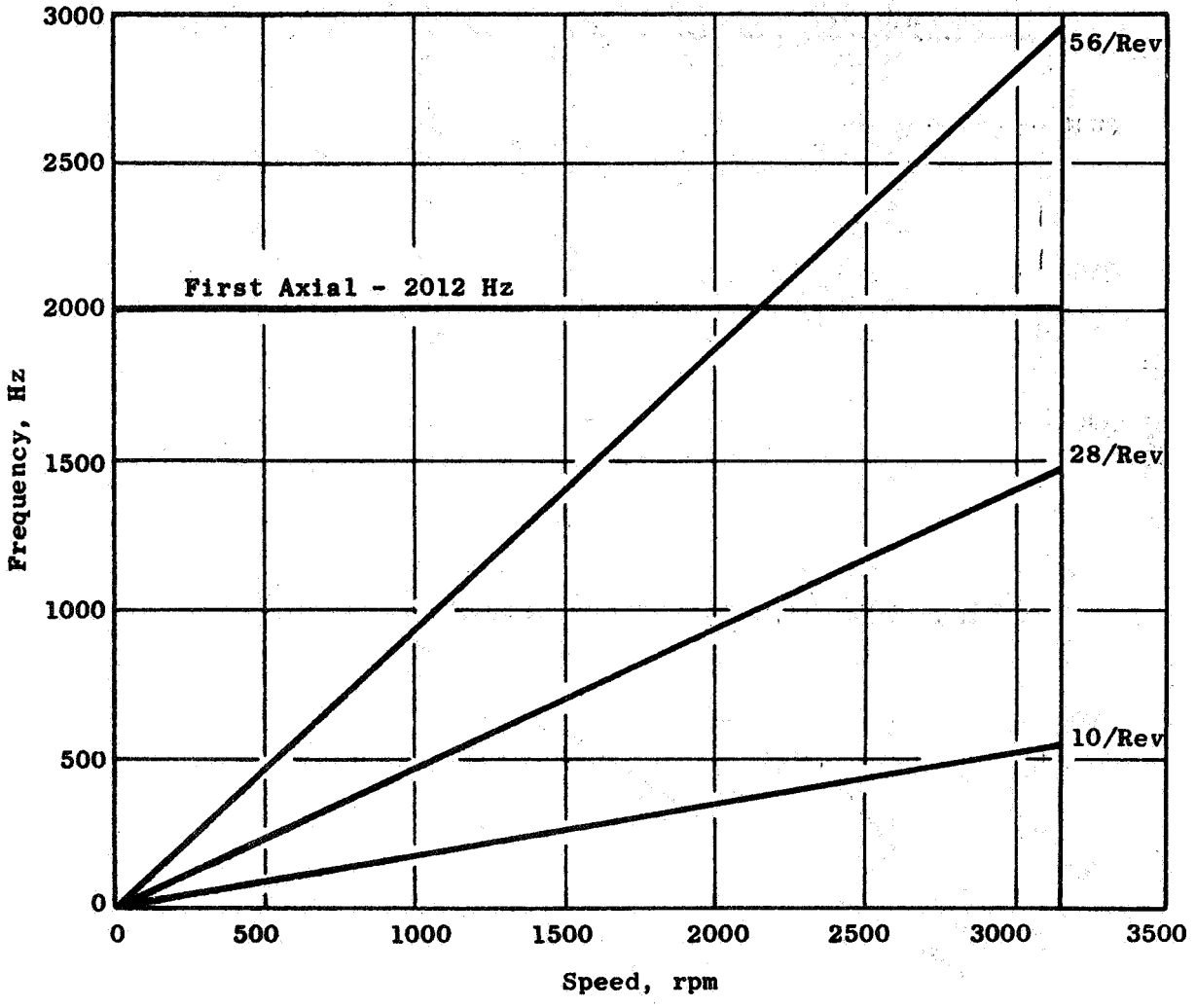

Figure 72. Most Probable Modes of Vibration, Stage One Blade.

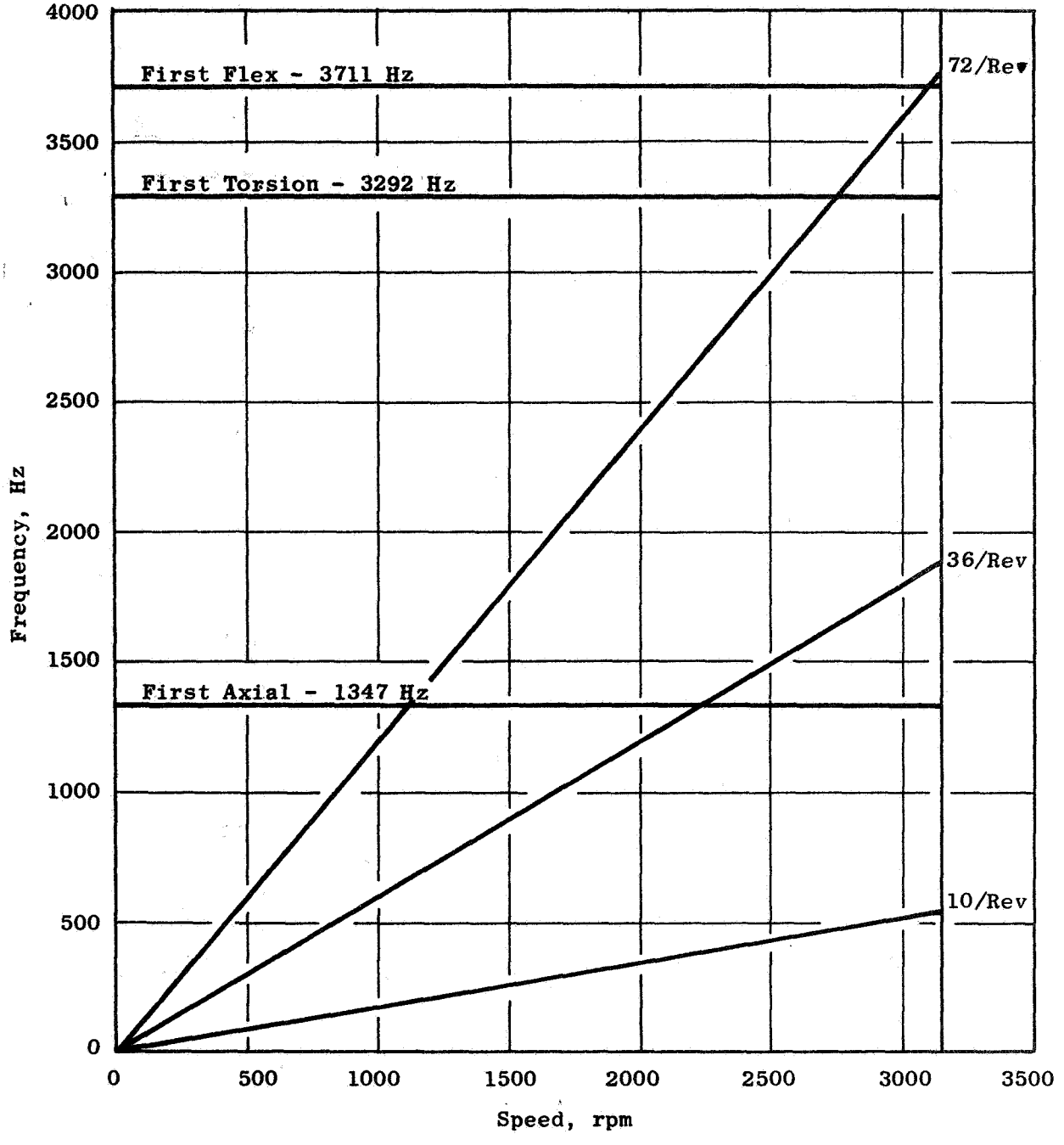

Figure 73. Most Probable Modes of Vibration, Stage Two Blade.

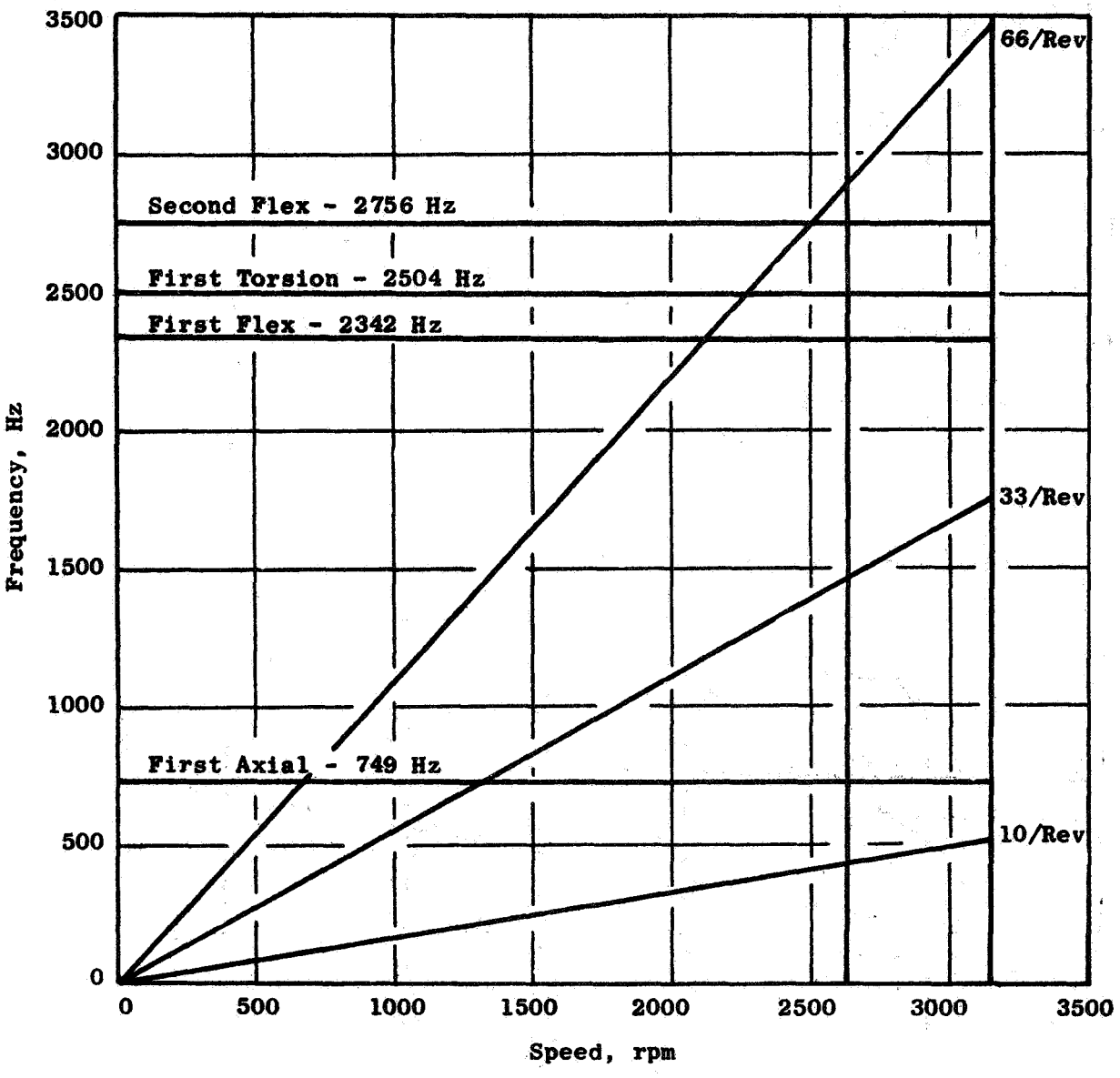

Figure 74. Most Probable Modes of Vibration, Stage Three Blade.

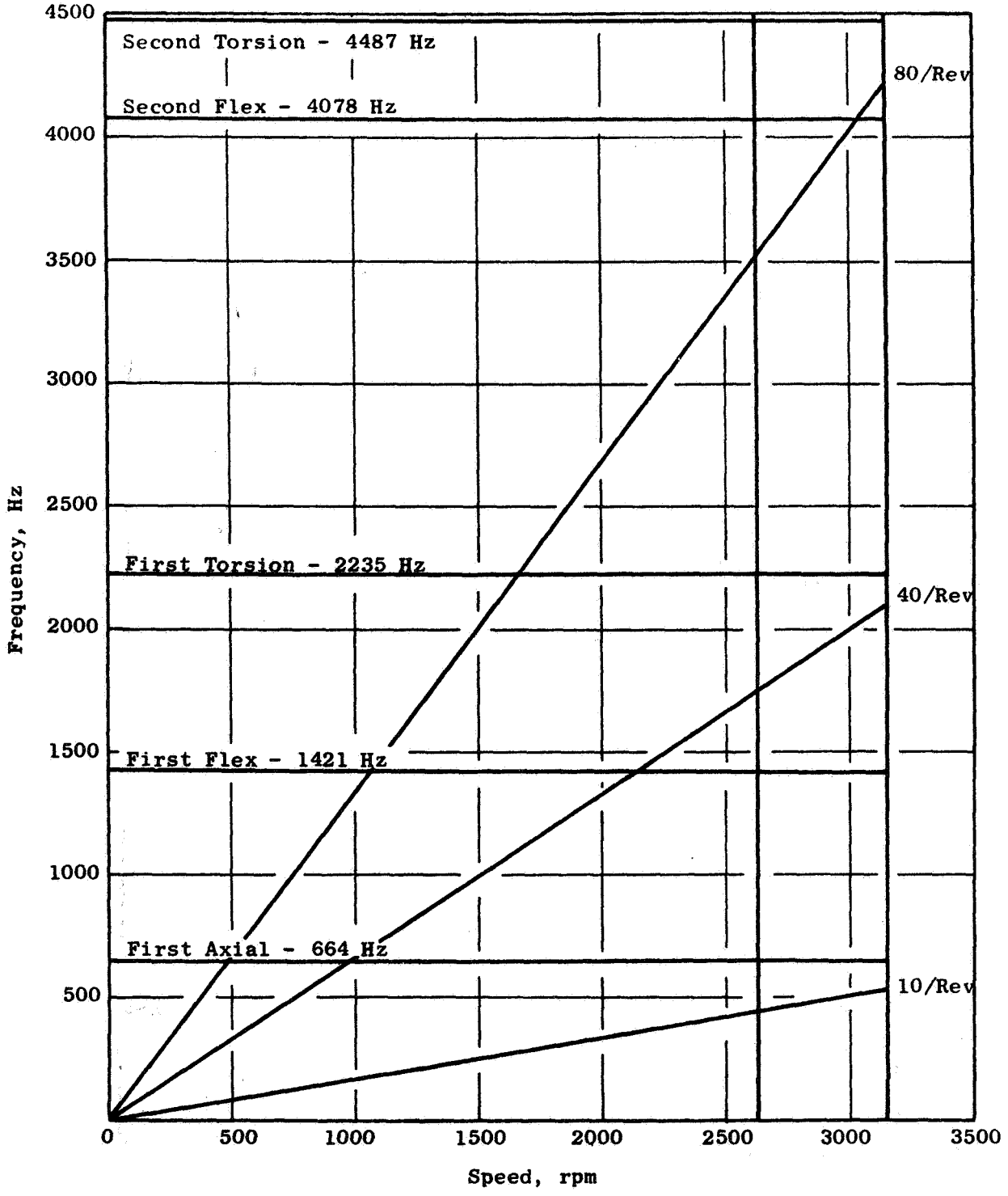

Figure 75. Most Probable Modes of Vibration, Stage Four Blade.

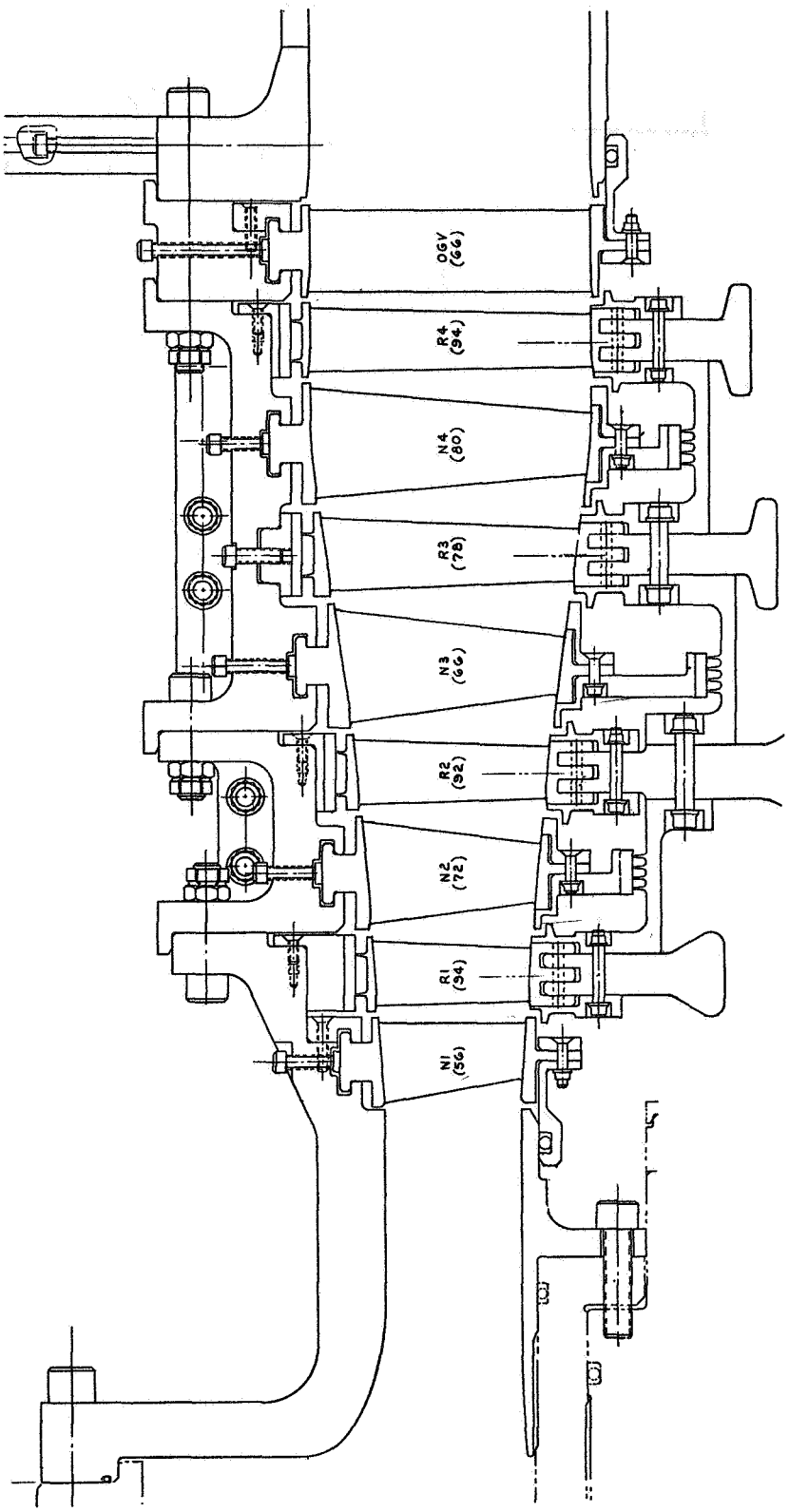

Figure 76. Mechanical Design Flowpath.

"The aeronautical and space activities of the United States shall be conducted so as to contribute . . . to the expansion of human knowledge of phenomena in the atmosphere and space. The Administration shall provide for the widest practicable and appropriate dissemination of information concerning its activities and the results thereof."

—NATIONAL AERONAUTICS AND SPACE ACT OF 1958

NASA SCIENTIFIC AND TECHNICAL PUBLICATIONS

TECHNICAL REPORTS: Scientific and technical information considered important, complete, and a lasting contribution to existing knowledge.

TECHNICAL NOTES: Information less broad in scope but nevertheless of importance as a contribution to existing knowledge.

TECHNICAL MEMORANDUMS: Information receiving limited distribution because of preliminary data, security classification, or other reasons. Also includes conference proceedings with either limited or unlimited distribution.

CONTRACTOR REPORTS: Scientific and technical information generated under a NASA contract or grant and considered an important contribution to existing knowledge.

TECHNICAL TRANSLATIONS: Information published in a foreign language considered to merit NASA distribution in English.

SPECIAL PUBLICATIONS: Information derived from or of value to NASA activities. Publications include final reports of major projects, monographs, data compilations, handbooks, sourcebooks, and special bibliographies.

TECHNOLOGY UTILIZATION PUBLICATIONS: Information on technology used by NASA that may be of particular interest in commercial and other non-aerospace applications. Publications include Tech Briefs, Technology Utilization Reports and Technology Surveys.

Details on the availability of these publications may be obtained from:

SCIENTIFIC AND TECHNICAL INFORMATION OFFICE

NATIONAL AERONAUTICS AND SPACE ADMINISTRATION

Washington, D.C. 20546